A Survey of Methods to Study Zinc Porphyrin Aggregates in Various Media

A Thesis Submitted to
the College of Graduate Studies and Research
in Partial Fulfillment of the Requirements
for the Degree of Master of Science
in the Department of Chemistry
University of Saskatchewan

by

Jaclyn O'Brien
Department of Chemistry
University of Saskatchewan

Permission to Use

In presenting this thesis in partial fulfilment of the requirements for a Postgraduate degree from the University of Saskatchewan, I agree that the Libraries of this University may make it freely available for inspection. I further agree that permission for copying of this thesis in any manner, in whole or in part, for scholarly purposes may be granted by professors Ronald P. Steer and Matthew F. Paige who supervised my thesis work or, in their absence, by the Head of the Department or the Dean of the College in which my thesis work was done. It is understood that any copying or publication or use of this thesis or parts thereof for financial gain shall not be allowed without my written permission. It is also understood that due recognition shall be given to me and to the University of Saskatchewan in any scholarly use which may be made of any material in my thesis.

Requests for permission to copy or to make other use of material in this thesis in whole or part should be addressed to:

Head of the Department of Chemistry

University of Saskatchewan

Saskatoon, Saskatchewan

S7N 5C9

Canada

Abstract

Metalloporphyrin aggregation is critical for triplet-triplet annihilation (TTA) to occur. In order to maximize the efficiency of TTA, to use as a mechanism of photon upconversion in dye-sensitized solar cells, it is important to understand the phenomenon of absorber aggregation. The aggregation of ZnTPP in polymer films was investigated by fluorescence anisotropy and total internal reflection fluorescence microscopy (TIRFM). Single molecule spectroscopy (SMS) and spectromicroscopy were the techniques used to study single molecules and multimolecular aggregates of ZnTPP/ZnTPPS in polymer films/adsorbed on glass substrates.

Fluorescence anisotropy measurements consistently showed depolarized emission from films most concentrated with ZnTPP. This observation was likely a result of energy transfer in and among porphyrin aggregates. Fluorescence intensity decays were also obtained and they illustrated a pattern of decreased fluorescence lifetime (i.e. faster decays) as the concentration of porphyrin in the film increased. These results are consistent with the formation of aggregates, and their increased presence in more concentrated films. The formation of these aggregates quenches the fluorophore's fluorescence, resulting in the observed shorter fluorescence lifetimes.

TIRFM was performed to study the structure of these polymer films doped with ZnTPP. It was determined that these films consisted of discrete domains and thus lacked homogeneity, and the presence of aggregates was clearly visible. Time-resolved TIRFM measurements were also performed but no interesting results were collected.

SMS and spectromicroscopy were the final techniques employed to study porphyrin aggregation. Preliminary measurements were performed with polymer films doped with ZnTPP, and the single step decay time trajectories collected indicated that single molecules were being studied. Furthermore, emission spectra of these molecules were collected and they were similar to those obtained for a bulk measurement, but the bands were slightly shifted in comparison. These measurements were repeated with ZnTPPS adsorbed to glass substrates. Two different patterns of decay trajectories were measured: (i) single step decays corresponding to single ZnTPPS molecules and (ii) multi step/complex decays representative of multimolecular aggregates. Emission spectra were also collected for the multimolecular aggregates, and they were consistent with those of an ensemble measurement but slightly blue-shifted. Such a shift is common when studying aggregates on such a highly polar surface. Thus, these results demonstrate that ZnTPPS aggregates form even at concentrations as low as 10^{-8} M, and can be studied using SMS despite their weak fluorescence emission.

Acknowledgements

I would first like to thank both of my supervisors, Ron Steer and Matt Paige, for their continued support over the last two years. Both have been incredibly patient with me, and I am grateful for how they both have always made time to help me, whether it was with my research or in making decisions for my future career. Most importantly, their enthusiasm for their work has been truly inspiring, and is something I will never forget.

I would also like to thank the members of both research groups. I have been introduced to a number of great people over the years, and they have made my time at the University of Saskatchewan enjoyable and memorable. In particular, I would like to thank my fellow co-worker Yin Lu. She has been an incredible help to me, and I really don't believe I would have had the same experience if it wasn't for her consistent willingness to help me with my project, and in understanding the theory behind it all.

I was very fortunate to have been able to perform some of my research at the University of Melbourne in Australia, and I would like to thank everyone there that helped me out. In particular: Emma Hooley, Xiaotao Hao, Trevor Smith, Toby Bell, Alison Funston, Ken Ghiggino and Ben Robotham.

I would also like to thank NSERC and the Department of Chemistry at the University of Saskatchewan for their financial support.

Finally, I would like to thank my friends and family for their continued support, constant encouragement and infinite patience. I genuinely appreciate their

confidence and optimism and truly hope that I reciprocate such acts of kindness in their lives.

Table of Contents

List of Figures

List of Tables

List of Abbreviations

A	Absorbance
A	Cross-sectional area of the laser beam used in calculating the signal-to-noise ratio
BBO	Beta barium borate
CCD	Charge coupled device
cw	Continuous wave
D	Dichroic miror
DSSC	Dye sensitized solar cell
EMCCD	Electron multiplying CCD
F	Fluorescence
f	Focal length
FL	Focusing lens
fs	Femtoseconds
FWHM	Full-width at half maximum
G	G-factor
IC	Internal conversion
ICCD	Intensified CCD
I_{HV}	Intensity of vertically polarized emission when excited by horizontally polarized light
I_{HH}	Intensity of horizontally polarized emission when excited by horizontally polarized light
ISC	Intersystem crossing
I_{VV}	Intensity of vertically polarized emission when excited by vertically polarized light
I_{VH}	Intensity of horizontally polarized emission when excited by vertically polarized light
N	Number of atoms in a molecule
n	Number of monomer units in a porphyrin array
NA	Numerical aperture
NaOH	Sodium hydroxide
ns	Nanoseconds
OL	Objective lens
P	Phosphorescence
PH	Pinhole
PMMA	Poly(methyl methacrylate)
ps	Picoseconds
PVA	Poly(vinyl alcohol)
r	Anisotropy
rpm	Rotations per minute
r(t)	Anisotropy at time t
R6G	Rhodamine 6G
S	Sample
SCAN	Sample scan stage
SMS	Single molecule spectroscopy
SNR	Signal-to-noise ratio

TIRFM	Total internal reflection fluorescence microscopy	ZnTBP	Zinc tetrabenzoporphyrin
TTA	Triplet-triplet annihilation	ZnTPP	*meso*-tetraphenylporphine zinc
VR	Vibrational relaxation	ZnTPPS	*para*-sulfonated derivative of ZnTPP

List of Symbols and Mathematical Terms

a_1	Contribution of τ_1 to overall decay
a_2	Contribution of τ_2 to overall decay
A_0	Fitting constant
C_b	Background count rate per watt of excitation power
d	Exponential decay distance
$\vec{E}$	Electric field vector
F_{coll}	Angular collection factor of the detector
F_{filter}	Filter transmission
F_{opt}	Transmission factor for the optical losses
$h\nu_f$	Fluorescent photon
I_0	Initial intensity
I(0)	Intensity of evanescent wave at the interface of two media
I(t)	Intensity at time t
I(z)	Intensity of evanescent wave as it passes a distance z through the n_2 medium
k_f	Rate constant of emission
$\sum k_{nr}$	Sum of all rate constants of all nonradiative pathways
n	Refractive index of the medium between the sample and objective when calculating NA
$n_{1,2}$	Refractive indices of media light travels through in TIRFM calculations
N	Number of molecules
N_A	Avogadro constant
N_d	Dark count rate
n_Q	Quantum efficiency of the detector
$\vec{P}$	Absorption transition moment
$P_0/h\nu$	Number of excitation photons per second
S_0	Ground singlet state
S_1	First excited singlet state
S_2	Second excited singlet state
T	Detector counting interval
T_1	First excited triplet state
β	Angle between absorption and emission transition moments
ε	Molar extinction coefficient
λ	Excitation wavelength
λ_0	Excitation wavelength in a vacuum
θ	Incident angle in TIRFM
θ	Collection angle of the objective in calculating NA
θ_c	Critical angle
σ_p	Absorption cross section of a molecule

Φ_F	Fluorescence quantum yield	Γ	Point group of molecule
γ_r	Rate of fluorescence	Γ_{tot}	Total frequency width of the absorption
τ	Fluorescence lifetime	Ψ_e'	Upper electronic wavefunction of the transition
τ_1, τ_2	Average excited state lifetimes	Ψ_e	Lower electronic wavefunction of the transition
τ_{on}	Photobleaching time constant	μ_e	Electric dipole moment operator

Chapter 1: Introduction

Aggregation is a natural phenomenon observed amongst many different aromatic fluorescent molecules. This self-assembly of molecules is a result of π-π stacking interactions between the molecules in the system being studied. These π-π stacking interactions are essentially the sum of all noncovalent interactions, including: dispersion and electrostatic interactions, and solvophobic effects. Aggregation is most often observed in fluid and solid media. The formation of aggregates has an effect on the overall system. For example, aggregation can quench or induce fluorescence emission. In this thesis, the formation and properties of zinc porphyrin aggregates in various media were studied using fluorescence and spectroscopy techniques. In the following paragraphs, the techniques utilized in this work and the theory necessary to understand the results observed are explained.

1.1 An Introduction to Photophysics

Light-induced processes are essential to the functioning of the natural world as photon absorption initiates a number of important reactions, including those involved in photosynthesis, and ozone formation and depletion. When a molecule absorbs a photon of light, it becomes energetically excited, and will dissipate the absorbed energy of the photon by producing either a chemical (photochemistry) or physical (photophysics) change to the molecule. Photophysical processes are mainly observed in the work described in this thesis, and they include both radiative (fluorescence/phosphorescence) and radiationless processes.

Fluorescence is defined as the emission of light by an electronically excited molecule in which the radiative decay occurs between electronic states of the same electron spin multiplicity (from $S_1 \rightarrow S_0$, for example). S_0 indicates the ground singlet electronic state of a molecule where all of its electrons are spin-paired and occupy the orbitals of lowest energy. When a molecule absorbs a UV-visible photon of specific energy, it can be promoted to a higher excited electronic state. The electron in excited singlet states (S_n, $n \geq 1$) is of opposite spin to the electron remaining in the ground state.[1] Electronic excited states can relax back to the ground state through either nonradiative (internal conversion) or radiative (that is, fluorescence) pathways. Electronically excited molecules can also undergo intersystem crossing (ISC), a nonradiative transition between electronic states of different spin multiplicity, for example from $S_1 \rightarrow T_1$. T_1 denotes the first excited triplet state of the molecule. It differs from S_1 in that the two unpaired electrons in T_1 have parallel spins.[1] According to the spin-multiplicity selection rule[2], transitions from $T_1 \rightarrow S_0$ are forbidden, but still take place at slow rates due to spin-orbit coupling. If this transition involves an emission of a photon, the luminescence observed is called phosphorescence. In this thesis, phosphorescence will not be discussed further. Instead fluorescence will be the main focus of this work. Other processes can also take place when the molecule is in the triplet state, including triplet-triplet annihilation, which will be discussed later in this chapter.

In addition to the spin-multiplicity selection rule, the symmetry and parity of the molecule must also be considered to determine if a particular electronic transition is optically allowed. The symmetry selection rule states that an electronic transition

is only allowed when the product of $\Gamma(\Psi_e^{'}) \otimes \Gamma(\mu_e) \otimes \Gamma(\Psi_e)$ is totally symmetric. Γ represents the irreducible representation of the electronic wavefunction of the molecule being studied, μ_e is the electric dipole moment operator, and $\Psi_e^{'}$ and Ψ_e correspond to the upper and lower electronic wavefunctions of the transition, respectively. The parity selection rule is an extension of this general symmetry based selection rule which states that for a centrosymmetric molecule, electronic transitions between states of the same parity (gerade (g) means even, and ungerade (u) means odd) are forbidden. That is, transitions are only allowed between states of different parities, $g \leftrightarrow u$, for example. Figure 1.1 shows a Jablonski diagram that is often used to illustrate the transitions discussed above.

Nonlinear, polyatomic molecules have 3N-6 normal modes of vibration, where N is equal to the number of atoms in the molecule. In the following diagram, the vibrational levels that are attributed to each electronic energy level are shown schematically as horizontal lines of a smaller weight. At thermal equilibrium, molecules occupy these vibrational states in numbers that follow the Boltzmann distribution; at room temperature, most occupy the lowest energy vibrational level of the ground electronic state. In addition, there are a number of rotational energy levels associated with each vibrational energy level that are not shown in Figure 1.1.

Vibrational relaxation (VR) refers to the relaxation of vibrationally "hot" populations to that population characteristic of thermal equilibrium where the ground vibrational level within an electronic state is most highly populated. This process occurs very quickly in condensed media, and as a result most electronic transitions occur from the ground vibrational level of an electronic state. In fact, most of the S_1

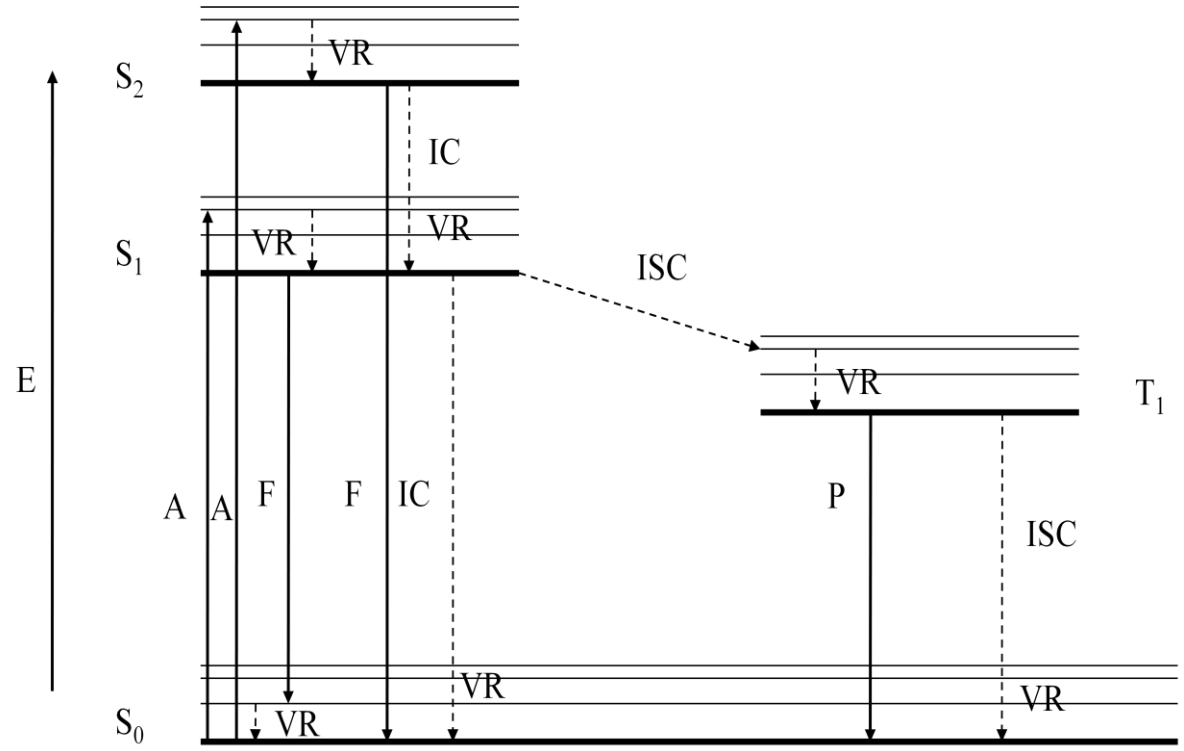

Figure 1.1 A simplified Jablonski diagram. Full arrows represent radiative transitions and the dashed arrows indicate nonradiative transitions. A = absorption, F = fluorescence, IC = internal conversion, ISC = intersystem crossing, P = phosphorescence, VR = vibrational relaxation, S_0 = ground singlet state, S_1 = first excited singlet state, S_2 = second excited singlet state, and T_1 = first excited triplet state. Higher-order states are not shown.

fluorescence originates from the ground vibrational level of S_1, and T_1 phosphorescence from the lowest vibrational level of T_1.[1] Moreover, when a molecule decays through fluorescence or phosphorescence it normally decays to one

of the higher vibrational levels of the ground state. As a result, the energy of the photons emitted during fluorescence and phosphorescence is typically lower than that of the photons that were initially absorbed. Consequently, if one were to compare the absorption and fluorescence emission spectra of a molecule, it would be seen that the emission spectrum would be displaced to longer wavelengths (red-shifted) in comparison to that of the absorption spectrum. If large structural changes do not accompany photon absorption, the emission spectrum of a molecule is often the mirror image of its absorption spectrum. This is due to the same transitions occurring in both absorption and emission as a result of similarly spaced vibrational levels in the two electronic states, which are also not severely displaced. According to the Franck-Condon principle, all electronic transitions are vertical, that is, they occur without nuclear displacement. Therefore, the most probable transition in absorption will most likely be the most probable transition in emission (See Figure 1.2 A). The difference in energy between the maxima in the absorption and emission spectra is called the Stokes' shift (See Figure 1.2 B).[1]

A molecule's fluorescence can be described quantitatively by its quantum yield and lifetime. The quantum yield, Φ_F, is a measure of the probability that a one-photon absorption event will lead to the emission of a photon. As such, it is a ratio of the number of photons emitted to the number that were absorbed in the same sample over the same time period. In equation 1.1, k_f is the rate constant of emission for the fluorescing molecule, and $\sum k_{nr}$ is the sum of all rate constants of all nonradiative pathways by which it relaxes back to the ground state. The closer the quantum yield

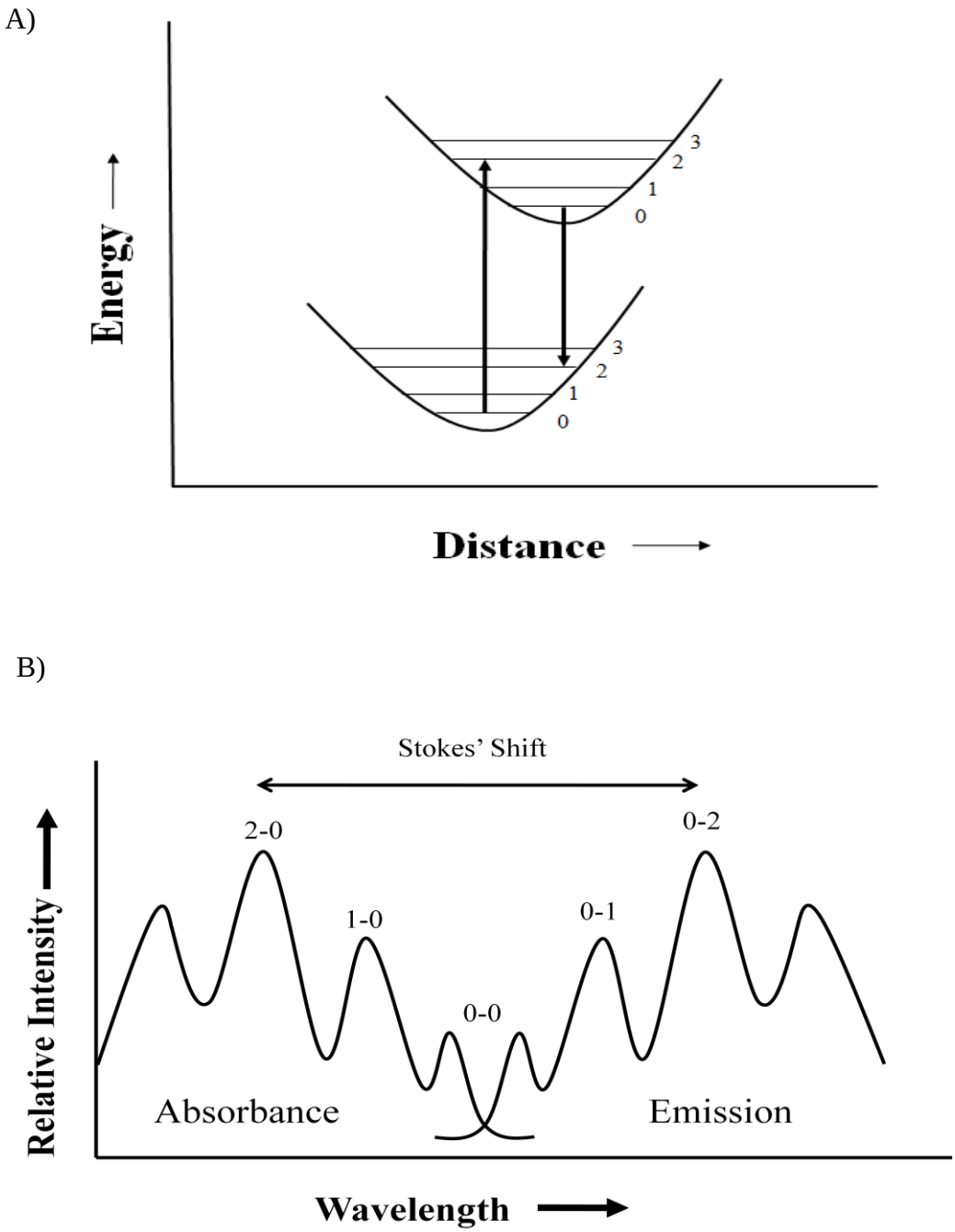

Figure 1.2 Schematic diagrams illustrating **A)** the Franck-Condon principle and **B)** the mirror image rule. The numbers indicate the vibrational levels in the ground and excited states between which the transition occurs.

is to unity (that is, $\sum k_{nr} << k_f$), the more fluorescent the molecule will be. Nonradiative decay pathways compete with fluorescence, resulting in a quantum yield less than one.

$$\Phi_F = \frac{k_f}{k_f + \sum k_{nr}} \tag{1.1}$$

The fluorescence lifetime (τ) is defined as the time it takes for $1/e$ of the emitting excited state population to decay to other electronic states. Moreover, it's a measure of the amount of time that an ensemble of molecules stays in the excited state and can be calculated using the following expression:

$$\tau = \frac{1}{k_f + \sum k_{nr}} \tag{1.2}$$

Equation 1.3 can be rearranged to determine the average lifetime of an excited state that relaxes back to the ground state via a single exponential decay. Molecules that decay from the excited state in this way exhibit first-order kinetic behaviour. In the following equation, I_0 is the initial intensity and $I(t)$ is the intensity at time t.

$$I(t) = I_0 e^{-t/\tau} \tag{1.3}$$

Multi-exponential decays can be observed in samples with significant intermolecular interactions. Second-order decays, for example, have two different decays for two different excited species in the sample. The formation of multi-molecular aggregates is one phenomenon that can cause these types of decays.

Equation 1.4 can be rearranged to determine the lifetimes of the two excited states in a second-order decay;

$$I(t) = a_1 e^{-\tau_1/t} + a_2 e^{-\tau_2/t} \qquad (1.4)$$

Where α_1 and α_2 represent the contribution of each lifetime to the overall decay, and whose sum is always equal to one. τ_1 and τ_2 are the average excited state lifetimes.

1.2 Porphyrins

Molecules or fragments of larger entities that emit fluorescence are called fluorophores. Most often, fluorophores in organic molecules are aromatic. Porphyrins are a group of fluorescent molecules that were the subject of this research.

Porphyrins are fully conjugated tetrapyrroles with varying side groups. These macrocycles are often studied because they mimic natural light harvesting systems.[3] As such, porphyrins have been proposed as ideal candidates for use in dye sensitized solar cells (DSSCs)[4-6], photodynamic therapy[7-10] and oxygen sensors[11,12], to name a few of their applications. Solutions of these compounds are highly coloured, as they have strong absorption bands in the visible region of the electromagnetic radiation spectrum. The tetrapyrrole can be complexed with a metal to form a metalloporphyrin (See Figure 1.3 for typical examples).

Porphyrins, and their metallated derivatives, have many spectroscopic properties that make them attractive to work with. For instance, many are chemically stable, they are strong absorbers of visible light, most are structurally rigid and many

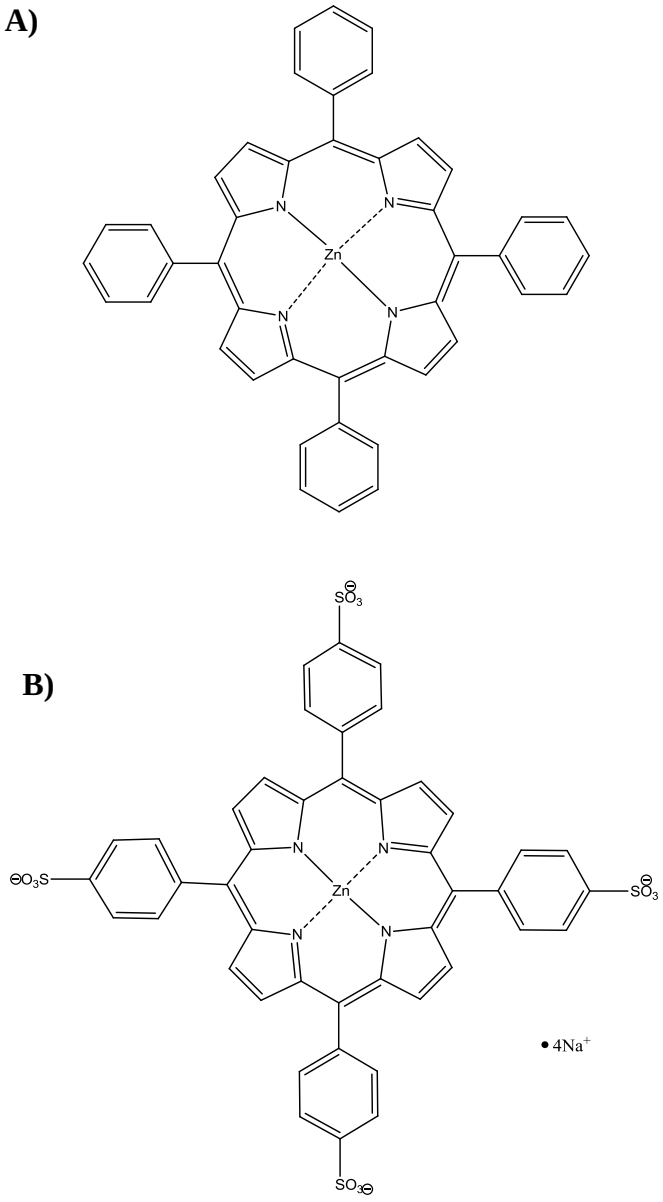

Figure 1.3 The chemical structure of **A)** *meso*-tetraphenylporphine zinc, ZnTPP, and **B)** its *para*-sulfonated derivative, ZnTPPS. The dashed bonds represent coordinate covalent bonds.

are planar, which minimizes the rates of nonradiative decay pathways.[13] In addition, they are rare in that several types of porphyrins have been found to fluoresce strongly from two singlet excited states ($S_2 \rightarrow S_0$ and $S_1 \rightarrow S_0$).[3] The observed emission from the S_2 state violates Kasha's rule, which states that molecules with closed shell singlet ground states only fluoresce from the lowest excited singlet state (that is, S_1 which gives rise to the porphyrin Q bands).[14] The first observation of S_2 emission (porphyrin Soret band) from a porphyrin (zinc tetrabenzoporphyrin, ZnTBP) was in 1971.[15] Nonetheless, since S_2 has such a short lifetime it was difficult to learn more about these states until recently with the development of ultrafast laser technology.[3]

The two metalloporphyrins that will be discussed in this thesis are *meso*-tetraphenylporphine zinc, ZnTPP, and its *para*-sulfonated derivative, ZnTPPS (see Figure 1.3). The latter has the same structure as ZnTPP, but each of the phenyl rings are sulfonated in the para position to make it soluble in water. The quantum yields for the S_1 and S_2 fluorescence of ZnTPP are: 2.67×10^{-2} and 1.84×10^{-3}, respectively.[16,17] The lifetimes of the S_1 and S_2 excited states of ZnTPP are 1.96 ns and 1.38 ps, respectively, all in dilute ethanol solutions at room temperature.[17] Figure 1.4 shows the absorption and emission spectra for ZnTPPS in aqueous solution.

Porphyrins and their metallated derivatives are known to form multimolecular aggregates,[18,19] in which multiple molecules stack on top of one another and are held together by π-π interactions. Aggregation occurs in solution at micromolar porphyrin concentrations,[3,20-23] and has even been seen spectroscopically at concentrations less than 10^{-5} M.[24] This phenomenon has also been observed in thin polymer films,[25] and on glass cover slips at concentrations of 10^{-8} M of the dye.[26] As such, the aggregation

of porphyrins is unavoidable and may seem problematic if one wanted to study the dye in an unaggregated state. Nonetheless, the natural formation of these aggregates can promote certain phenomena, such as triplet-triplet annihilation (TTA), which can only be observed when they are present. In the porphyrins that radiate from S_2, TTA is a mechanism for non-coherent photon upconversion, the generation of photons that are higher in energy than the photons that are initially absorbed. TTA involves the interaction of two triplet states to form two singlet states, one of higher and one of lower energy. That is, $2T_1 \rightarrow S_n + S_0$, where $n \geq 1$. In some porphyrin systems (ZnTPP, for example), TTA generates excited S_2 state molecules with high efficiency. Thus, photon upconversion can occur in the one chromophore system by:

$$S_0 + h\nu \rightarrow S_1$$

$$S_1 \rightarrow T_1,$$

$$2T_1 \rightarrow S_2 + S_0,$$

$$S_2 \rightarrow S_0 + h\nu_f.$$

TTA in metalloporphyrins has been observed in both solution and solid-state phases.[25,27-41] In order for a fluorophore to undergo TTA, it needs to have a large S_1-T_1 energy gap to prevent back ISC to the S_1 state, and its T_1 state must be relatively long lived. Many metalloporphyrins exhibit both of these characteristics (for ZnTPP, $\Delta E(S_1\text{-}T_1) = 4015\ cm^{-1}$ and $\tau(T_1)$ has been reported to be 1.2 ms and 0.6 ms in benzene solution, and 6.86 ms in PMMA films)[42,43] making them an ideal subject for TTA study. Furthermore, the d^{10} zinc porphyrins studied in this thesis were chosen because they do not have any interfering charge transfer states between the S_1 and S_2

A)

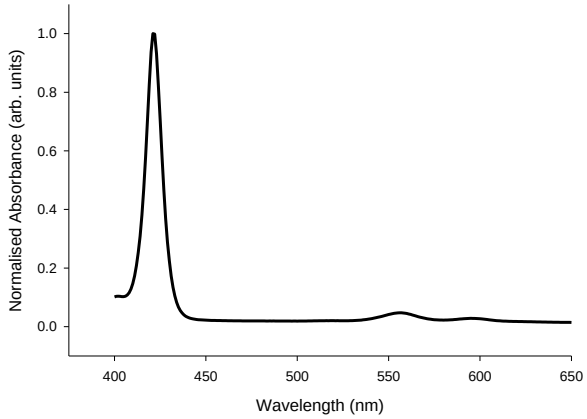

B)

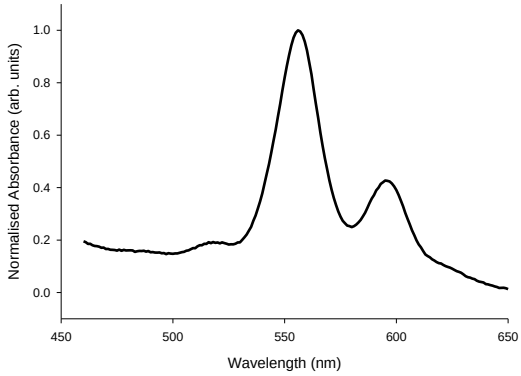

Figure 1.4 A) Normalised absorption spectrum of 1 x 10^{-5} M ZnTPPS in water displaying both the Soret (ca. 420 nm) and Q-bands (ca. 550 and 600 nm). **B)** Normalised absorption spectrum of ZnTPPS in water showing only the Q-bands. **C)** Normalised emission spectrum of 5 x 10^{-4} M ZnTPPS in water. λ_{ex} was 532 nm in order to provide a close spectral match to the excitation laser used in the microscopy and spectromicroscopy measurements discussed in Chapter 3. The Q emission spectra have not been corrected for reabsorption effects.

C)

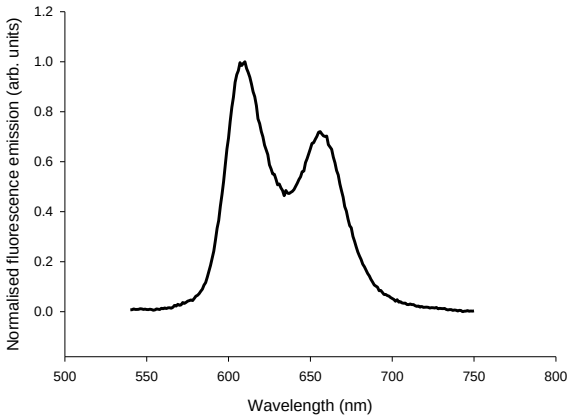

states, since Zn(II) species have filled d shells. More so, ZnTPP is so well studied that it can be considered a model compound for further spectroscopic studies.

Solar photon upconversion has been proposed as a method to improve the solar-to-electrical energy conversion efficiencies of dye-sensitized photovoltaic cells. It has been proposed that the TTA observed with metalloporphyrins in the solid state could be incorporated into DSSCs as the mechanism used to achieve photon upconversion.[25] Nonetheless, before this is done, it would be advantageous to further understand absorber aggregation in thin polymer films and on solid substrates. In this thesis, efforts to learn more about these metalloporphyrin aggregates will be described. Fluorescence anisotropy, total internal reflection fluorescence microscopy (TIRFM), and single molecule fluorescence spectroscopy were the techniques chosen to study these aggregates. Anisotropy measurements were performed to see if they would provide insight into aggregation phenomena as a function of porphyrin loading in the film. TIRFM was used to examine the homogeneity of dye in doped polymer

films by exciting the fluorophores present only at the interface of the film and glass substrate. Finally, in order to fully understand how these porphyrin aggregates form and behave, they were studied at the single molecule level using fluorescence spectroscopy and microscopy. The theory underlying these techniques will be discussed in the following sections of this chapter.

1.3 Techniques Used to Study ZnTPP Aggregates in Polymer Films

1.3.1 Fluorescence Anisotropy

Fluorophores absorb photons only when the electric field vector ($\vec{E}$) associated with the photons has a non-zero component that is parallel to the absorption transition moment of the molecule ($\vec{P}$). As such, when one employs plane polarized excitation light, only the molecules with transition moment vectors that are oriented in a favourable way ($\vec{E}$ // $\vec{P}$) will be excited. This selective excitation results in emission that is also polarized, at least initially. The extent of polarization of the emission can be measured as anisotropy, which is defined as:

$$r = \frac{I_{VV} - I_{VH}}{I_{VV} + 2I_{VH}} \qquad (1.5a)$$

In the above equation, r is the emission anisotropy. For the terms I_{VV} and I_{VH}, I signifies the emission intensity, the first subscripted letter represents the direction of polarization of the excitation light used (vertical), and the second subscripted letter stands for the direction of polarization (vertical or horizontal) of the emission collected from the sample.

Anisotropy measurements can provide information about the environment of the fluorophore in a sample, and on the relative orientations of its absorption and emission transition moments. If the emission detected is polarized, then a nonzero anisotropy is observed. However, if the emission is completely depolarized, the anisotropy falls to a value equal to zero. Depolarized emission can result from (i) non parallel absorption and emission transition moments (that is, one excites in one transition but measures the fluorescence from another transition), (ii) energy transfer and (iii) rotation of the fluorophore in the excited state prior to emission. The latter is particularly likely when studying small fluorescent molecules in solutions of low viscosity.[1]

Anisotropy measurements can be steady-state and time-resolved. For steady-state measurements, one excites a sample with continuous plane polarized light (oriented vertically, for example), and collects the sample's horizontally and vertically polarized emission through another polarizer. If this is done at various emission wavelengths, a graph of the fluorescence anisotropy versus wavelength can then be obtained using equation 1.5a.

After values for the anisotropy (r) are determined, the angle (β) between the absorption and emission transition moments in the fluorophore can be calculated using equation 1.6. In this equation r is the anisotropy observed, but it is not a result of fluorophore rotation or energy transfer.[1]

$$r = \frac{2}{5}\left(\frac{3cos^2\beta - 1}{2}\right) \tag{1.6}$$

The largest value for r is 0.40 and that corresponds to absorption and emission transition moments that are parallel. In contrast, the lowest r value is -0.20 which represents transition moments in the fluorophore that are perpendicular to one another. Of course, if β is known a priori then it can be used to solve for r.[1]

For time-resolved measurements, the sample is excited by a vertically polarized pulsed laser, and then one collects the sample's emission (both horizontally and vertically polarized) through another polarizer over the full lifetime of the fluorescent species (see Figure 1.5). Using the following equation, one can then make a plot of the fluorescence anisotropy as a function of time.[1]

$$r(t) = \frac{I_{VV}(t) - I_{VH}(t)}{I_{VV}(t) + 2I_{VH}(t)} \qquad (1.5b)$$

Fluorescence anisotropy was employed in this thesis because it can provide information on the state of ZnTPP aggregation in a sample. When these measurements are performed in the solid state (e.g. in polymer films that are doped with ZnTPP) it is unlikely that the fluorophore will rotate fast enough to cause significant depolarization of the emission over the short time (nanoseconds) of the excitation experiment. In addition, both the transition moments for the Soret and Q bands in ZnTPP are parallel, so both absorption and emission events could occur in the two different transitions and still should not cause depolarized emission.[44] As a result, if the emission detected in these samples is depolarized then it is more likely a result of energy transfer between ZnTPP molecules in an aggregate and/or between aggregates themselves during the lifetime of the excited species. Thus, if anisotropies close to zero are observed, and change as a function of porphyrin loading in the films,

then this constitutes additional evidence that ZnTPP aggregation occurs as a function of loading.

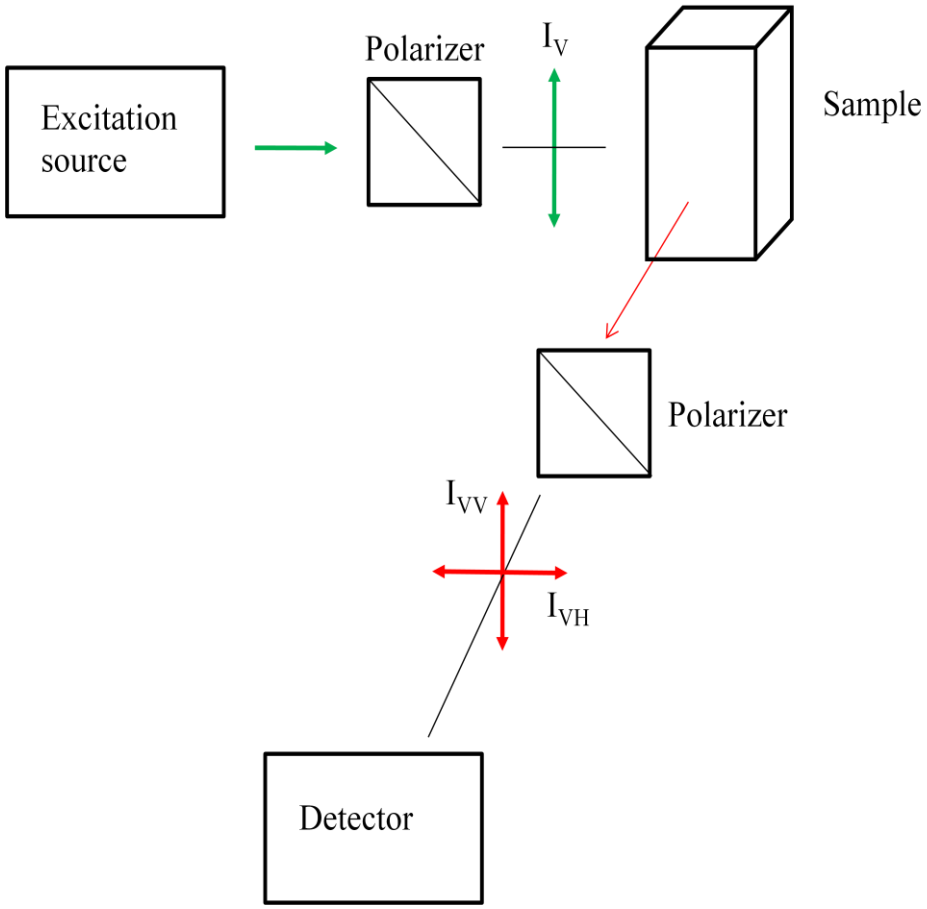

Figure 1.5 A schematic diagram showing how fluorescence anisotropy measurements are performed.

1.3.2 Total Internal Reflection Fluorescence Microscopy

Total internal reflection fluorescence microscopy (TIRFM) is a technique that can be used to study fluorophores at the interface between two media having different refractive indices (here between a glass cover slip and a ZnTPP/polymer film of lower refractive index). When the sample is excited at an angle that is greater than the critical angle (see equation 1.7), then the excitation light will be totally reflected from the sample at the interface.

$$\theta_c = \sin^{-1}\left(\frac{n_2}{n_1}\right) \qquad (1.7)$$

Here θ_c is the critical angle and n_1, n_2 are the refractive indices of the initial and final media the light travels through, respectively. At the same time, an evanescent wave is produced that excites fluorophores that are very close to the interface of the film and the glass slide (see Figure 1.6). An evanescent wave is a standing wave whose intensity decays exponentially from the boundary where it was formed into the medium of n_2, as described by equation 1.8.[45]

$$I(z) = I(0)e^{(-z/d)} \qquad (1.8)$$

$I(z)$ is the intensity of the wave as it passes a distance z through the n_2 medium, $I(0)$ is the intensity of the wave at the interface of the two media and d is the exponential decay distance represented by the following expression.

$$d = \frac{\lambda_0}{2\pi}(n_2^2 sin^2\theta - n_1^2)^{-1/2} \qquad (1.9)$$

λ_0 is the excitation wavelength in a vacuum, θ is the incident angle and n_1, n_2 were defined earlier. An evanescent wave usually penetrates less than 200 nm into the second medium, with a depth that is determined by the characteristics of the system (i.e., excitation wavelength, incident angle and refractive indices of the two media involved) being studied.[45]

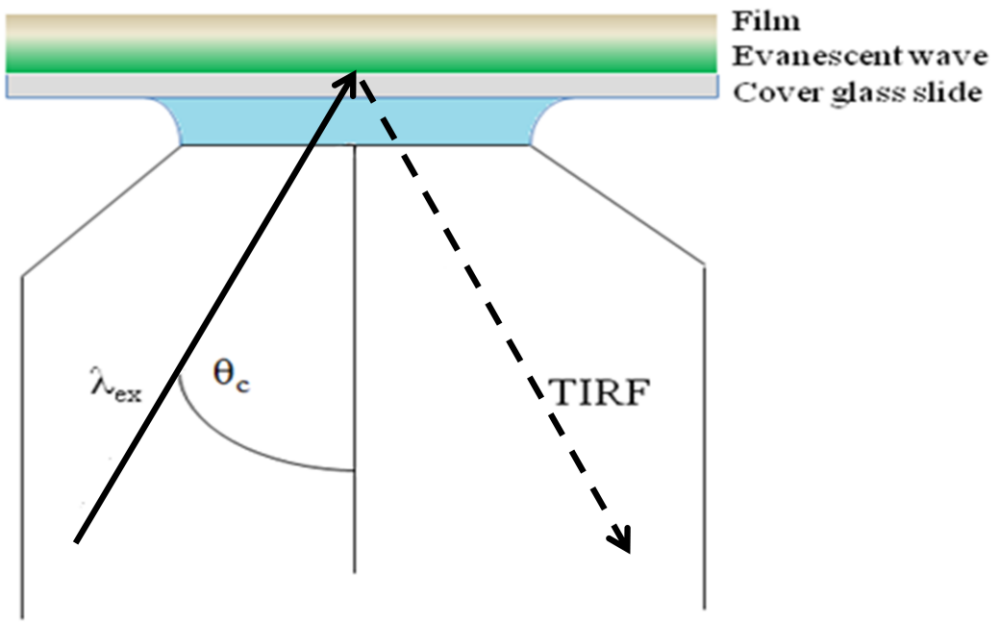

Figure 1.6 A schematic diagram illustrating TIRFM. The excitation is totally internally reflected from the glass cover slide, resulting in the penetration of an evanescent wave into the film.

The microscope configuration employed for TIRFM measurements is the same as that for epifluorescence (see section 1.4.5) except that the last mirror in the excitation path is placed on a translation stage. To perform TIRFM experiments, the translating mirror needs to be moved to ensure that the excitation is coupled through the extreme edge of the objective. In contrast, for epifluorescence measurements the mirror is moved to direct the laser beam through the center of the objective.[45]

As was stated previously, only the molecules located within the first 200 nm depth from the interface will be excited using TIRFM. Fewer molecules are being excited, which results in a decreased background signal. Thus, this technique is very sensitive (can even be used in single molecule detection experiments) and can provide information regarding the homogeneity of the porphyrin film.[45,46]

1.4 Single Molecule Fluorescence Spectroscopy

Single molecule spectroscopy (SMS) is a spectroscopic technique that enables one to study a single molecule in isolation from all but the medium in which it is fixed. Using this technique, information about the molecule of interest can be obtained that might otherwise be lost in the ensemble averaging that is observed in bulk measurements. At the single molecule level, each individual molecule may be surrounded by a slightly different environment which will affect its observed behaviour. Such behaviour, which would otherwise be obscured in a bulk measurement, can be studied using SMS. A means of optical excitation (normally a laser) induces an electronic transition of the molecule that results in the emission of detectable fluorescence. The fluorescence that is detected provides information about

the molecule being studied and its local environment. After a number of single molecules are individually excited, one can construct a frequency histogram of the distribution of values for a particular experimental parameter (fluorescence intensity, photobleaching time, etc.). While the molecule of interest is being excited, one must remember that there are also a number of solvent or host molecules surrounding it. These host molecules, along with the instrumentation itself, can be the source of noise that will significantly decrease the signal-to-noise ratio (SNR) of the measurement. As a result, it is very important to ensure that there are no fluorescent impurities in the solvent/host, and that the only molecule being excited is the one that is of interest. The latter can be achieved by exciting with a physically narrow laser beam and using a very low concentration (~10^{-9} M) of the compound being studied.[45] SMS has become more widely used in the last two decades as a result in the advancement of the necessary technology (i.e. detectors, filters, optics and microscopes).[46] At this time, many different fields use this extremely sensitive technique in their research, and it will surely become more popular as the technology for it continues to improve.

1.4.1 Background Signals

Even with repeated, sequential excitation, a single molecule does not emit high intensity fluorescence. Thus any background or noise signals need to be limited to ensure that the photons being emitted by the excited molecule are easily detected. Signal from a single molecule can be maximized in the following ways. A small probing volume must be employed to reduce any unwanted fluorescence from other molecules in the system and to limit the extent of Raman scattering. It's also important that the excitation is not at a high enough power to exceed the saturation

threshold of the molecule's absorption, and thus prevent it from absorbing any more excitation photons. As such, these extra excitation photons can then contribute unfavourably to background and noise. The molecules to be studied using SMS should also have certain characteristics, including: high photostability, a large absorption cross section, a fluorescence quantum yield close to unity, rigid structures (limits the nonradiative decay pathways and makes it more likely for the excited state to relax via fluorescence) and a low yield of triplet state formation as a result of ISC, as this prevents the absorption and emission of photons for a period of time equal to the triplet state's lifetime.[45]

1.4.2 Absorption Cross Section and Photobleaching Time of the Fluorophore

The probability that a single molecule will absorb an excitation photon is σ_p/A, where A is the cross-sectional area of the laser beam, and σ_p is the absorption cross section of the molecule. A large value for σ_p means that the photons from the laser are effectively absorbed by the molecule, maximizing the potential for observed fluorescence. It is important to maximize σ_p in order to detect single molecules. The following expression demonstrates how to determine σ_p for a randomly oriented single molecule:

$$\sigma_p = 2\pi \left(\frac{\lambda}{2\pi}\right)^2 \left(\frac{\gamma_r}{\Gamma_{tot}}\right) \tag{1.10}$$

In the above equation, λ is the wavelength of excitation, γ_r is that rate of fluorescence and Γ_{tot} is the total frequency width of the absorption.[45] One can also use equation 1.11 to calculate σ_p at ambient temperature:

$$\sigma = \frac{2.303\epsilon}{N_A} \tag{1.11}$$

where ε is the molar extinction coefficient ($Lmol^{-1}cm^{-1}$) and N_A is the Avogadro constant. Absorption cross-sections can also depend on the excitation intensity because if the absorption becomes too high, then the molecule won't be able to decay back to the ground state at a sufficiently fast rate (i.e. the transition becomes "saturated"), which will then decrease the number of excitation photons that can be absorbed.[45] Thus, it's important not to use a laser power that is too high as the excitation source can saturate the absorbers and the extra excitation photons will contribute to increased background and noise.

Photobleaching is another important consideration in single molecule measurements. The photobleaching of a molecule refers to a chemical change that prevents the molecule from being able to absorb and/or emit more photons. Many molecules studied by single molecule methods emit ca. 10^6 photons before photobleaching. Since photobleaching is often a result of photo-oxidation of the molecule, simply removing oxygen from the environment being studied can prolong the life of the fluorescing molecule.[45] One can introduce argon or nitrogen gas to the system being studied[47] or perform these measurements on samples in a vacuum.[48]

1.4.3 Signal-to-Noise Ratio

In order to obtain interpretable results in SMS it is extremely important to reduce noise and any background signals that would interfere with detecting the fluorescence. Residual fluorescence is one contributor of background signals. It can

originate from the optics and/or colored filters used in the experimental set up. Furthermore, there can be red-shifted emission from the excitation source that may be of similar energy to the fluorescence from the single molecule. Background can also arise from elastic Rayleigh scattering of the excitation photons and Raman scattering from solvent/host molecules. Scratch-free substrates, interference filters with the necessary transmission windows and ultrapure solvents need to be employed in SMS measurements to reduce these background signals.[45] It's also important to use an objective with a high numerical aperture (NA) to maximize the amount of fluorescence detected. NA is defined by the following equation:

$$NA = n \sin \theta \tag{1.12}$$

where n is the refractive index of the medium between the sample and objective and θ is the collection angle of the objective. Oil is often the medium of choice for SMS experiments due to its high refractive index (n = 1.51). Oil immersion objectives are available with a NA higher than 1.4.[45]

The SNR is critical for single molecule measurements. Most detectors, especially charge coupled device (CCD) detectors, have a constant dc offset value that occurs even in the absence of light. In addition to the offset are the dark counts from the detector, and background signals. The signal from the single molecule is then observed when the detected emission is statistically larger than the sum of the dark counts and background signals.[45] Thus, it is very important that the signal from the single molecule be significantly more intense than the background and dark levels

in order to obtain a sufficiently high SNR. The following equation can be used to calculate SNR for both confocal and wide-field microscopic configurations.

$$SNR = \frac{D\Phi_F \left(\frac{\sigma_p}{A}\right)\left(\frac{P_0}{h\nu}\right)T}{\sqrt{\left(\frac{D\Phi_F \sigma_p P_0 T}{Ah\nu}\right) + C_b P_0 T + N_d T}} \quad (1.13)$$

Here, Φ_F is the fluorescence quantum yield of the molecule of interest, A is the area of the excitation beam, T is the detector counting interval, σ_p is the absorption cross section, $P_0/h\nu$ is the number of excitation photons per second, N_d is the dark count rate and C_b is the background count rate per watt of excitation power. D is equivalent to $n_Q F_{coll} F_{opt} F_{filter}$ where n_Q is the quantum efficiency of the detector, F_{coll} is the angular collection factor of the detector, F_{opt} is a transmission factor for the optical losses and F_{filter} is the filter transmission.[45,49] This expression further illustrates the need to select a molecule with a high quantum yield and absorption cross section, and to use a small excitation spot. An intense laser will increase SNR, but again one must not exceed saturation of the optical transition. These parameters are optimized in the experimental set up in order to obtain the highest possible SNR. In order to identify the fluorescence of a single molecule, the SNR needs to be greater than one, but a value higher than this is often required.

1.4.4 CCD Detectors Used in SMS

The detectors used in SMS need to be of high quantum efficiency and sensitive enough to detect single molecule fluorescence with little dark noise. There are two classes of detectors used in SMS experiments: single-element and two-

dimensional array detectors.[45] The latter was the only type of detector used in the experiments discussed in this thesis, and it is further described in this section.

Two different CCD detectors were employed in the experiments that will be presented in this thesis. First, a Princeton Instruments back-illuminated Si CCD array with liquid-nitrogen cooled detector was used. This type of detector has a quantum efficiency of about 70 - 80% in the red and infrared.[45] This detector works at temperatures of ca. - 120 ºC as a result of cooling by liquid nitrogen,[45] a temperature at which the number of dark counts are significantly reduced. This type of CCD is often used in the recording of emission spectra from single molecules.[50-53] The second type of CCD to be discussed are electron multiplying (EMCCD) cameras (manufactured by Andor Technology and Roper Scientific). An EMCCD detector is the same as a normal CCD except that it has an added gain register that is inserted between the normal serial register and the output amplifier. In the gain register, electrons are multiplied by impact ionization. Obtaining multiplication gains in this way not only improves the overall signal, but also drastically reduces noise, because charge multiplication occurs before the output amplifier. This CCD camera also has a high quantum efficiency in the red and infrared.

1.4.5 Microscope Configurations in SMS

There are several microscope configurations that can be used to study the fluorescence emission from individual molecules. The two that were used in the studies described in this thesis are confocal and epifluorescence microscopy. Confocal microscopy utilizes a laser beam that excites a very small spot on the

sample. The diameter of the spot can be diffraction limited (approximately λ/2). In this set up, the fluorescence collected from a single molecule is passed through a pinhole that is located in the optical path after light passes through the microscope. The pinhole is employed to eliminate scattered light and, in particular, any fluorescence that did not originate from the focal plane. After the pinhole the fluorescence is directed either to a single element detector, or into a grating spectrometer that disperses the emission onto a CCD detector to obtain a fluorescence spectrum of the multiple photons emitted from a single molecule.[45] The set up will be further discussed in Chapter 3 of this thesis.

Epifluorescence microscopy is one technique for wide-field imaging of single molecules. In this technique the excitation source is used to illuminate an area of the sample that is several microns in diameter. To do this the excitation light is passed through a focusing lens before it enters the microscope. Plan Apo (apochromatic and flat field correction) objectives are ideal to use in wide-field imaging as they correct for chromatic aberration and ensure a flat field.[45] Fluorescence from the sample passes back through the objective and dichroic mirror, then through two long pass filters to remove residual fluorescence before being focused onto a CCD detector. Using this technique, multiple single fluorophores in the sample can be viewed at the same time. As a result, their fluorescence intensity and relative positions can be compared, and one can observe individual molecules photobleach as a function of time. Histograms of the distributions of fluorescence intensity and photobleaching time for the single molecules can then be prepared with

the data obtained using this technique.[45] A schematic diagram of these microscope configurations is shown in Figure 1.7.

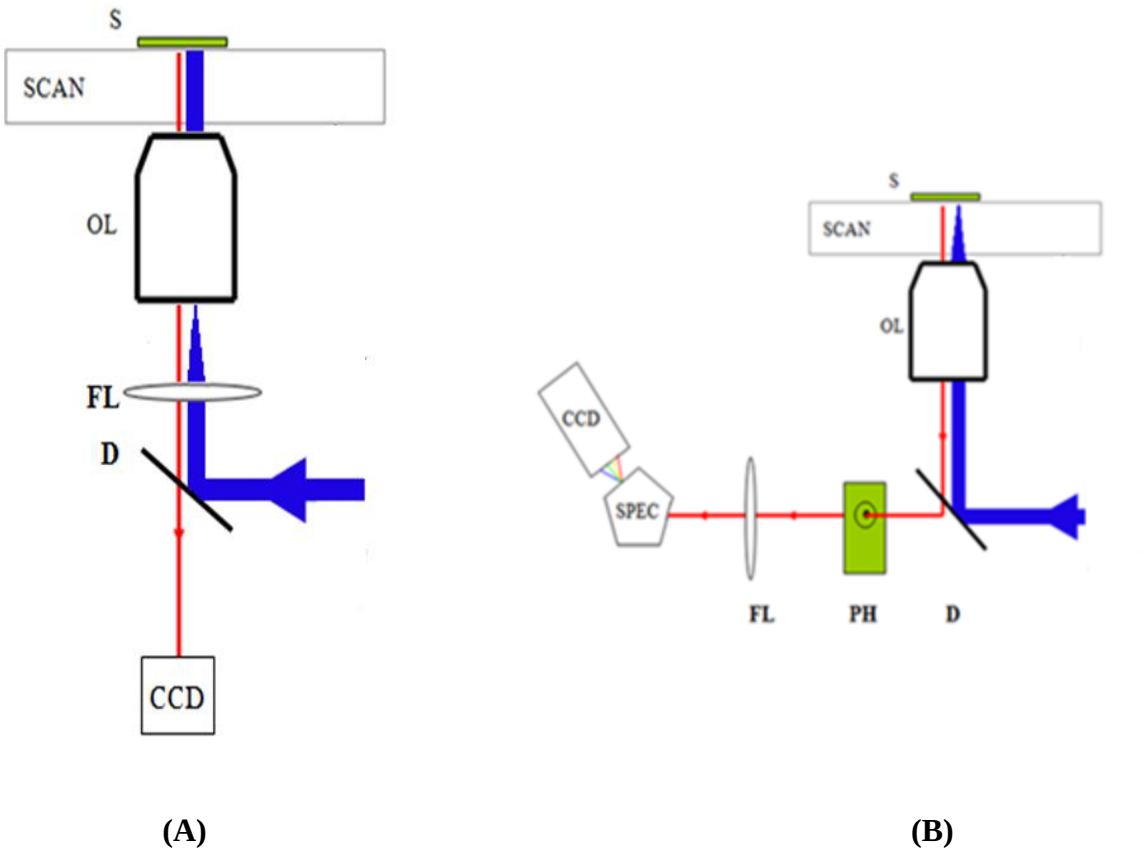

Figure 1.7 Schematic diagrams of the microscope configurations for A) epifluorescence and B) confocal microscopy. For comprehension, S = sample, SCAN = sample scan stage, OL = objective lens, FL = focusing lens, D = dichroic mirror, PH = pinhole and SPEC = spectrometer.

1.4.6 Studying Metalloporphyrins Using SMS

Metalloporphyrins are not ideal candidates for study using SMS, as they have very low quantum yields of fluorescence (for the S_1 state of ZnTPP, $\Phi_F = 2.67 \times 10^{-2}$)[17], have a high ISC yield to form dark triplet states and photodegrade in the presence of oxygen.[54] However, covalently linked porphyrin arrays have been observed by Kim et al. at the single molecule level using SMS.[13,55-59] These arrays have been studied by Kim's group as they mimic natural light harvesting systems, and can thus have a variety of applications, including being used as molecular photonic devices.

In one of Kim's publications, the emission of linked orthogonal ZnTPP arrays (consisting of n = 1 to 96 ZnTPP monomer units) was reported.[55] Using SMS, fluorescence time trajectories (plots of fluorescence intensity as a function of time) of these arrays were collected and they consisted of a series of discrete photobleaching steps (with a poor signal-to-noise ratio). Each decay in the time trajectory corresponds to the photobleaching of a single ZnTPP molecule in the array, which means that each monomer absorbs light independently. This type of fluorescence time trajectory was observed for porphyrin arrays with up to 8 ZnTPP monomers. When the system consisted of more than 8 ZnTPP monomers, more complex photobleaching behaviour was observed as a result of increased nonradiative pathways, assigned by Kim et al. to the greater nonlinearity in the structure of these longer arrays. Fluorescence emission spectra were also collected for these arrays in solution at bulk concentrations, and at the single molecule level in poly(methyl methacrylate) (PMMA) films. The emission bands for the arrays in these two

systems were in different positions, and the observed spectral shifts were attributed to the difference in the local environment of the fluorophores in the arrays.

These works published by Kim et al. focus on the study of porphyrin arrays, but they have also shown a fluorescence time trajectory for a single ZnTPP molecule.[55] Nonetheless, the signal-to-noise ratio is poor, making it difficult to be convinced that the trajectory is anything more than noise. In addition, no emission spectrum was reported for the single ZnTPP molecule sample to prove that the weak fluorescence observed was from a porphyrin. To the best of our knowledge, no one else has reported the detection of single metalloporphyrin molecules. Even though Kim's reports are preliminary, they do suggest that it might be possible to use SMS to study individual ZnTPP molecules, despite their unfavourable characteristics to be detected using this technique.

1.5 Motivation for This Project

In order to potentially use TTA as a mechanism of photon upconversion in DSSCs, it is important to further understand the role of absorber aggregation in controlling TTA efficiencies and energy transfer in and between ZnTPP aggregates. Fluorescence anisotropy and TIRFM techniques can be employed to learn more about ZnTPP aggregation in these films. It is also advantageous to understand how a single ZnTPP (or ZnTPPS) molecule behaves compared to the aggregated form. More information about the environment surrounding the fluorophore can be obtained at the single molecule level because the ensemble averaging present in bulk measurements is absent. Thus, the focus of this project is to study ZnTPP/ZnTPPS in the solid state

to gain further information regarding the formation of their aggregates and their behaviour at the single molecule level. The object is to gain more insight concerning the use of such a system in a DSSC to improve its overall solar-to-electrical energy conversion efficiency and to make its production and use more affordable.

Chapter 2: Bulk ZnTPP Fluorescence Spectroscopy Measurements

Two types of bulk fluorescence experiments were performed: fluorescence anisotropy (time-resolved and steady-state) and total internal reflection fluorescence microscopy (TIRFM). Both the experimental details and results for these experiments are described in this chapter.

2.1 Materials Investigated

Meso-tetraphenylporphine zinc, ZnTPP, was purchased from Porphyrin Systems. Poly(methyl methacrylate), PMMA, (MW = 75 000, 200 micron beads) was bought from Polysciences Inc. Toluene was used as the solvent in these experiments. Sigma-Aldrich, ≥ 99.5% ACS spectrophotometric grade was the type used for fluorescence anisotropy and most TIRFM measurements. AnalaR, Merck, Minimum assay 99.5% was used in the time-resolved TIRFM measurements. All chemicals were used as received.

2.2 Sample Preparation and Instrumentation

2.2.1 Fluorescence Anisotropy

2.2.1.1 Time-Resolved Fluorescence Anisotropy

Three solutions of different ZnTPP concentrations (10%, 3.3% and 1.5% by mass ZnTPP) were prepared by mixing various volumes of 1 mM ZnTPP in toluene, and 2% PMMA in toluene (m/v). For each concentration of ZnTPP, three different films were prepared (1, 3 and 10 layers) using a spin casting technique. For each layer, 120 μL of solution was added to a clean microscope coverglass slide (22 mm x

22 mm, VWR), which was then spin coated for 1 minute at 1000 rpm using a Laurell Technologies Corporation Spin Coater Model WS-400BX-6NPP1LITE.

These measurements were performed using a cavity dumped, mode-locked Titanium:Sapphire laser (Coherent Mira 900, 76 MHz rep rate) that was pumped by a solid state laser (Coherent Verdi V10). Its 800 nm output was frequency doubled using a BBO single crystal (INRAD, 561-044, TSS 28.7º) to 400 nm. The light was then passed through a polarizer (Broadband Rhomb polarization rotator) to ensure that the excitation light was vertically polarized. The excitation light was then directed to the sample, whose emission, in both the vertical and horizontal directions, was collected through another polarizer (Polaroid HNP'B). Under normal circumstances, the emission would be passed through a monochromator before it reaches the detector. For these measurements, however, the monochromator was removed and replaced by a 570 nm long pass filter. The reason for doing this is due to the detector's decreased efficiency in the red region of the spectrum. Q band emission from ZnTPP is in the red, and as a result more counts were obtained when the long pass filter was used than when the monochromator was in place. Finally, the emission was detected by a multichannel plate photomultiplier detector (Edinburgh Instruments TCC900 with an Eldy EM132-1 microchannel plate photomultiplier). CMCA software was used when collecting data and SPC decay fit software was used after data collection.

2.2.1.2 Steady-State Fluorescence Anisotropy

The thin PMMA films doped with ZnTPP were prepared in the same manner as described above for the time-resolved fluorescence anisotropy measurements. To perform steady-state fluorescence anisotropy measurements, two polarizers (Cary Eclipse manual polarizer accessory) were introduced into a Varian Cary Eclipse Fluorescence Spectrophotometer. One was placed in the path of the excitation beam to ensure only vertically polarized light excited the sample. The other polarizer was used to collect both the horizontally and vertically polarized emission from the sample. For these measurements, the samples were excited in both the Soret band (420nm) and in the Q band (550nm), and the anisotropy values obtained from the different excitation wavelengths were compared.

2.2.2 Total Internal Reflection Fluorescence Microscopy (TIRFM)

Films were prepared in the same way as described above for the fluorescence anisotropy experiments (this time on circular microscope coverglass slides), but for each concentration of ZnTPP, only one layer was deposited. In addition, a 1 μM ZnTPP solution in toluene was prepared and from that dilutions were performed with 1% PMMA in toluene (m/v) to make 10^{-7} M and 1 nM ZnTPP solutions. Single layer films were prepared from these solutions using the same spin casting technique as described above. It is important to note, however, that with the 1 μM ZnTPP solution, 1 layer of 1% PMMA in toluene (m/v) was spin coated followed by an additional layer from the 1 μM ZnTPP solution. For time-resolved TIRFM

experiments, films were prepared from a solution of 4 μM ZnTPP in toluene. Once again, for these films, the first layer was PMMA and the second contained the dye.

For these measurements a Nikon ECLIPSE TE2000-U microscope was used. A 408 nm cw Coherent argon ion laser (Coherent Radius 405) was used as the excitation source when images of the sample were obtained. In contrast, for the time-resolved TIRFM experiments the Ti:Sapphire laser described above was used and frequency doubled to provide an output of 400 nm. A fibre optic was used in both cases to deliver the excitation light to the microscope and through the Plan Apo TIRF 60x/1.45 oil immersion objective lens to excite the sample. For the preliminary images obtained, the sample's emission was collected using a Nikon Digital Camera (CoolPix 4500). For the more detailed images an EMCCD was used as the detector (Princeton Instruments Acton, Photon Max 1024). In addition, for the time resolved TIRFM experiments, a fast-gating intensified CCD (LaVision PicoStar HR12 Imager QE) was used as a detector.

2.3 Results and Discussion

2.3.1 Fluorescence Anisotropy

Absorber aggregation is an important phenomenon to further understand because it can provide insight on how to improve the efficiency of TTA for use in DSSCs. As was previously described in section 1.3.1, fluorescence anisotropy measurements can provide information regarding ZnTPP's environment in the film from the extent of emission polarization. Depolarized emission could be a result of three different processes, briefly: (i) fluorophore rotation in the excited state, (ii) non

parallel absorption and emission transition moments and (iii) energy transfer. It is unlikely that ZnTPP would rotate significantly in the film over the short time (ns) of the excitation experiment. Small molecules rotate rapidly in fluid solution, on a timescale of 40 ps or less, whereas protein molecules (larger molecules with molecular weights around 25kDa) take ca. 10 ns to rotate under the same conditions.[1] Rotational times are directly proportional to a molecule's moment of inertia (i.e. the greater the moment of inertia, the more time it takes for the molecule to rotate), and to the viscosity of the medium the molecule is in. ZnTPP is not a small molecule, but it's also not as large as a protein, and thus its rotational time would be in the range described above (i.e. most likely ca. hundreds of picoseconds in solution). The viscosities of polymers are on the order of 10^4 to 10^7 Pa.s, which are 10^7 to 10^{10} times larger than that of water.[60] Thus, when ZnTPP is studied in a solid, polymer medium, the rotational time will be dramatically increased, which would not allow the molecule to rotate over the short time (a few ns) of the experiment. In addition, it is known that both the Soret and Q bands transition moments are in the same plane,[44] and thus depolarized emission as a result of (ii) is doubtful. Thus, if depolarized emission is detected it is most likely a result of energy transfer between ZnTPP molecules in close proximity (i.e. in an aggregate). Both time-resolved and steady state anisotropy measurements were performed to determine if ZnTPP's fluorescence was depolarized, and the results will be described in the following sections.

2.3.1.1 Time-Resolved Fluorescence Anisotropy

Initially the fluorescence anisotropy for polymer films doped with three different ZnTPP concentrations (and for each concentration, three different conditions

with respect to the number of layers) was investigated using time-resolved anisotropy. The first observation made in these experiments was a rapid decay in the intensity of the sample's emission as the concentration of ZnTPP in the film increased (See Figure 2.1). Presumably this rapid decay is due to the formation of aggregates in the film which would be responsible for quenching the sample's fluorescence.[25] Lifetimes were calculated for the decays and they were noticeably shorter in the films more concentrated with ZnTPP. The lifetimes for the 1.5%, 3.3% and 10% by mass ZnTPP samples (10 layers) where the emission was vertically (i.e. I_{VV}) and horizontally (i.e. I_{VH}) polarized were calculated and are shown in the following table.

Emission	**τ for 1.5% by mass ZnTPP in PMMA film (ns)**	**τ for 3.3% by mass ZnTPP in PMMA film (ns)**	**τ for 10% by mass ZnTPP in PMMAfilm (ns)**
I_{VV}	1.78	1.29	0.63
I_{VH}	1.86	1.35	0.66

Table 2.1 Lifetimes calculated from the fluorescence intensity decays for 1.5%, 3.3% and 10% by mass ZnTPP (10 layers) in PMMA films. The lifetime was calculated for both the vertically (I_{VV}) and horizontally (I_{VH}) polarized emission. See Figures A.1-A.6 for fluorescence decays and their best single exponential fit.

These lifetimes clearly get shorter as the concentration of ZnTPP in the film increases. At higher ZnTPP concentrations, the formation of aggregates will be greater, resulting in more intermolecular interactions that will decrease the amount of fluorescence that is emitted. The lifetimes calculated for both horizontally and vertically polarized emission were similar for the samples with the same concentration of dye. The lifetimes measured for the most dilute film are the ones most consistent with that measured for ZnTPP in dilute ethanol solutions (τ = 1.96 ns for the S_1 excited state).[17] The decays for the 10 layer films at the three different ZnTPP concentrations are shown below.

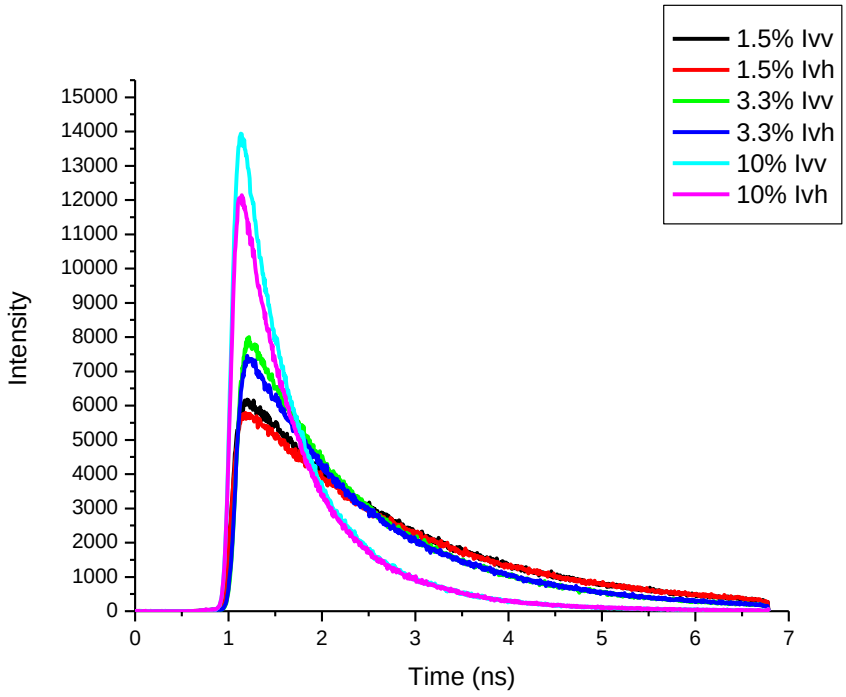

Figure 2.1 Fluorescence decay curves of 10 layer films of various ZnTPP concentrations in PMMA. λ_{ex} = 400 nm (pulsed), 120 μW (average power).

One should also note that the I_{VV} decays are slightly more intense than the I_{VH} decays. This is a result of the emission polarizer and/or emission monochromator being more efficient at passing vertically polarized light than horizontally polarized light.[1] To correct for this, one must calculate the G-factor, whose value is dependent on the emission wavelength using the following equation.

$$G = \frac{I_{HV}}{I_{HH}} \tag{2.1}$$

Thus, a sample is excited with horizontally polarized light and both the vertically and horizontally polarized emission intensities are measured, using the maximum counts for each condition to calculate G. If G = 1 than that means that both vertically and horizontally polarized light are passed through the system with the same efficiency. However, if G is not equal to 1 the detection system is sensitive to one more than the other. For all measurements G must be calculated, and if it is not equal to 1 it must be incorporated into the anisotropy equation as follows.

$$r(t) = \frac{I_{VV}(t) - GI_{VH}(t)}{I_{VV}(t) + 2GI_{VH}(t)} \tag{2.2}$$

For all anisotropy measurements described in this thesis, G was calculated as described above and its value was taken into account in subsequent calculations.

From the decays in Figure 2.1, the fluorescence anisotropy was calculated using equation 1.5b, and plotted as function of time. It should also be noted that in these experiments the emission polarizer was manually switched between collecting the horizontally and vertically polarized fluorescence for each separate sample. When these measurements were repeated again (as discussed later in this section), the

emission polarizer automatically switched between these two positions by computer control.

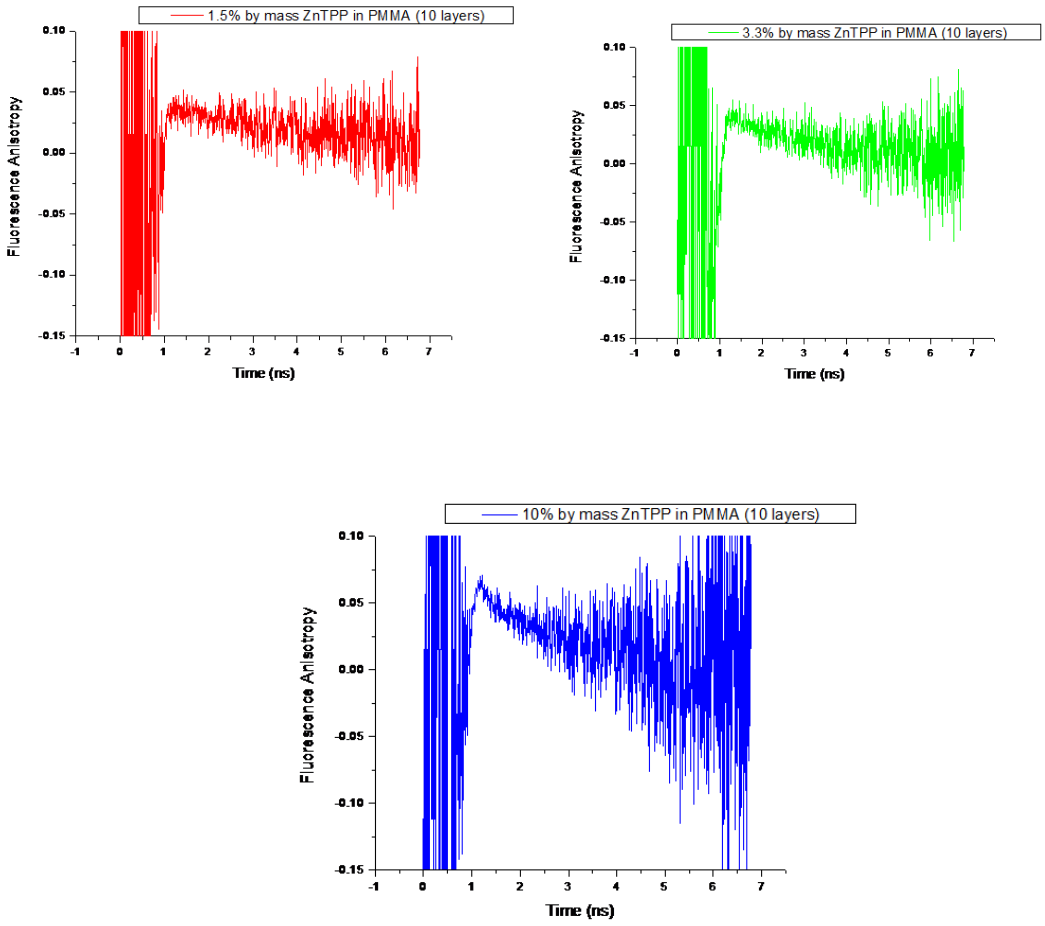

Figure 2.2 A plot of fluorescence anisotropy as a function of time for 10 layered films at three different ZnTPP concentrations in PMMA. λ_{ex} = 400 nm (pulsed), 120 μW (average power).

The anisotropy data above is noisy due to the small differences in intensity between the vertically and horizontally polarized fluorescence. When calculating these anisotropies, one is always taking the small difference between two large numbers, resulting in small anisotropy values and noisy decays as a function of time.

The time-resolved fluorescence anisotropy measurements were repeated (see below) using the emission polarizer that automatically switched between collecting vertically and horizontally polarized fluorescence. Different samples were used in these measurements, but they were prepared in the same way as the samples used for the first anisotropy measurements.

Once again, the decays look similar to the ones described earlier in that the more concentrated ZnTPP films decay faster than the other films. In addition, the lifetimes calculated from these decays showed the same trend as was observed in the previous data. The lifetimes for the samples consisting of 1.5%, 3.3% and 10% by mass ZnTPP for the decays of the vertically and horizontally polarized emission were calculated and are shown in Table 2.2.

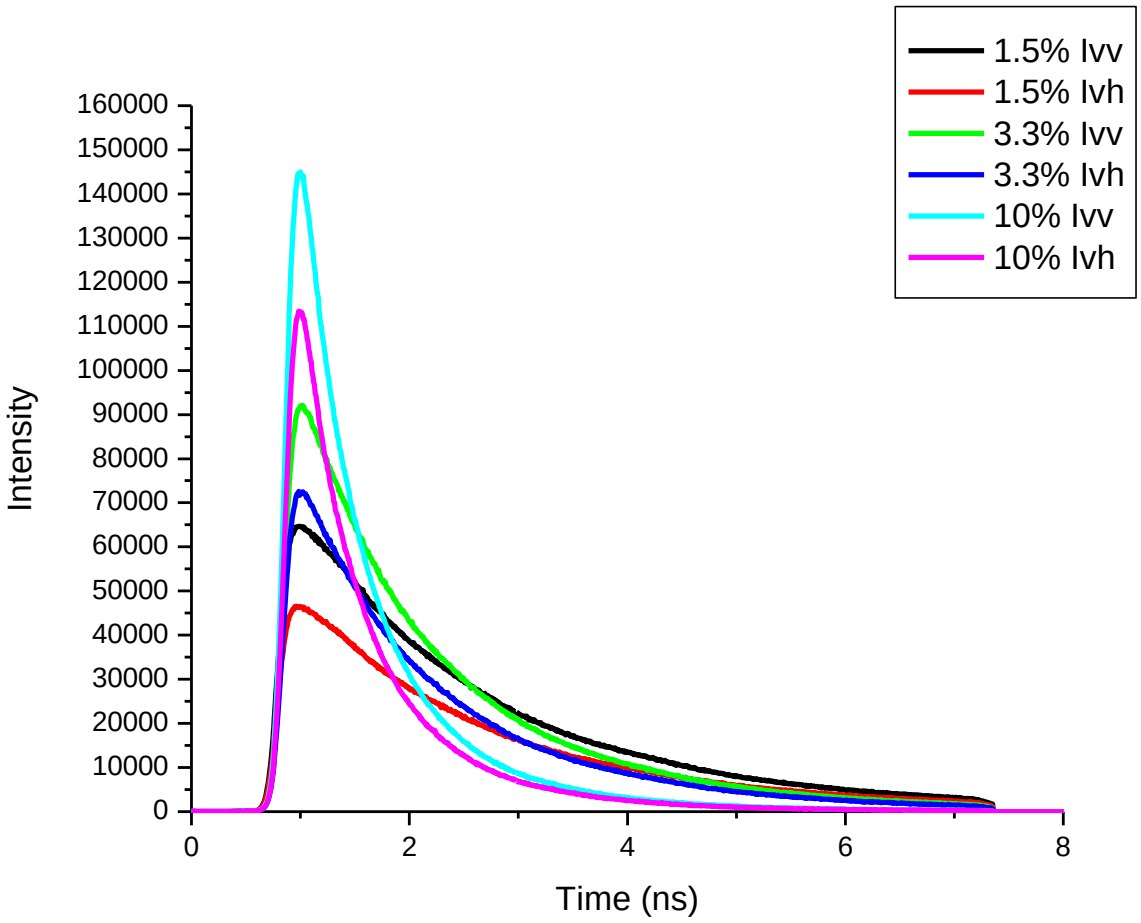

Figure 2.3 Fluorescence decay curves of 10 layer films of various ZnTPP concentrations in PMMA. λ_{ex} = 400 nm (pulsed), 140 μW (average power).

Emission	τ for 1.5% by mass ZnTPP in PMMA film (ns)	τ for 3.3% by mass ZnTPP in PMMA film (ns)	τ for 10% by mass ZnTPP in PMMAfilm (ns)
$\mathbf{I_{VV}}$	1.91	1.37	0.65
$\mathbf{I_{VH}}$	1.92	1.35	0.65

Table 2.2 Lifetimes calculated from the fluorescence intensity decays for 1.5%, 3.3% and 10% by mass ZnTPP in PMMA films. The lifetime was calculated for both the vertically (I_{VV}) and horizontally (I_{VH}) polarized emission. See Figures A.7-A.12 for fluorescence decays and their best single exponential fit.

From these decays, the anisotropy was calculated and plotted as a function of time.

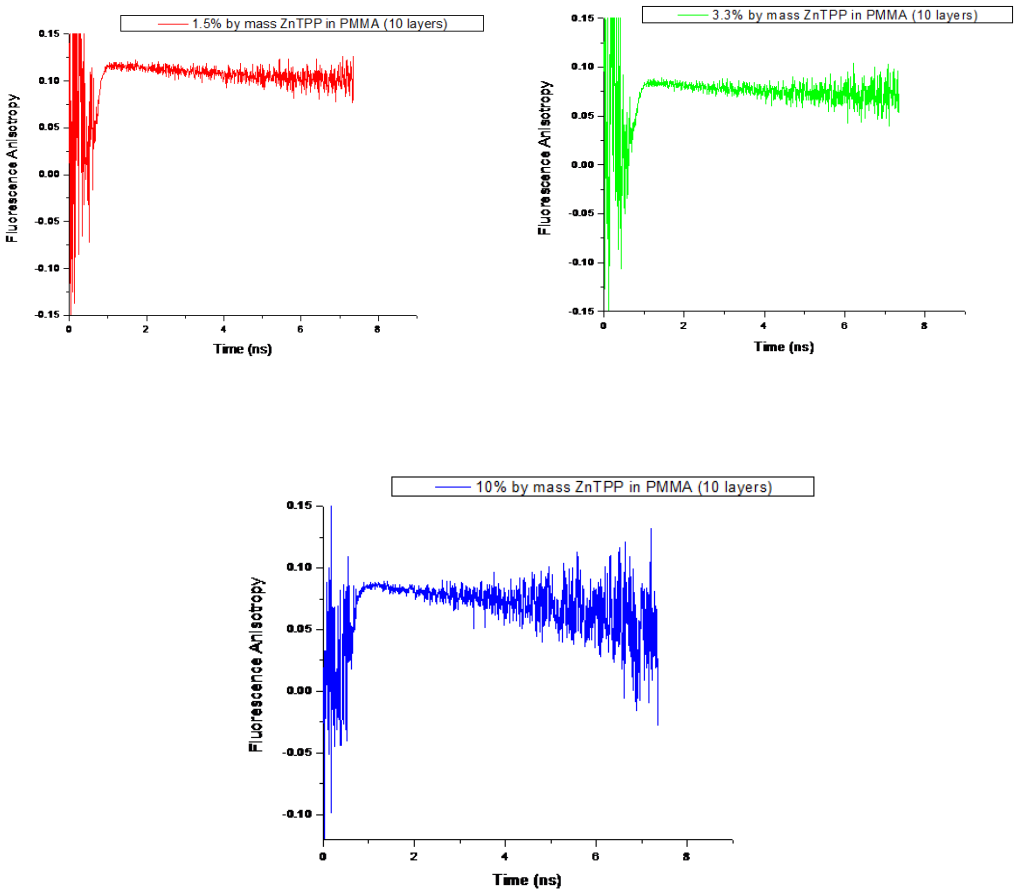

Figure 2.4 Fluorescence anisotropy as a function of time for various concentrated ZnTPP 10 layered films in PMMA. λ_{ex} = 400 nm (pulsed), 140 μW (average power).

Based on the anisotropy data from the first experiment, it appears that the emission is being depolarized at all concentrations of ZnTPP in the films. When the experiment was repeated, however, the results were not reproducible. In fact, in the repeated experiment, the emission only looked depolarized in the film with the highest ZnTPP concentration. Since the anisotropy decays are less noisy when the

experiment was repeated, we believe that these data are more reliable. The depolarization observed is most likely a result of energy transfer in an aggregate of ZnTPP molecules, or between different aggregates. This is supported by the facts that (i) the fluorescence decay times decrease with increasing ZnTPP concentration (due to more interactions between ZnTPP molecules) and (ii) the greatest time-dependent fluorescence anisotropy is found in the most concentrated samples where aggregation will be greatest, and thus where there will be more opportunities for energy transfer between ZnTPP molecules in close proximity. To ensure that photophysics (i.e. exciting in the Soret band, and observing the emission from the Q bands) was not responsible for the depolarization of the emission, steady-state fluorescence anisotropy measurements were performed where the fluorophore was excited both in the Soret and in the Q bands. These measurements will be discussed in the next section.

2.3.1.2 Steady-State Fluorescence Anisotropy

Steady-state fluorescence anisotropy measurements were performed to determine if the emission depolarization observed in Figures 2.2 and 2.4 was a result of intramolecular photophysics, i.e. due to a change in direction of the transition dipole moment associated with the radiationless transition from S_2 to S_1. In the time-resolved experiments the sample was excited into the Soret band, and the fluorescence was measured from the Q bands. The concern here is that the depolarization observed might be a result of exciting the fluorophore into one band and observing the emission from another. Thus, steady-state fluorescence anisotropy measurements were performed on the same films that were studied using the time-

resolved approach (i.e. for the very first experiment of this kind), and the plots of anisotropy as a function of wavelength were compared for the two different wavelengths of excitation (420 nm in the Soret band and 550 nm in the Q band). The plots for 10% by mass ZnTPP in PMMA films (10 layers) are shown in Figure 2.5.

After inspecting the plots in Figure 2.5, one can see that the anisotropy values at the wavelengths of the Q bands (600 and 650 nm) are similar for both excitation wavelengths. This indicates that the depolarization observed previously was unlikely due to a change in direction of the transition dipole moment following S_2-S_1 decay. This result was somewhat expected as it has been previously reported that these transition moments are in the same plane,[44] and, as such, further suggests that the emission depolarization observed is caused by electronic energy transfer between, and among, aggregated ZnTPP molecules. It is not known yet how the ZnTPP molecules are oriented with respect to each other in the aggregate, however, it is most likely that the molecular planes are somewhat variable, and thus not just coplanar (H-type aggregate) or stacked like a deck of cards (J-type aggregate). One can distinguish between these two types of aggregates by measuring a UV-vis spectrum. If a blue-shift is observed then that is a result of the formation of H-aggregates, whereas J-aggregates are responsible for a red-shift in the spectrum.[61] The absorption spectra of these films have been previously measured, but no significant red or blue-shift was observed.[25] The width of the bands increased, however, as the concentration of ZnTPP increased. This is further spectroscopic evidence of ZnTPP aggregation. Nonetheless, the conclusions that can be made from these fluorescence anisotropy experiments are that porphyrin aggregation in thin polymer films is

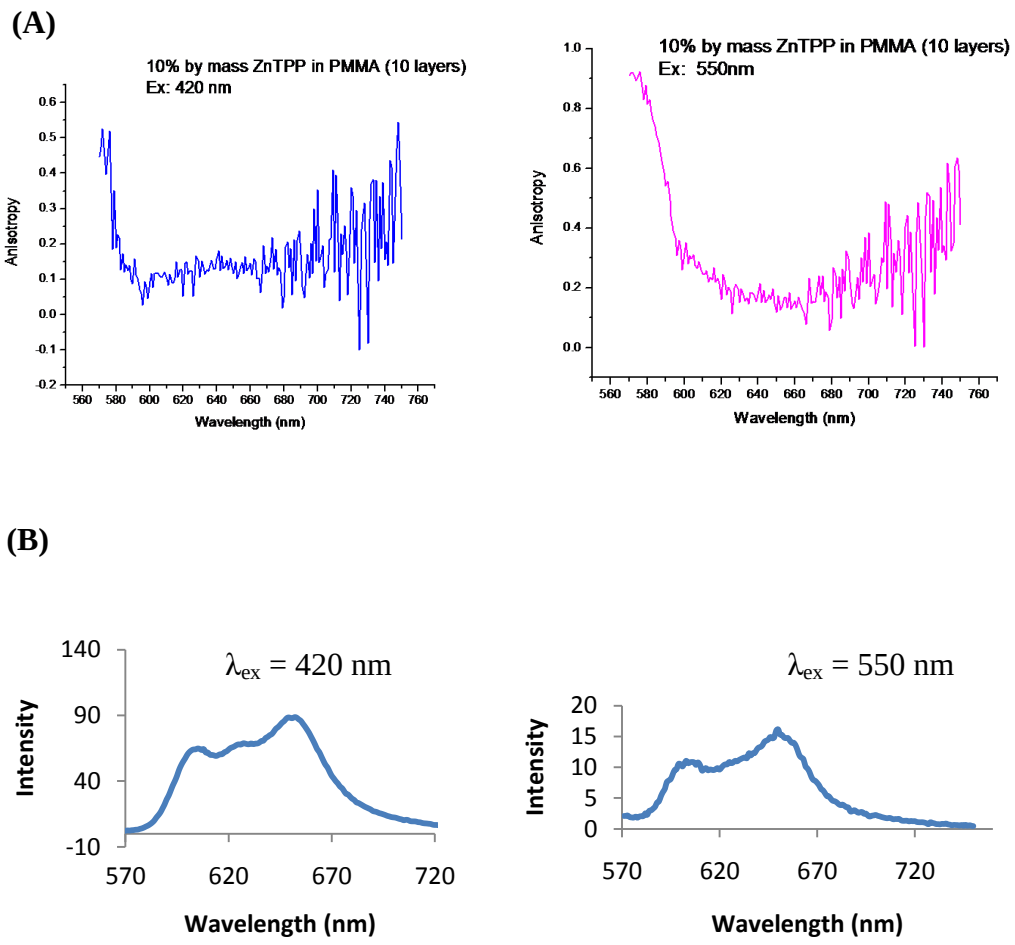

Figure 2.5 (A) Plots of anisotropy as a function of wavelength for a 10% by mass ZnTPP in PMMA film (10 layers) when excited with 420 nm and 550 nm light. **(B)** Emission spectra collected for the same film when excited with 420 nm and 550 nm light. The anisotropy observed at wavelengths less than 580 nm is an artefact, as there is no net ZnTPP fluorescence at those wavelengths.

extensive, as are the interactions between ZnTPP molecules in an aggregate and those among different aggregates.

2.3.2 Total Internal Reflection Fluorescence Microscopy (TIRFM)

Total internal reflection fluorescence microscopy (TIRFM) was another technique employed to study ZnTPP aggregation in PMMA films. This technique can provide information on the structure of the film (i.e. homogeneity of fluorophore distribution) by exciting the ZnTPP molecules that are present only at the interface of the doped polymer film and the glass substrate. The theory of this technique was described in detail in section 1.3.2. Briefly, it involves exciting the sample at an angle greater than the critical angle, resulting in total internal reflection of the excitation light and the penetration of an evanescent wave into the first 100 nm or so of the film. This evanescent wave is responsible for exciting the fluorophores it interacts with, and their detected fluorescence allows the structure of the film to be studied. It is important to know whether these films are homogeneous, as this will clarify their applications. In a DSSC, for instance, a homogeneous film is desired to ensure that a fluorophore in the film is always being probed by optical excitation, regardless of where the light is focussed on the sample. If the dye is not excited it prevents the subsequent steps to convert solar energy to electricity from taking place. This would interfere with the working DSSC and affect its efficiency, which is undoubtedly a problem.

Initially, single layer films having the same concentrations of ZnTPP in PMMA that were used in the anisotropy measurements were studied. A Nikon digital

camera was used as the detector, but unfortunately it was not sensitive enough to collect images that showed any structure. Instead only the red emission from S_1 that is expected was observed. Non-TIRFM images were also collected, and for these it was not just the first 100 nm (or so) of the film being excited.

TIRFM

Non-TIRFM

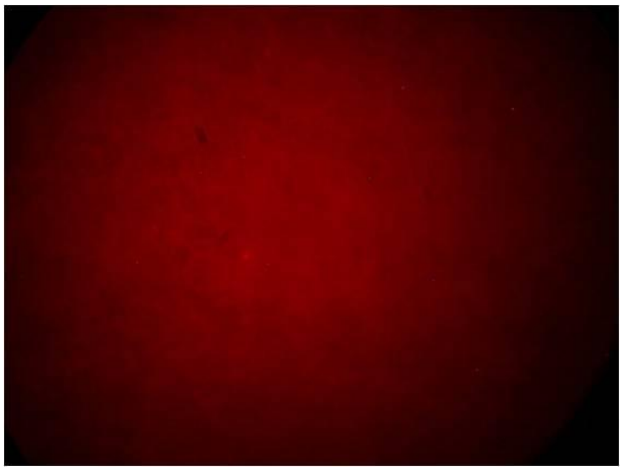

Figure 2.6 TIRFM and non-TIRFM Images collected on the same segment of the sample using a Nikon camera for a 10% by mass ZnTPP in PMMA film (1 layer). λ_{ex} = 408 nm (cw), at a power of 0.1 mW.

These initial survey experiments showed that the concentration of ZnTPP in the film would need to be decreased and a more sensitive detector would need to be used if any structure in the film was to be observed. The following images were therefore collected using an EMCCD camera.

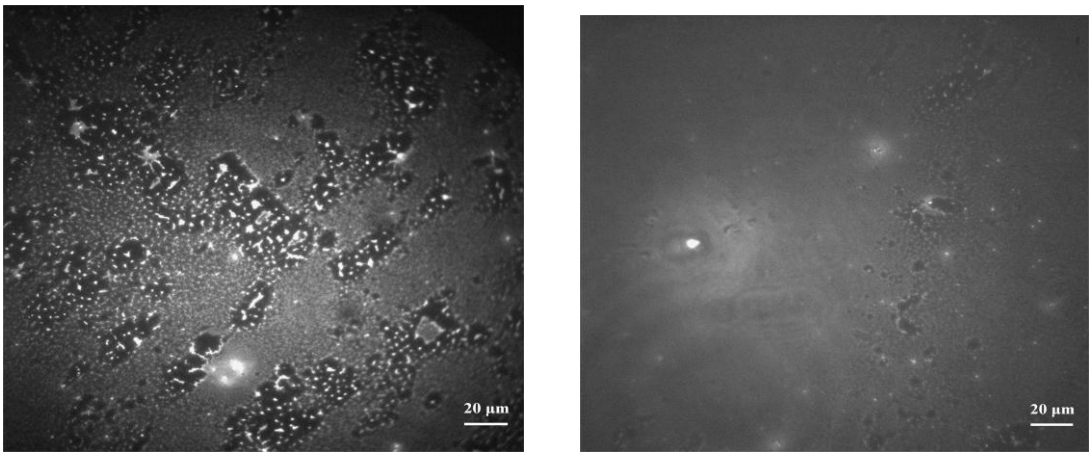

TIRFM Non-TIRFM

Figure 2.7 TIRFM and non-TIRFM images collected on the same segment of the sample using an EMCCD camera for a 1 µM ZnTPP in PMMA film (1 layer). λ_{ex} = 408 nm (cw), at a power of 0.1 mW.

The above TIRFM image clearly shows that these films are not homogeneous. A variety of structures are observed at the film-substrate interface, including aggregates. When the whole film is excited (see non-TIRFM image above), similar

structures are observed, albeit the TIRFM image more clearly illustrates such structures, because background signals are minimized as fewer molecules are being excited. The collection of these images provides evidence that ZnTPP is not distributed homogeneously in the PMMA film, but rather accumulates in different areas of the polymer and forms aggregates.

Using the same detector, films were prepared with a decreased concentration of ZnTPP in PMMA. For these dilute ZnTPP concentrations there was not much difference between the TIRFM and non-TIRFM images. Samples consisted of uniform films with a few bright spots, possibly assignable to single molecules or small aggregates. One example is shown below.

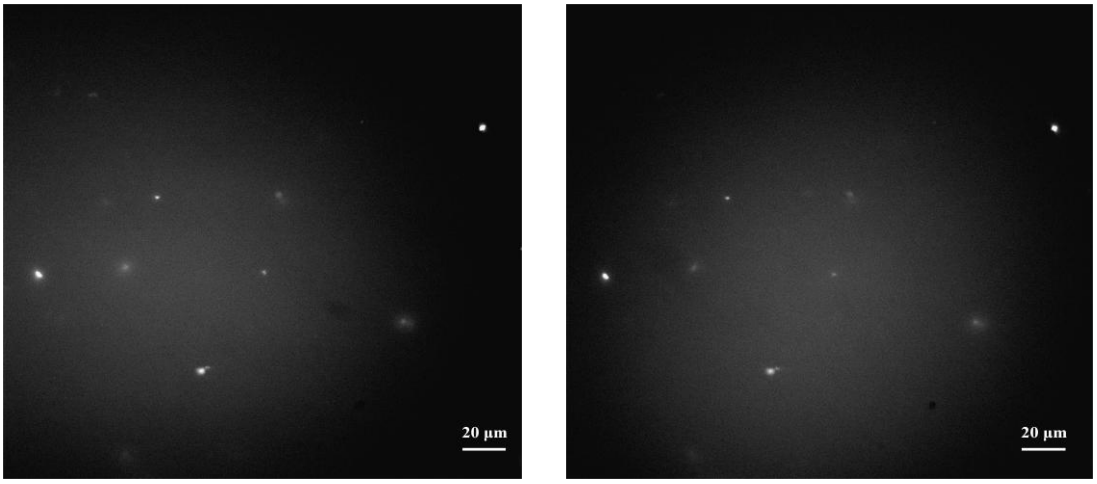

TIRFM Non-TIRFM

Figure 2.8 TIRFM and non-TIRFM images collected on the same segment of the sample using an EMCCD camera for a 10^{-7} M ZnTPP in PMMA film (1 layer). λ_{ex} = 408 nm (cw), at a power of 0.1 mW.

By using a fast-gated, intensified CCD (ICCD) camera, time-resolved TIRFM images could be collected and used to obtain fluorescence lifetime information about the samples. Briefly, an ICCD consists of a photocathode, a microchannel plate and a phosphor screen. Photons are first detected by the photocathode which produces electrons that are intensified by the microchannel plate. The electrons are then directed towards the phosphor screen where photons are generated and then focused onto the CCD chip. The ICCD is similar to the EMCCD in that, for both, charge multiplication occurs before the output amplifier which helps in reducing noise.

Samples of 1.6 μM and 4 μM ZnTPP in PMMA films were measured using this time-resolved TIRFM approach. Plots of the decay in emission intensity as a function of time for various spots on the sample were produced. Three different areas were measured. A fluorescence decay curve was produced for the whole sample, for a small area on the film where aggregates were suspected to be located and for an area where no aggregates would be found. Figure 2.9 shows four images that, when compiled with many others, can generate a video showing how the fluorescence intensity of the sample changes over time. Data can be extracted from the images in a video (see Figure 2.10 and 2.11) to develop a fluorescence intensity decay curve. The images in these experiments were collected every 200 ps. These measurements had a time resolution of 60 ps and the full-width at half maximum (FWHM) of the excitation pulse of the laser was 120 fs.

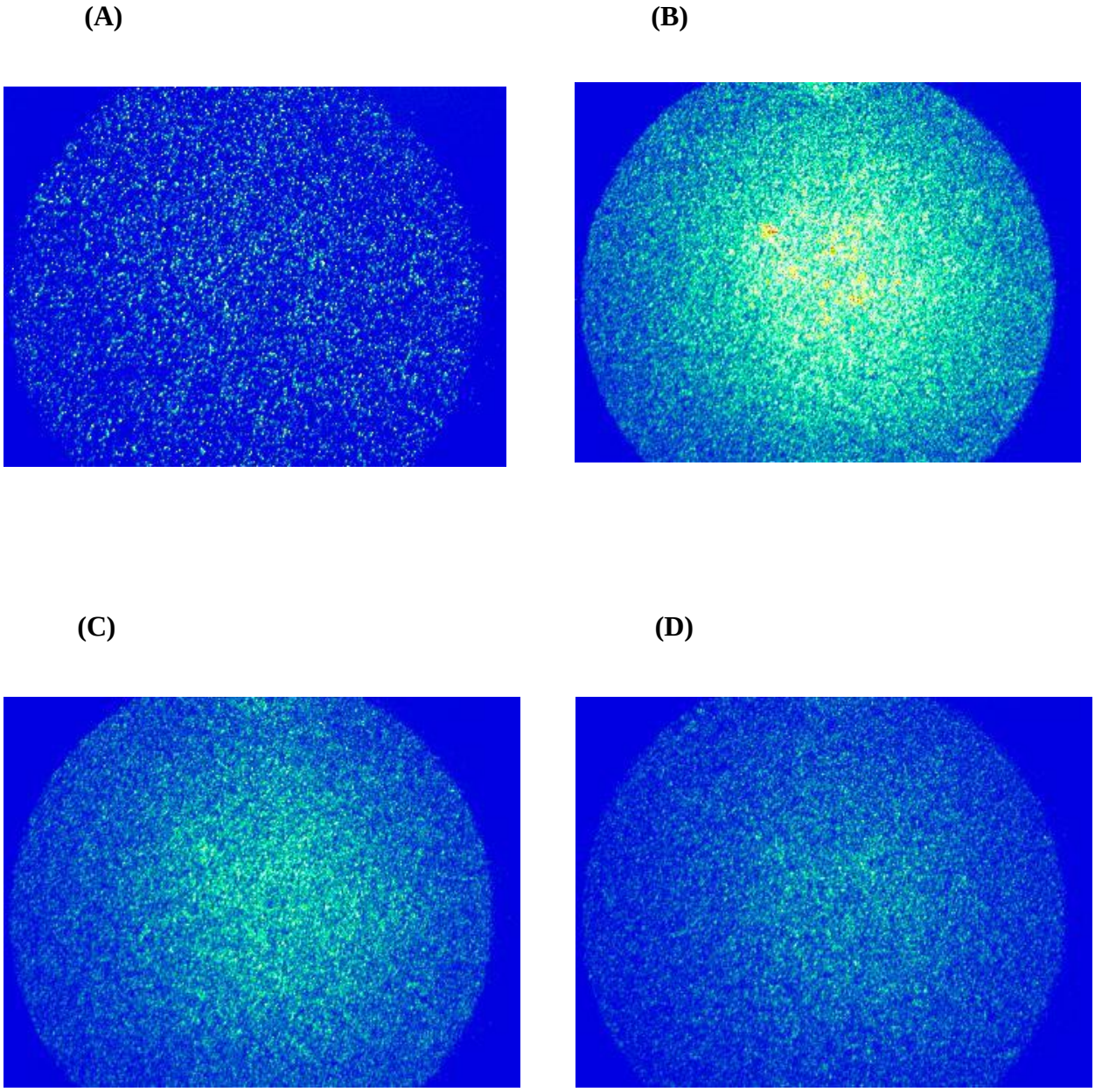

Figure 2.9 Images of a PMMA film doped with 4 μM ZnTPP collected A) 0.2, B) 2.4, C) 3.6 and D) 4.4 ns after excitation with a 400 nm, pulsed laser, with an average power of 0.4 mW. These measurements were performed in TIRFM mode.

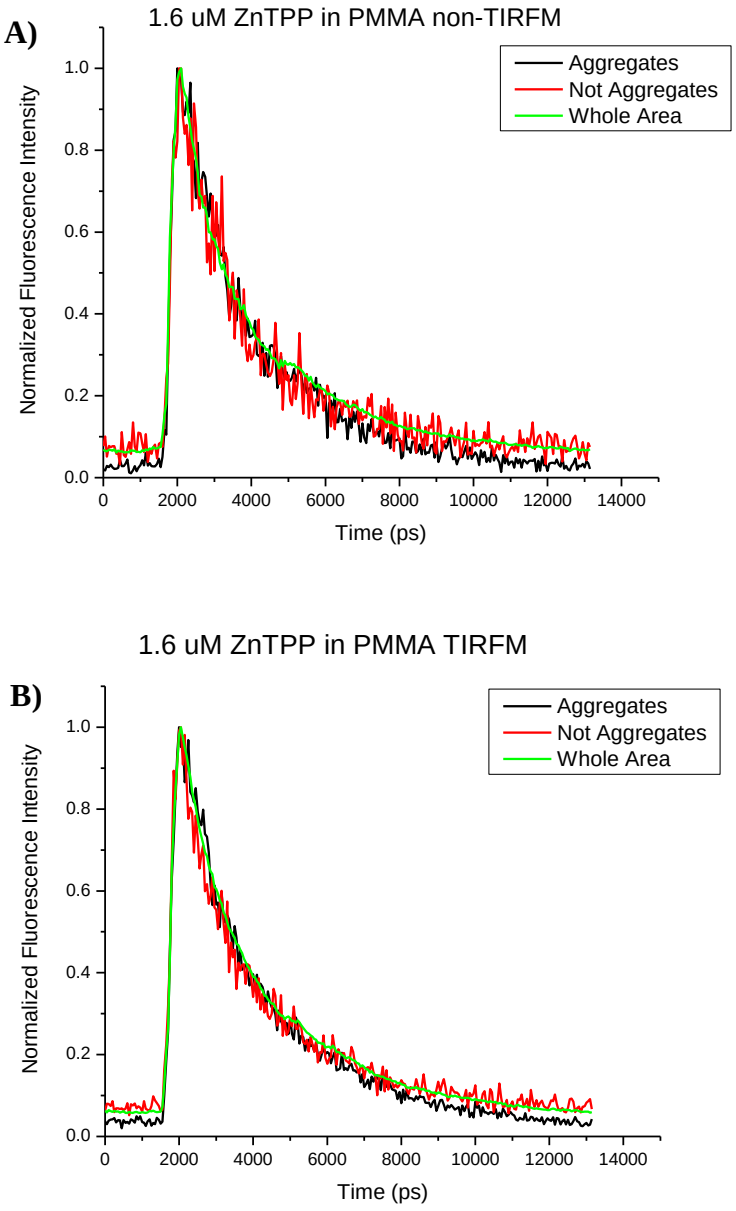

Figure 2.10 Normalized fluorescence decays as a function of time for a 1.6 μM ZnTPP in PMMA film. Decays were obtained in both TIRFM and non-TIRFM modes for three different areas of the film: whole area (A, B and E), aggregates (A, B and C) and not aggregates (A, B and D). λ_{ex} = 400 nm, pulsed excitation at an average power of 0.4 mW.

C)

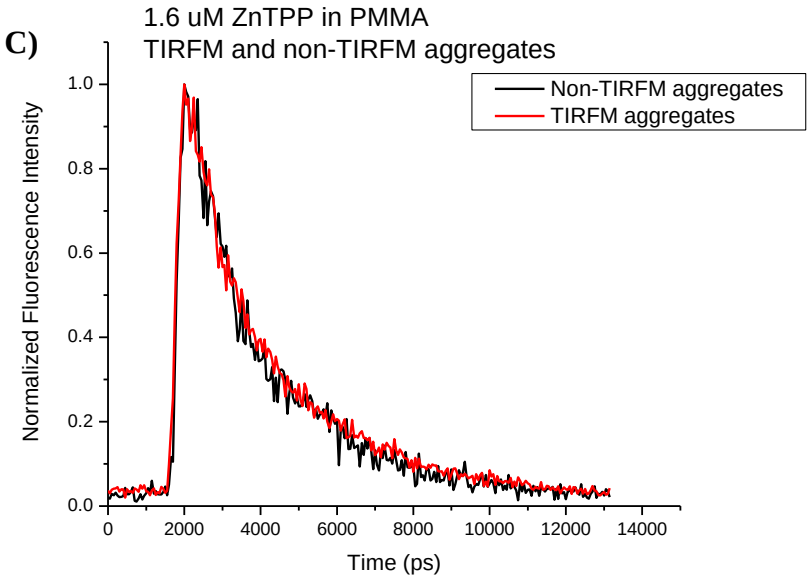
1.6 uM ZnTPP in PMMA
TIRFM and non-TIRFM aggregates
Non-TIRFM aggregates
TIRFM aggregates
Normalized Fluorescence Intensity
Time (ps)
0.0
0.2
0.4
0.6
0.8
1.0
0
2000
4000
6000
8000
10000
12000
14000

D)

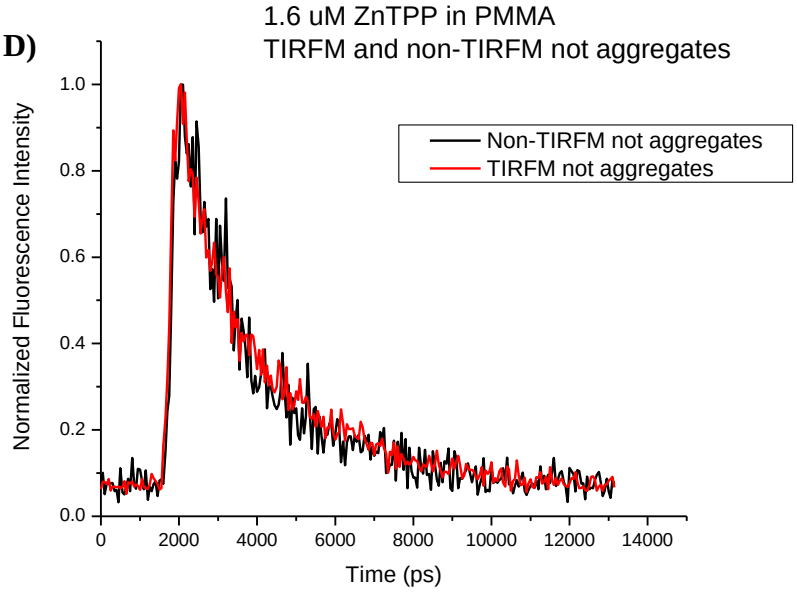
1.6 uM ZnTPP in PMMA
TIRFM and non-TIRFM not aggregates
Non-TIRFM not aggregates
TIRFM not aggregates
Normalized Fluorescence Intensity
Time (ps)
0.0
0.2
0.4
0.6
0.8
1.0
0
2000
4000
6000
8000
10000
12000
14000

E)

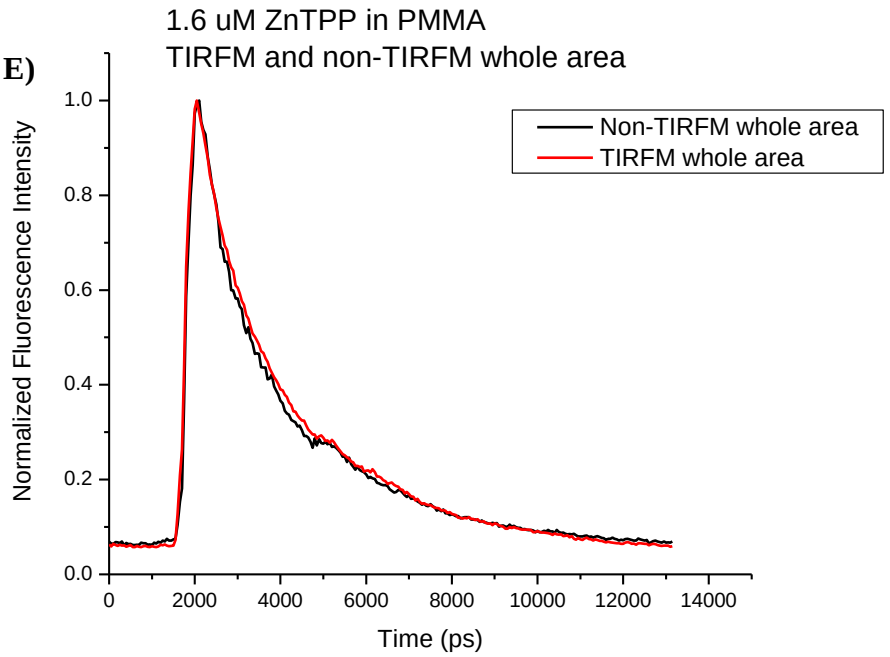
1.6 uM ZnTPP in PMMA
TIRFM and non-TIRFM whole area
Non-TIRFM whole area
TIRFM whole area
Normalized Fluorescence Intensity
Time (ps)
0.0
0.2
0.4
0.6
0.8
1.0
0
2000
4000
6000
8000
10000
12000
14000

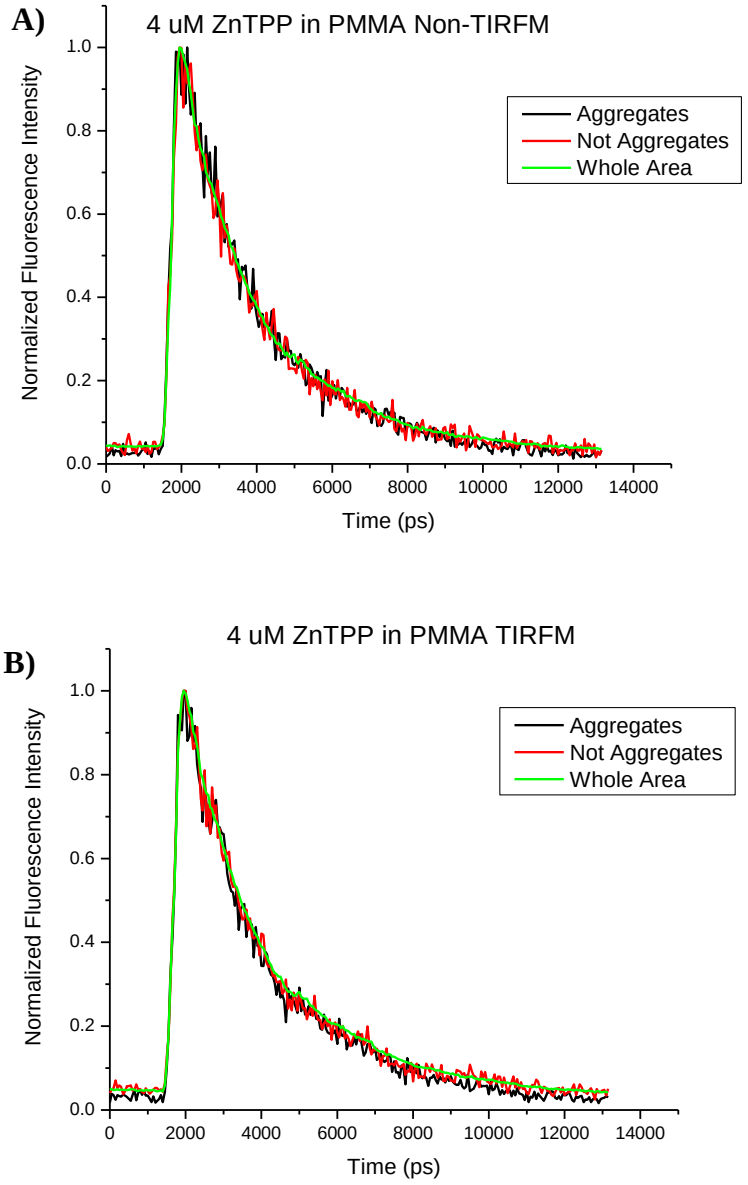

Figure 2.11 Normalized fluorescence decays as a function of time for a 4 μM ZnTPP in PMMA film. Decays were obtained in both TIRF and non-TIRF modes for three different areas of the film: whole area (A, B and E), aggregates (A, B and C) and not aggregates (A, B and D). λ_{ex} = 400 nm, pulsed excitation at an average power of 0.4 mW.

C)

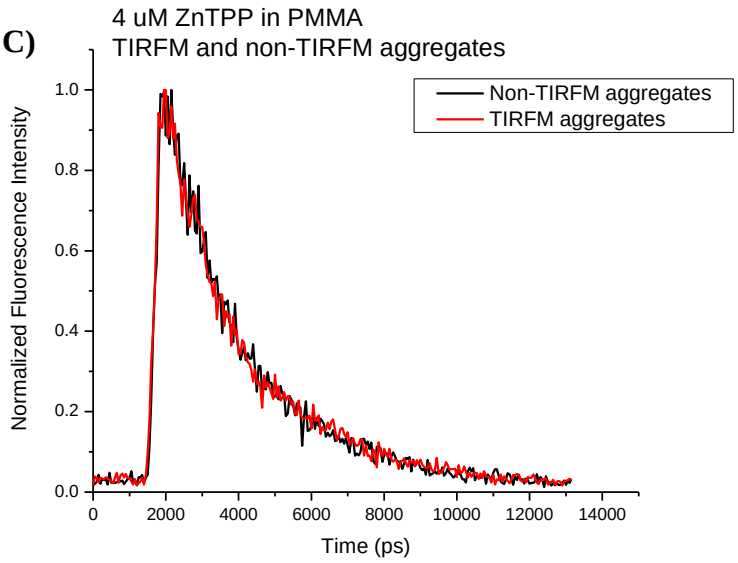
4 uM ZnTPP in PMMA
TIRFM and non-TIRFM aggregates
Non-TIRFM aggregates
TIRFM aggregates
Normalized Fluorescence Intensity
Time (ps)
0.0
0.2
0.4
0.6
0.8
1.0
0
2000
4000
6000
8000
10000
12000
14000

D)

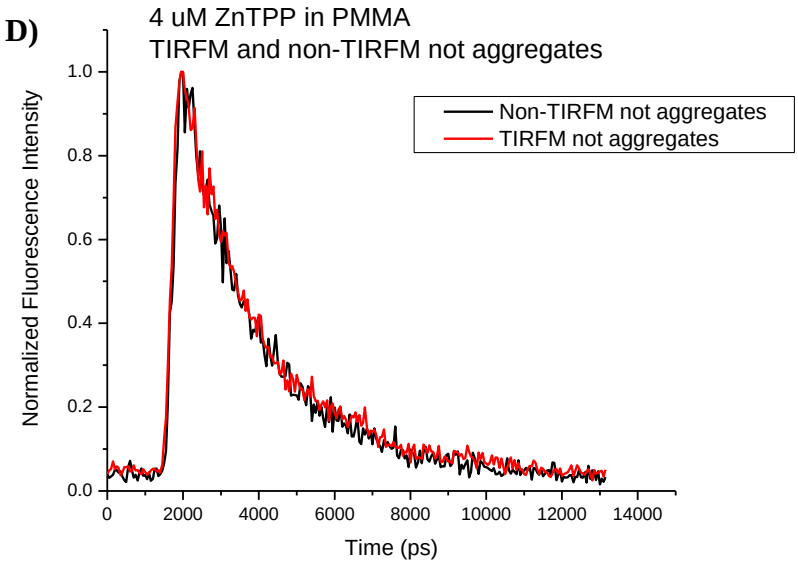
4 uM ZnTPP in PMMA
TIRFM and non-TIRFM not aggregates
Non-TIRFM not aggregates
TIRFM not aggregates
Normalized Fluorescence Intensity
Time (ps)
0.0
0.2
0.4
0.6
0.8
1.0
0
2000
4000
6000
8000
10000
12000
14000

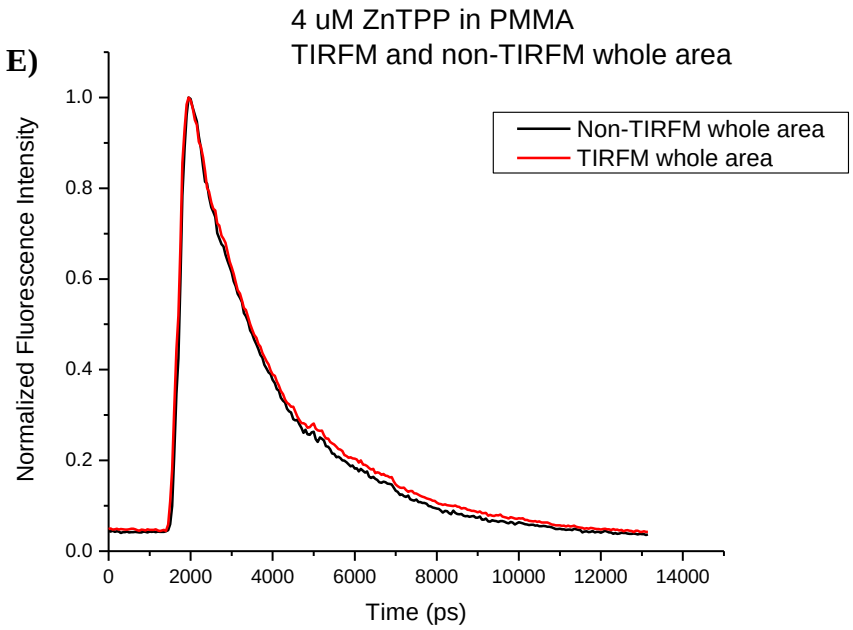

After comparing the above data, one concludes that all the decays are similar. The fluorescence decays, and the corresponding lifetimes (all around 2 ns, for both TIRFM and non-TIRFM modes, see Figures A.13-A.24 for fluorescence decays and their best single exponential fit), are very much alike for the three different areas examined in the film. In Figure 2.12, the decays for the two ZnTPP concentrations are compared. To be consistent with the anisotropy results, one would expect the more concentrated ZnTPP film to decay faster due to greater aggregation. Nevertheless, the fluorescence decays for both concentrations are very similar, with lifetimes around 2 ns. The concentrations of ZnTPP being compared in this experiment are not as different as the concentrations studied using fluorescence

anisotropy, which were different by up to 8.5% by mass ZnTPP. It's possible that the amount of absorber aggregation in these films is similar leading to essentially the same fluorescence intensity decays. If that is the case, then these experiments should be repeated using films with a more drastic difference in their concentration of ZnTPP in an effort to acquire more evidence to support the claim that porphyrin aggregation quenches the fluorescence of its respective monomers. Furthermore, in these measurements the films consisted of one layer of PMMA and the dye solution was spin casted on top. It is possible that when the dye solution is deposited onto the PMMA layer, it dissolves some of the polymer, allowing some of the ZnTPP molecules to diffuse into it. Assuming that the evanescent wave would not penetrate past the PMMA layer, which is about 200 nm thick (the average penetration distance of an evanescent wave), only the select few of ZnTPP molecules that diffused into the PMMA will be excited. The ZnTPP molecules being excited in these films are more isolated than the ones in the normal PMMA film, and, as such, significant aggregation may not be occurring. Thus, this lack of aggregation is another potential reason for why a significant change in lifetime is not observed in these films when different areas are excited.

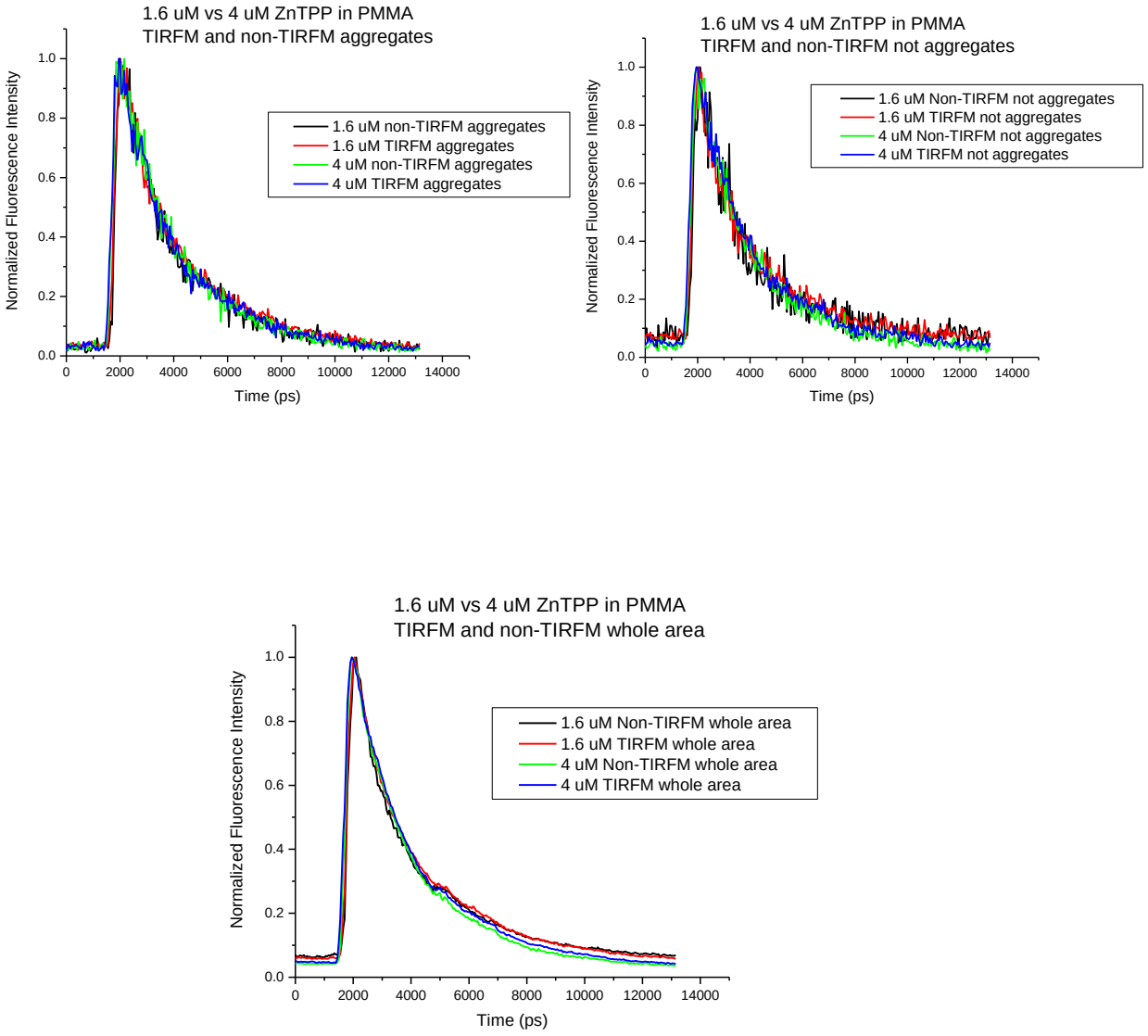

Figure 2.12 The comparison of normalized fluorescence decays as a function of time for 1.6 and 4 μM ZnTPP in PMMA film. Decays were obtained in both TIRFM and non-TIRFM modes for three different areas of the film: whole area, aggregates and not aggregates. λ_{ex} = 400 nm, pulsed excitation at an average power of 0.4 mW.

2.4 Conclusions

This chapter describes how fluorescence anisotropy and TIRFM techniques were employed to study absorber aggregation in PMMA films doped with ZnTPP. Fluorescence anisotropy measurements were performed to determine if depolarized emission was detected as a result of ZnTPP aggregation. TIRFM was used to learn more about the structure of the film, to see if it was homogeneous and if it consisted of detectable aggregates.

In the fluorescence anisotropy experiments, depolarized emission was observed in these films consistently at the highest ZnTPP concentration investigated. The time dependence of the anisotropy is most likely a result of energy transfer between ZnTPP molecules of an aggregate and among different aggregates in the polymer film. This hypothesis is further supported by the faster decays of fluorescence intensity as a function of time as the concentration of ZnTPP in the film increased. The formation of aggregates is more plentiful at higher ZnTPP concentrations and thus the increased interactions between ZnTPP molecules are responsible for quenching the dye's fluorescence, resulting in the observed shorter lifetime. In addition, fluorophore rotation in the excited state and photophysics were ruled out as reasons for the depolarization observed.

TIRFM studies of the structure of films revealed that the films are not homogeneous, and that aggregates of the dye are indeed formed. The time-resolved TIRFM measurements, unfortunately, did not provide any further insight into the relationship between ZnTPP aggregation and fluorescence quenching, nevertheless,

further samples with a significantly different ZnTPP content should be investigated by this technique.

Chapter 3: Single ZnTPP Molecule Fluorescence Spectroscopy

This chapter will describe experiments aimed at observing fluorescence emission from single porphyrin molecules. Wide-field microscopy, along with spectromicroscopy was used to determine if single porphyrin molecules could be detected in thin polymer films or on glass substrates. This chapter is based on material that has been submitted for publication.[26]

3.1 Materials Investigated

Two different porphyrins were studied in this project: (i) *meso*-tetraphenylporphine zinc, ZnTPP, (Porphyrin Systems) and (ii) its *para*-sulfonated derivative, ZnTPPS, (Frontier Scientific). In addition, two polymers were investigated: (i) poly(methyl methacrylate), PMMA, (MW = 75 000, 200 micron beads) and (ii) poly(vinyl alcohol), PVA, (MW = 78 000). Both were purchased from Polysciences Inc. Chloroform (Fluka, for UV-spectrophotometry $\geq$ 99.8%) and water (Millipore, resistivity = 18 MΩcm) were used as solvents. All chemicals were used as received.

3.2 Instrumentation and Sample Preparation

Preliminary measurements with ZnTPP were performed at the University of Melbourne. These experiments were repeated at the University of Saskatchewan, but due to a number of setbacks (contaminated polymers and organic solvents), ZnTPPS (a water soluble derivative of ZnTPP) was investigated since the water available was free of fluorescent impurities. Nonetheless, the work with both of these porphyrins will be discussed in this chapter.

3.2.1 Wide-Field Microscopy

At the University of Melbourne, films were prepared by a spin casting technique. A few drops of 1% PMMA in chloroform were added to a clean microscope coverglass slide (22 mm x 22 mm, VWR) and then spin coated at 4000 rpm for 75 seconds using a Specialty Coating System (SCS) P6700 Series Spin Coater. Then a few drops of ca. 1 nM ZnTPP in chloroform were added to the same slide and spin coated at the same speed and time as for the first polymer coating. The microscope coverglass slides were cleaned by sonicating them in a solution of acetone for twenty minutes, then in an aqueous 10% NaOH solution for twenty minutes, and then in Millipore water for another twenty minutes (this last step was repeated twice). The slides were then dried under nitrogen before being treated with UV light generated ozone for another twenty minutes. Control experiments were performed to ensure that the glass slides and the polymer were free of fluorescent impurities. After the samples were prepared they were promptly imaged using the single-molecule microscope.

This project was continued at the University of Saskatchewan with films prepared using water-soluble ZnTPPS. These films were prepared by spin coating a few drops of ca. 10^{-8} M ZnTPPS in Millipore water onto a clean microscope coverglass slide (22 mm x 22 mm, VWR) at 1000 rpm for 1 minute using a Laurell Technologies Corporation Spin Coater Model WS-400B-6NPP/LITE. The microscope coverglass slides were cleaned by passing them through a propane torch a minimum of 10 times. After the films were prepared, they were immediately imaged using the single-molecule microscope. To be confident that the only fluorophores

being imaged were that of ZnTPPS, control samples of the coverglass slides alone and the slides that had been spin coated with water were also imaged. In both control experiments, no significant fluorescent impurities were seen using the fluorescence microscope. These films were not prepared with a protecting layer of polymer, because solutions of PMMA and PVA spin coated onto coverglass slides were both found to contain an unacceptable amount of fluorescent impurities. As a result, they could not be used while imaging single ZnTPPS molecules as they would have obscured the porphyrin's fluorescence. The source of fluorescent contaminants in the polymers and solvents is unknown at this time, although the antioxidants that are added to them to prevent the formation of peroxides and the products of their photochemically-initiated radical reactions are likely contributors. This is one area, in particular, where the technology needs to advance for this field of research to continue to develop.

The instrumentation for the wide-field microscopy at the University of Melbourne employed a cw 532 nm pumped solid-state diode SLOC laser (Shanghai Laser & Optics Century Co., Ltd.) to excite the sample. The laser passed through a 10 μm pinhole and then through a neutral density filter to control the laser power. The beam was then directed to a lens (Thorlabs, f = 25 cm) that focused the beam into an inverted microscope (Olympus IX 71), and through a dichroic mirror that reflects the excitation light but transmits the Stokes' shifted fluorescence. The beam was focused through a high numerical aperture oil immersion objective lens (Olympus UPlanSApo 100x/1.40 oil) onto the sample, with an illumination spot of ca. 1 mm diameter. Fluorescence from the sample was then collected by the objective and

passed back through the microscope, through an emission filter (550 nm long pass) and into a CCD camera (Princeton Instruments PhotonMax 512).

At the University of Saskatchewan, similar instrumentation was employed. A 532 nm cw pumped solid-state diode laser (vertical polarization, Dragon Lasers, Chang Chun, China) was used as the excitation source. The beam was passed through neutral density filters, then a Glan-Thompson Polarizer and a zero-order quarter wavelength plate for 532 nm to make the laser output circularly polarized. The beam was passed through a focusing lens (f = 75 cm), directed into the back of the microscope (Nikon Eclipse TE2000-U), reflected from a dichroic mirror (Omega 540 DRLP) and finally focused onto the sample with a Nikon Plan-Apo 60x/1.40 oil immersion objective. The fluorescence from the sample then passed back through the objective, through two different 540 nm long pass filters (Omega Optical) and into the CCD detector (Cascade 512F, Photometrics). The CCD was operated using MetaMorph software, which was also used for data analysis.

3.2.2 Spectromicroscopy

Spectromicroscopy measurements were also performed at both universities. The samples were prepared in the same way as was described in section 3.2.1.

The spectromicroscopy instrumentation at the University of Melbourne is very similar to the wide-field microscopy set-up described above, except that it does not include the focusing lens found in the wide-field system. As a result, the objective focuses the beam onto a small spot (tens of microns) on the sample that lies on an x-y piezo stage (Physik Instrumente P-517). In addition, after the fluorescence passes

back through the objective lens, and through a filter, it also passes through a pinhole (~100 μm). From there the fluorescence was either directed into: (1) an avalanche photodiode detector (Perkin Elmer SPCM-AQR-14) coupled with a photon counting card (TimeHarp 200) for time resolved data, or (2) a spectrograph (HJY Triax 550) with a liquid nitrogen cooled CCD attached (HJY Symphony) for recording spectra. Figure 3.1 shows a schematic diagram of the interchangeable wide-field/spectromicroscopy instrumentation at the University of Melbourne.

For spectromicroscopy measurements at the University of Saskatchewan, the focusing lens in the wide-field set-up was removed, allowing the excitation to be focused by the objective into a small spot (~ 2 μm) on the sample. The sample's fluorescence was passed through the same long-pass filters as described above and was focused into an imaging spectrograph (MS125 Spectrograph, Newport (Oriel) Instruments). The spectrograph dispersed the output onto an electron multiplying CCD detector (iXon, Andor Technology), producing a 2D spectrum of the region on the sample being investigated. The instrument was wavelength calibrated using an Hg pen lamp. The quantum efficiency of the CCD did not vary significantly over the spectral region of interest, so it was not necessary to correct collected emission spectra for a wavelength-dependent response of the detector. A frame exposure time of 100 ms was used, and the CCD pixels were binned to maximize the SNR in the collected emission spectra.

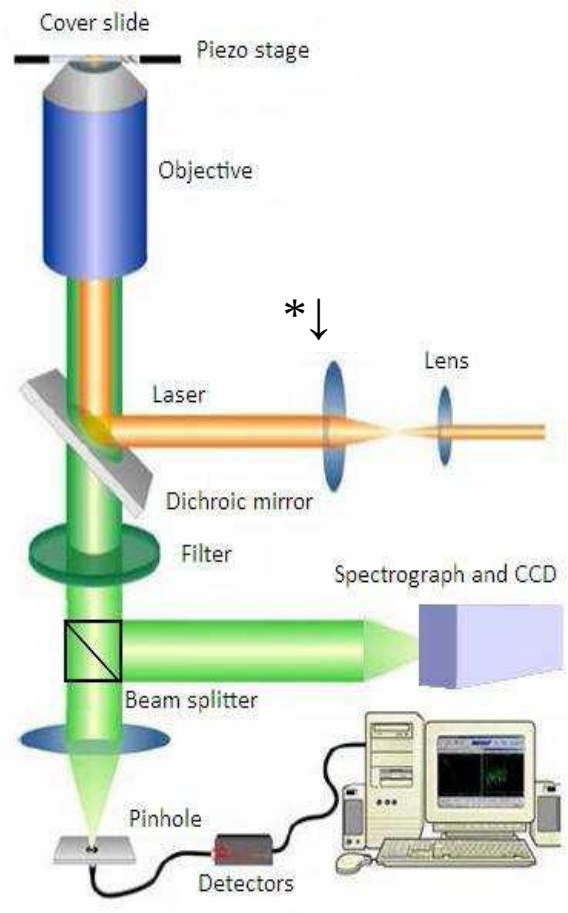

Figure 3.1 Schematic diagram of the confocal microscope that was used for single molecule fluorescence detection.[62] The asterisk (*) in the diagram indicates the position of the focusing lens for wide-field microscopy. Figure taken, with permission, from reference 62.

3.3 Results and Discussion

SMS was employed to study single molecules and aggregates of ZnTPP in polymer films and ZnTPPS on glass substrates. As noted previously, it is imperative to fully understand absorber aggregation in order to maximize the efficiency of TTA so it can be used as a successful mechanism for photon upconversion in DSSCs. In addition, it is important to study lone molecules to acquire information that may be lost due to the ensemble averaging in bulk measurements. Knowing how a single ZnTPP or ZnTPPS molecule behaves may provide more information on the aggregates they form at higher concentrations. Nonetheless, as has been previously described, porphyrins are difficult molecules to study using SMS, mainly because of their low fluorescence quantum yield ($\Phi_F = 2.67 \times 10^{-2}$ in the S_1 for ZnTPP).[17] To put this into perspective, one can compare porphyrins to R6G molecules ($\Phi_F = 0.95$),[63] a dye often used in single molecule measurements. After examining their respective fluorescence quantum yields, one can see that the fluorescence from R6G would be much more intense (making it that much easier to see it as a single molecule) than that from a porphyrin. In addition, porphyrins are difficult to study using SMS because they photodegrade in the presence of oxygen and readily form dark triplet states.[54] Nevertheless, porphyrins have a short fluorescence lifetime (the less time the molecule spends in the excited state, the more opportunities it will have to absorb photons that can potentially lead to fluorescence emission) and absorb strongly at the excitation wavelength used, all characteristics that are favourable for a dye to have in order to be studied at the single molecule level.

3.3.1 Wide-Field Microscopy

Wide-field microscopy was used to image the single porphyrin molecules in the polymer film or on the glass substrate. Figure 3.2 shows what a collected image commonly looks like.

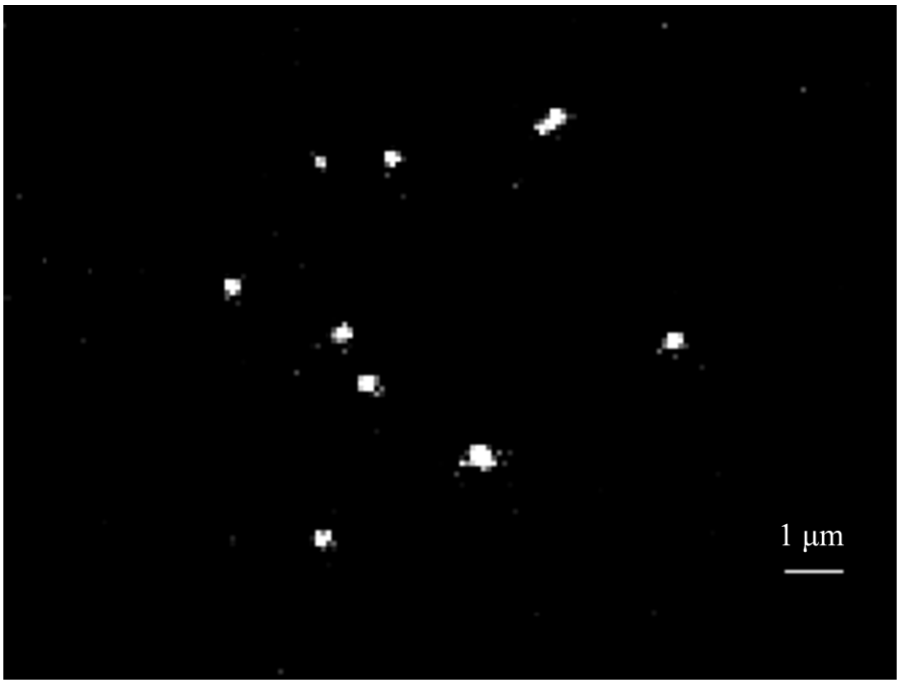

Figure 3.2 An image obtained using wide-field microscopy for a 1 nM ZnTPP in PMMA film. The nonfluorescent background is black, and the emission from ZnTPP molecules is represented by the white spots in the image. λ_{ex} = 532 nm (cw), ca. 5 kW/cm^2.

Videos were recorded that showed the fluorescence from molecules in the film until they ultimately photobleached. Time trajectories were obtained from these videos for the various fluorescent spots on the film. From these time trajectories, one can determine if the fluorescence from a single molecule is being measured. A single step photobleaching decay in these plots of fluorescence emission as a function of time is characteristic of a single molecule, and a series of multistep decays is representative of more than one molecule, possibly a multimolecular aggregate.

Preliminary wide-field microscopy measurements were performed at the University of Melbourne with ca. 1 nM ZnTPP in PMMA films. Time trajectories were obtained that showed single step photobleaching (see Figure 3.3), which are characteristic of single molecules.

A histogram of single-molecule fluorescent intensities can be generated after a number of single ZnTPP molecules in the film are measured. Figure 3.4 shows the distribution of fluorescent intensities for the molecules in the film studied. Such a trend of distributions is expected to be seen from the emission of individual molecules, as each molecule is in a slightly different microenvironment. In the polymer film, different ZnTPP molecules are surrounded by different functional groups, charges and atoms, and this will affect the intensity of their emission.[45] This histogram, however, does show that about 40% of the molecules in the film being studied had emission intensities between 5000 and 10 000 counts. Thus, these molecules were in similar environments, resulting in similar emission intensities.

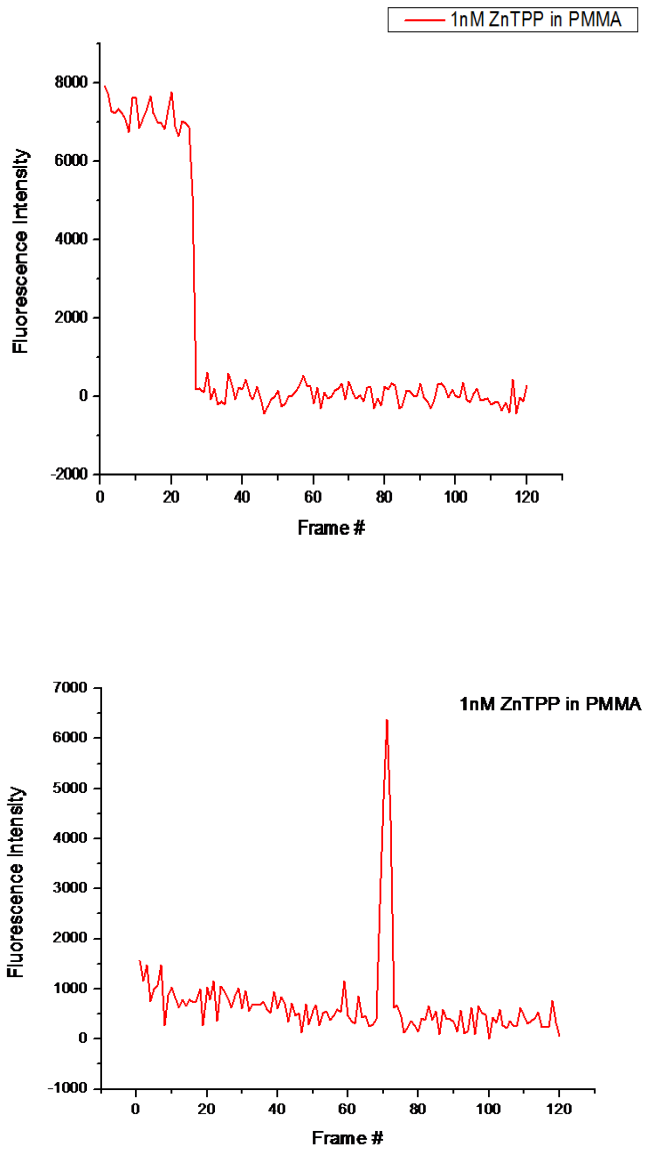

Figure 3.3 Plots of fluorescence intensity as a function of frame number for possible single molecules in a PMMA film doped with 1 nM ZnTPP. λ_{ex} = 532 nm (cw), ca. 5 kW/cm^2.

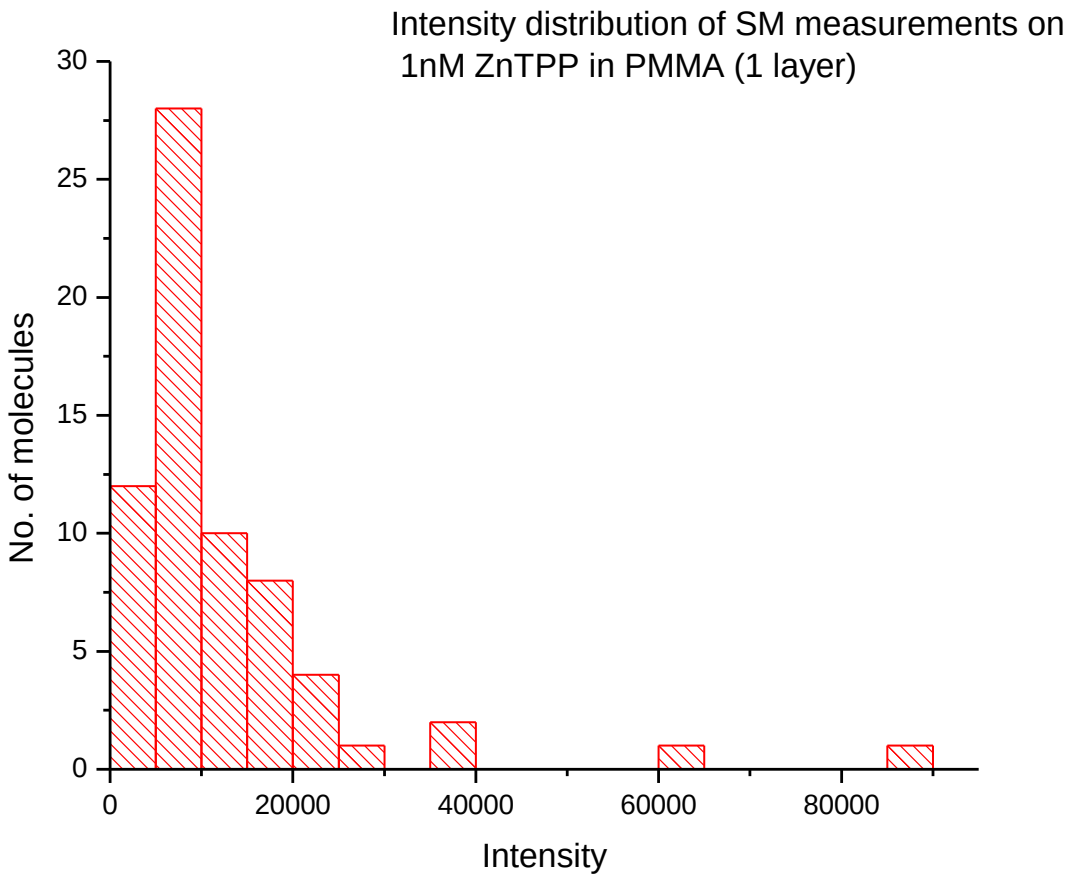

Figure 3.4 Histogram of individual ZnTPP molecules in a PMMA film. λ_{ex} = 532 nm (cw), ca. 5 kW/cm^2.

The results obtained at the University of Melbourne warranted further investigation before any firm conclusions could be made. The wide-field microscopy experiments were repeated (and spectromicroscopy characterization, which will be discussed in the next section) with ZnTPPS at the University of Saskatchewan. Time trajectories and histograms of photobleaching times and fluorescence intensities for

single ZnTPPS molecules were obtained. Once again, the films of ZnTPPS studied were not coated with polymer like the ZnTPP films discussed above. Instead, the film was prepared by spin coating a water solution of the dye (ca. 10^{-8} M) on the coverglass slide. The results obtained with ZnTPPS were consistent with those for ZnTPP. However, data was also collected indicating ZnTPPS aggregates (described below), which were not detected in the experiments with ZnTPP. Nonetheless, the formation of ZnTPPS aggregates was expected, as the polar groups in the fluorophore, and the hydrophillic glass substrate the dye is adsorbed to, will undoubtedly promote the aggregation of ZnTPPS molecules.

Using the wide-field microscopy set up at the University of Saskatchewan, time trajectories were collected and two different types of photobleaching behaviour were observed in these films: (i) single-step decays and (ii) a more complex decay route, including multiple decay steps or one long gradual (nearly exponential) decrease in intensity. The single-step photobleaching behaviour is likely a result (see Figure 3.5 A,B) of single ZnTPPS molecules. At the dilute concentration of dye used, it is easy to spatially resolve single molecules (i.e. each molecule is spaced by a distance greater than the excitation laser spot size), which further supports the notion that individual ZnTPPS molecules are being observed. The more complex photobleaching decays are most likely that of multimolecular aggregates. Two examples are shown in Figure 3.6 A,B. In **A)** two photobleaching events occur in succession, suggesting that the area being studied consisted of an aggregate made up of at least two emitting ZnTPPS molecules. This multi-step behaviour is common and has been seen in other single molecule studies of different fluorophores,[64,65] and

in Kim's study of ZnTPP arrays (discussed in Chapter 1).[55] The time-trajectory shown in **B)** shows a more complex behaviour in that the fluorescence intensity actually increased with time. Nonetheless, on the whole, the fluctuations in these trajectories suggest the photobleaching of individual emitters.

A)

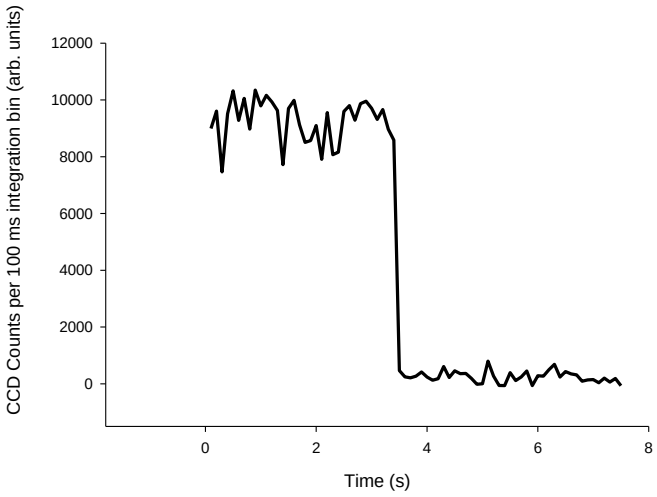

B)

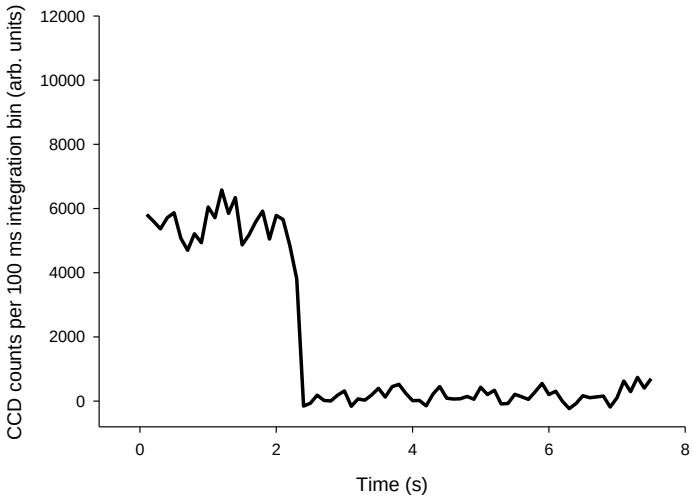

Figure 3.5 A,B) Single-molecule fluorescence time trajectories for individual molecules of ZnTPPS on microscope coverglass slides. The fluorescence intensity is plotted as CCD counts per 100 ms integration bin (arbitrary units) after the mean background signal has been subtracted. λ_{ex} = 532 nm, cw, 1.0 kW/cm^2.

A)

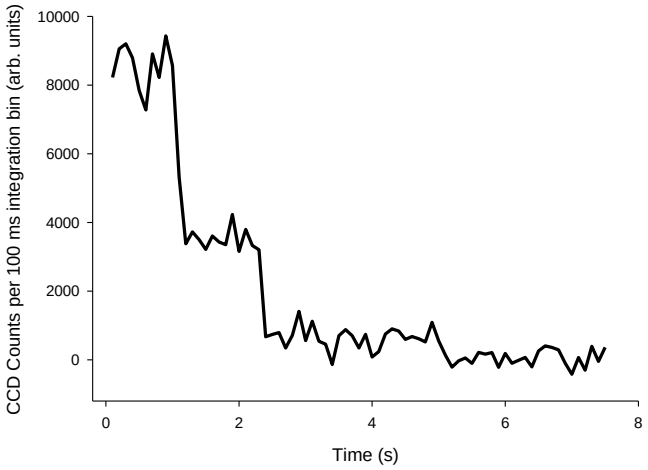

B)

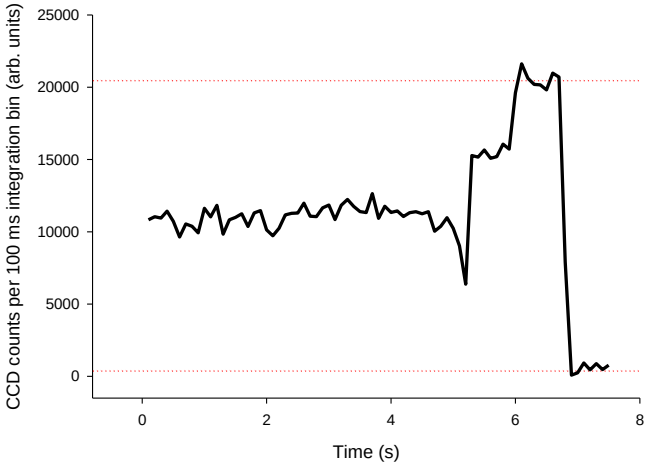

Figure 3.6 A) Fluorescence trajectory for a multimolecular aggregate of ZnTPPS with two discrete photobleaching events. **B)** Fluorescence trajectory for a multimolecular aggregate of ZnTPPS exhibiting more complex photobleaching behaviour. The dotted red lines show one of the single-step transitions observed in this time trajectory. λ_{ex} = 532 nm, cw, 1.0 kW/cm^2.

After collecting information from a number of single ZnTPPS molecules with time trajectories like that of type (i) (Figure 3.5 A,B), histograms of single molecule photobleaching times and single molecule fluorescence intensities were developed.

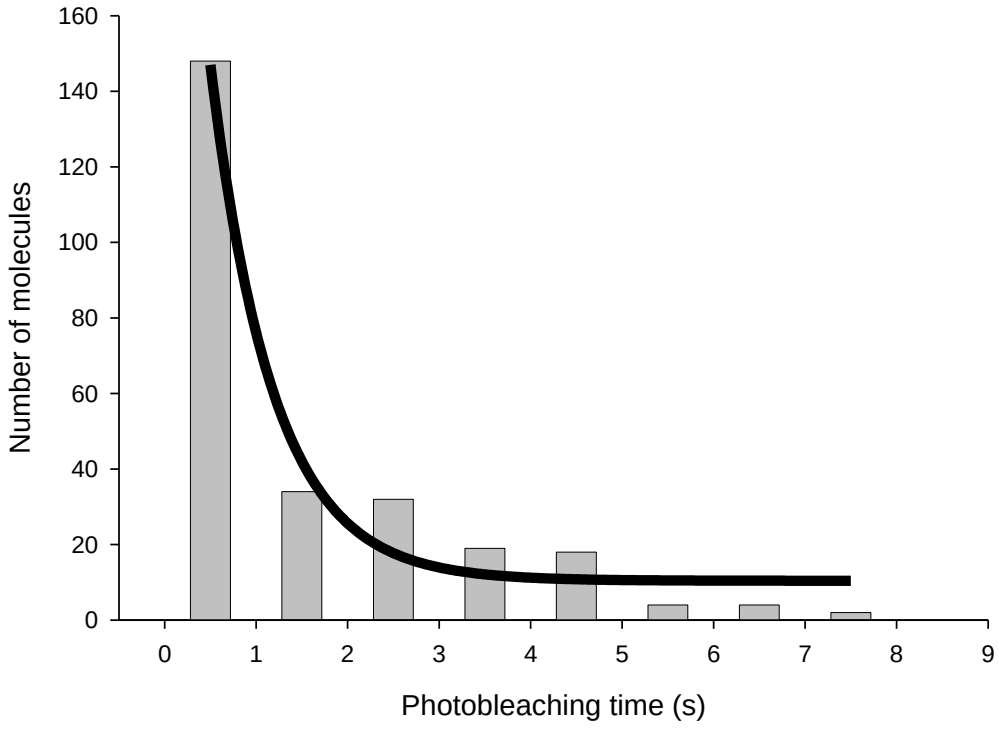

Figure 3.7 Histogram of photobleaching times for 261 individual ZnTPPS molecules collected from time-trajectories. λ_{ex} = 532 nm, cw, 1.0 kW/cm^2. The data were fit with a single exponential function ($N=A_0 \exp(-t/\tau_{on})$) where τ_{on} is the photobleaching time constant. τ_{on} was calculated to be 0.7 s.

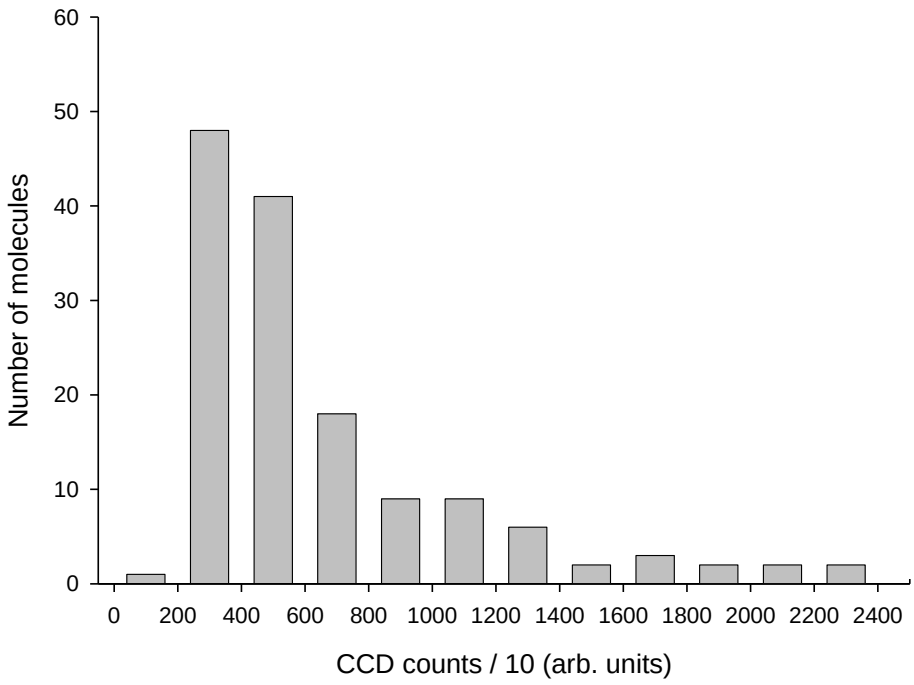

Figure 3.8 Histogram of individual ZnTPPS molecule fluorescence intensities (measured in CCD counts/10 (arb. units)). λ_{ex} = 532 nm, cw, 1.0 kW/cm^2.

The photobleaching time data shown in Figure 3.7 fits to a single-exponential decay curve ($N=A_0 \exp(-t/\tau_{on})$, where N is the number of molecules, A_0 a fitting constant and τ_{on} is a photobleaching time constant). This implies that there are individual emitters adsorbed on the glass substrate, as the decay follows first-order kinetics. If there were multiple excited species, then a fluorescence decay curve would have been observed for each, resulting in the overall decay curve not being single-exponential. To compare the results for ZnTPPS with R6G, the standard

organic dye discussed earlier, the values of τ_{on} for the dyes are 0.7 s and 2.0 s, respectively.[66] The τ_{on} value for R6G was obtained from imaging the dye in a polymer film under similar illumination intensity. From these τ_{on} values, one can see that R6G is notably more photostable, regardless of its polymer protective layer (i.e. polymer slows down the photobleaching rate), than ZnTPPS. Nevertheless, the τ_{on} value is reasonable as ZnTPPS is not expected to be easy to image at the single molecule level due to its involvement in oxygen-based photochemical reactions.[54]

The distribution of fluorescence intensities shown in Figure 3.8 also suggests the existence of individual emitters on the glass substrate. The average fluorescence intensity was 6100 counts, and this is similar to the intensities reported for a rhodamine-like calcium ion sensor (Calcium Green-1).[67] A significantly higher photobleaching rate was observed with ZnTPPS, and the measurements were performed using significantly greater illumination intensity. Nonetheless, this is an important observation as Calcium Green-1 is a much easier dye to study at the single molecule level because of its larger quantum yield and absorption cross-section. The observation of single Calcium Green-1 molecules with similar fluorescence intensities further suggests that single ZnTPPS molecules were detected.

After collecting information from a number of ZnTPPS aggregates with time trajectories like that of type (ii) (Figure 3.6 A,B), a histogram of the intensities for the individual photobleaching steps was prepared (see Figure 3.9).

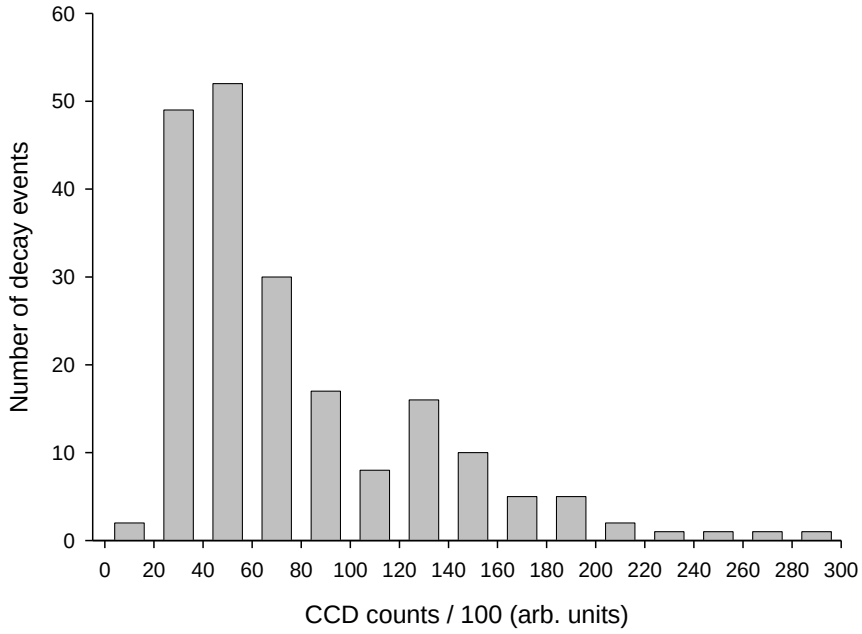

Figure 3.9 Histogram showing the fluorescence intensity of the discrete decay steps in multimolecular ZnTPPS aggregates (measured in CCD counts/100 (arb. units)). λ_{ex} = 532 nm, cw, 1.0 kW/cm^2.

The histogram of fluorescence intensities for the discrete decays in an aggregate (Figure 3.9) shows a similar distribution to that measured for individual ZnTPPS molecules (Figure 3.8). Furthermore, the average fluorescence intensities for both distributions are comparable: 6100 counts for individual ZnTPPS molecules and 7600 counts for the single emitters in an aggregate. This data provides further evidence that the sequential photobleaching steps in the aggregates are likely a result of individual molecules photobleaching in the aggregate. For the most part, the total

fluorescence intensity of each individual aggregate was greater than the intensity of individual constituent molecules, implying that the formation of aggregates does not readily quench the fluorescence of ZnTPPS. However, this conclusion may be influenced by a selection bias of the experiment, because if the emission was sufficiently quenched due to aggregation, then the emission from the ZnTPPS aggregates would not have been observable in these experiments.[25] If aggregation does not quench ZnTPPS's fluorescence than this contradicts the results in Chapter 2, where fluorescence quenching was readily observed as the formation of ZnTPP aggregates in the polymer film increased. Thus, these results are most likely a result of a selection bias in the experiment, where only aggregates whose emission was not sufficiently quenched were detected.

3.3.2 Spectromicroscopy

After studying these films using wide-field microscopy, it was important to obtain an emission spectrum of the dye in the film to ensure that the fluorescence observed in the measurements discussed above was from the porphyrin. Emission spectra are also useful in determining if aggregates are present in a film, as aggregation often results in spectral shifts (see previous discussion re. H- and J-aggregate formation). Once again, preliminary measurements were done at the University of Melbourne with PMMA films doped with ZnTPP. Similar measurements were then continued at the University of Saskatchewan with ZnTPPS films. Results from both studies will be discussed in this section.

At the University of Melbourne, the wide-field microscopy set-up discussed earlier was changed into a confocal one. As a result, the excitation beam was focused into a very small spot on the sample and its fluorescence was then passed through a spectrograph that was attached to a CCD detector. Figure 1.4 shows the absorption and emission spectra for ZnTPPS in water. The Q bands in both spectra are characteristic of S_1 emission from ZnTPP/ZnTPPS. The presence of these two bands in the emission spectra of the single molecules/aggregates provides sufficient evidence to prove that the fluorescence observed in the wide-field microscopy measurements was from the porphyrin of interest.

The emission spectrum of a film of ca. 1 nM ZnTPP in PMMA was obtained and consisted of ZnTPP's characteristic Q bands (see Figure 3.10), which are observed ca. 600 nm (the 0-0 transition) and 650 nm (the 0-1 transition) in a bulk measurement.[3] However, the band corresponding to the 0-0 transition was blue-shifted, and the one corresponding to the 0-1 transition was red-shifted. The dilute concentration of ZnTPP in the film being studied, along with the single-step photobleaching behaviour observed above in Figure 3.3, suggest that the emission spectra collected were for single porphyrin molecules. The maxima of the Q bands in the emission spectrum for a single ZnTPP molecule are expected to be at different wavelengths in comparison to that for a bulk solid phase sample, as there is a great amount of aggregation in the bulk sample, and this causes spectral shifts. At the dilute concentration of ZnTPP studied (ca. 1 nM), aggregation is very limited, and thus the position of the Q bands will be different than that for a sample high in

aggregation. Figure 3.10 shows the spectrum for the dilute ZnTPP film, along with one measured for a film of 1 μM ZnTPP in PMMA, the emission from a bulk sample.

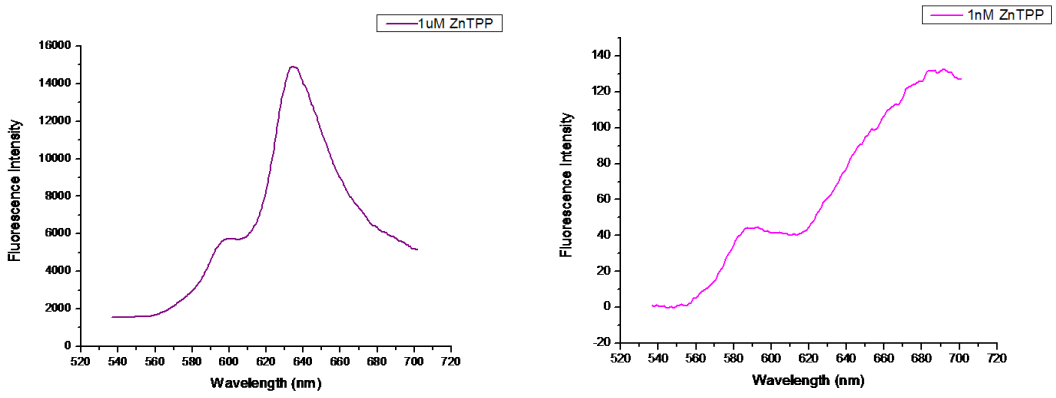

Bulk **Single Molecule?**

Figure 3.10 Emission spectra for concentrated (1μM) and dilute (1nM) ZnTPP in PMMA films. For the potential single molecule spectrum, five spectra were averaged and smoothing was performed (Adjacent Averaging, 10 points). λ_{ex} = 532 nm (cw), 56kW/cm^2 and 6.6 kW/cm^2 for the bulk and single molecule measurements, respectively.

These measurements were then repeated with ZnTPPS at the University of Saskatchewan with a modified version of the wide-field microscopy set-up discussed earlier in this chapter. The spectromicroscopy set-up was not optimized to detect single molecules; nevertheless, emission from the more strongly fluorescent multimolecular ZnTPPS aggregates could be detected. The emission spectrum

collected (see Figure 3.11) showed one band at 562 nm with a shoulder at 605 nm, and another sharp peak at 626 nm. It was determined, through control experiments, that the sharp peak at 626 nm was a result of Raman scattering. This peak was absent in the emission spectrum of a blank coverglass slide, but it was present in the emission spectrum of a hydrated glass slide (glass slide spin coated with water). As a result, this Raman scattering is due to the presence of water in the sample, and may be Raman scattering caused by an OH stretch. The difference in wavenumbers between the excitation and the 626 nm peak is 2.82×10^3 cm^{-1}, and this is in the OH stretching region (2700 – 3800 cm^{-1}), which further suggests the band observed is a result of an OH stretch.[68] The band at 562 nm and its shoulder are presumably assigned to the two Q bands characteristic of ZnTPPS. Even though these bands are blue-shifted with respect to their ensemble equivalents measured in water (610 nm and 656 nm, see Figure 1.4), the peak separation for the aggregates ($1.23 \times 10^3 \pm 50$ cm^{-1}) is very similar to that for the bulk samples ($1.15 \times 10^3 \pm 50$ cm^{-1}). The blue-shift observed with the aggregates is consistent with the formation of H-aggregates, even though the exact nature of the aggregate being studied is still unknown.[61]

As previously noted, fluorescence quenching is often a result of absorber aggregation, so if this was the case, one would not expect to be able to obtain emission spectra from multimolecular ZnTPPS aggregates. As these spectral results are still preliminary, it's difficult to know whether fluorescence quenching was occurring due to porphyrin aggregation and perhaps the most strongly fluorescent aggregates were just preferentially selected. To clarify this, more spectral analysis of the aggregates needs to be performed, along with ultrasensitive fluorescence lifetime

imaging measurements that will help in determining how the molecules are oriented in the aggregates.

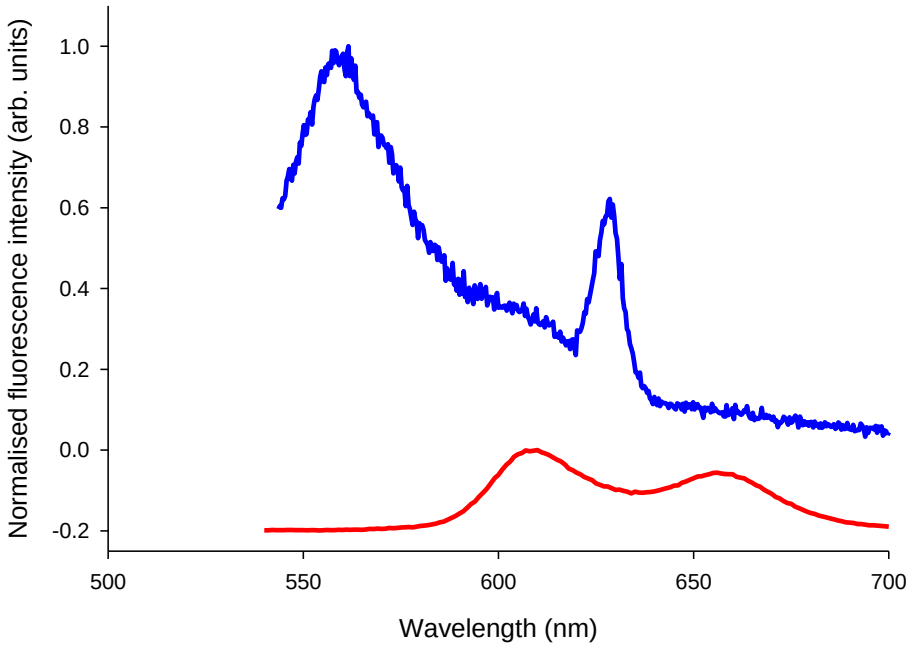

Figure 3.11 An average of 18 fluorescence emission spectra of ZnTPPS aggregates (blue) taken from a sample prepared at 10^{-8} M concentration via spectromicroscopy (λ_{ex} = 532 nm, cw, 17.0 kW/cm^2). For comparison purposes, the ensemble emission spectrum taken in water using a fluorimeter is shown inset (red).

It is difficult to compare the spectral shifts of ZnTPPS with those of ZnTPP in PMMA, because it is possible that the sulfonate functional groups in ZnTPPS and the hydrophilic glass surface of the slides that they are adsorbed to promote greater

fluorophore aggregation then what is observed in a polymer film. Thus, at this time, one should consider the results of these spectromicroscopy experiments as a demonstration that porphyrins can be detected at very dilute concentrations, despite previous claims suggesting porphyrins were poor candidates to study using SMS.

3.4 Conclusions

Preliminary measurements indicate that individual ZnTPP molecules can be detected in PMMA films. Single-step decay time trajectories and an emission spectrum consisting of two bands slightly shifted with respect to the Q bands characteristic of ZnTPP, were evidence that support this hypothesis. Further measurements with ZnTPPS were performed and both individual molecules and multimolecular aggregates of ZnTPPS on coverglass slides were examined by single-molecule fluorescence microscopy and spectromicroscopy. Single ZnTPPS molecules photobleached in one step, whereas multimolecular aggregates of ZnTPPS photobleached in a more complex manner. For the most part, the fluorescence time trajectories for the multimolecular aggregates consisted of discrete photobleaching steps, where each step corresponds to the photobleaching of an individual molecule. An emission spectrum was obtained for the more strongly fluorescent aggregates and it was blue-shifted in comparison with the emission spectrum collected from standard fluorimeter-based ensemble measurements. As a whole, these measurements demonstrate that metalloporphyrins can be detected at the single molecule level, and that the formation of its multimolecular aggregates occurs even at 10^{-8} M concentrations.

Chapter 4: Conclusions and Future Work

The overall goal of the work described in this thesis was to investigate the formation of porphyrin aggregates in polymer films and on solid glass substrates using a variety of techniques. Aggregation is critical for TTA to occur. The better understood the phenomenon of aggregation, the more efficient TTA can be as a means of photon upconversion in DSSCs. It is of great societal importance to improve the solar-to-electrical energy conversion efficiency of DSSCs, and to make them more affordable. Optimizing the TTA observed in polymer films doped with metalloporphyrins and introducing this system to DSSCs may be the approach that needs to be taken to significantly improve this technology. In this thesis, ZnTPP aggregation in the solid state was investigated to learn more about improving TTA efficiencies. Three different techniques were used; fluorescence anisotropy, TIRFM and SMS.

Fluorescence anisotropy measurements were performed to determine if anisotropy changed as a function of porphyrin loading in the films. Depolarized emission was observed in polymer films containing the largest concentration of ZnTPP. The emission was likely depolarized as a result of energy transfer in and among porphyrin aggregates, as the possibility of fluorophore rotation in the excited state and photophysical absorption-emission transition moment axis switching were reasoned to be unlikely. This conclusion is further supported by the fluorescence intensity decays measured. The decays became faster, with a shorter fluorescence lifetime, as the concentration of the porphyrin in the film increased. The fluorescence quenching observed is a result of the formation of aggregates, whose presence in

these films increases as they become more concentrated with dye. Thus, these results further demonstrate the natural phenomenon of porphyrin aggregation, and the spontaneous energy transfer that occurs between and among aggregates.

TIRFM was another technique employed in this thesis to study the structure of these polymer films doped with ZnTPP. If these systems were to be introduced to DSSCs, it would be ideal that they be homogeneous. However, after examining these films using TIRFM, it was determined that they lacked homogeneity, and instead consisted of a number of discrete structures, including those attributed to visible aggregates. Time-resolved TIRFM experiments were also performed to see where on the film the aggregates tended to form, but no concrete results were obtained, possibly a result of comparing films too similar in ZnTPP concentration, or perhaps the excitation of a nonrepresentative population of ZnTPP molecules, a result of how the films were prepared.

Finally, single molecule spectroscopy was employed to study ZnTPP in polymer films and ZnTPPS adsorbed to glass substrates. Both single porphyrin molecules and multimolecular aggregates were examined in these experiments using single molecule fluorescence microscopy and spectromicroscopy. Initially, PMMA films doped with ZnTPP were studied, and evidence of the observation of individual molecules was obtained in the single step decay time trajectories, and in collected emission spectra that were similar to those of an ensemble measurement, but whose bands were spectrally shifted. These measurements were repeated using samples of ZnTPPS adsorbed onto microscope coverglass slides. In these experiments, two different types of fluorescence time trajectories were observed: (i) single step decay

corresponding to single ZnTPPS molecules and (ii) a more complex decay behaviour consisting of multiple discrete steps or one gradual decrease in intensity that is representative of multimolecular aggregates. In (ii), each photobleaching step in the multi-level decay has been assigned to the photobleaching of individual ZnTPPS molecules. From these fluorescence time trajectories, histograms of the distribution of fluorescence intensity and photobleaching time were constructed for a number of ZnTPPS molecules. In addition, emission spectra were measured for the more strongly fluorescent aggregates. The Q bands were blue-shifted in comparison to those in an emission spectrum for a bulk measurement, but such a shift is expected when studying aggregates on highly polar surfaces. These measurements demonstrate that metalloporphyrins can be detected at the single molecule level, despite the fluorophore having suboptimal spectroscopic properties. Furthermore, the formation of aggregates was observed in these samples at porphyrin concentrations as low as 10^{-8} M. It is therefore reasonable to conclude that SMS is another technique that could be used to study metalloporphyrin aggregation and gain further insight regarding its role in photon upconversion processes.

There is still a great deal more to learn about absorber aggregation and its influence in photon upconversion. In order to use the metalloporphyrin/polymer system in DSSCs, it is important to ensure that the film is homogeneous, and thus requires further study on how this can be accomplished. It is also important to learn more about the nature of the porphyrin aggregates that were seen using SMS (i.e. J- or H-type aggregates, or perhaps both), and this can be done through further spectral analysis and fluorescence lifetime imaging experiments. In addition, since porphyrin

aggregation is essential for TTA to occur, it is necessary to explore the options to promote aggregation, so that the rate of TTA can be maximized. This might include introducing another species to the system that promotes intermolecular interactions between porphyrin molecules, and thus the formation of aggregates. Pyrazine is a bidentate ligand that can promote porphyrin aggregation, as it can coordinate to two zinc atoms in different ZnTPP molecules. As such, the ZnTPP molecules are forced to be close together (i.e. they are "linked") and this increased proximity might improve the efficiency of TTA between them. Nonetheless, TTA in these metalloporphyrin systems is a promising means of photon upconversion for use in DSSCs, and as such should be further studied to learn how to maximize its efficiency.

Chapter 5: References

(1) Lakowicz, J. R. *Principles of Fluorescence Spectroscopy* Second ed.; Kluwer Academic/Plenum: New York, 1999.

(2) Birks, J. B. *Photophysics of Aromatic Molecules*; Wiley-Interscience: New York, London, 1970.

(3) Gurzadyan, G. G.; Tran-Thi, T. H.; Gustavsson, T. *Journal of Chemical Physics* **1998**, *108*, 385-388.

(4) Campbell, W. M.; Jolley, K. W.; Wagner, P.; Wagner, K.; Walsh, P. J.; Gordon, K. C.; Schmidt-Mende, L.; Nazeeruddin, M. K.; Wang, Q.; Gratzel, M.; Officer, D. L. *Journal of Physical Chemistry C* **2007**, *111*, 11760-11762.

(5) Bell, T. D. M.; Ghiggino, K. P.; Haynes, A.; Langford, S. J.; Woodward, C. P. *Journal of Porphyrins and Phthalocyanines* **2007**, *11*, 455-462.

(6) Steer, R. P. *Journal of Applied Physics* **2007**, *102*, 3.

(7) Castano, A. P.; Demidova, T. N.; Hamblin, M. R. *Photodiag. Photodyn. Ther.* **2004**, *1*, 279-293.

(8) Mathai, S.; Smith, T. A.; Ghiggino, K. P. *Photochemical & Photobiological Sciences* **2007**, *6*, 995-1002.

(9) Nyman, E. S.; Hynninen, P. H. *Journal of Photochemistry and Photobiology B-Biology* **2004**, *73*, 1-28.

(10) Sternberg, E. D.; Dolphin, D.; Bruckner, C. *Tetrahedron* **1998**, *54*, 4151-4202.

(11) Gulino, A.; Giuffrida, S.; Mineo, P.; Purrazzo, M.; Scamporrino, E.; Ventimiglia, G.; van der Boom, M. E.; Fragala, I. *Journal of Physical Chemistry B* **2006**, *110*, 16781-16786.

(12) Kose, M. E.; Carroll, B. F.; Schanze, K. S. *Langmuir* **2005**, *21*, 9121-9129.

(13) Yang, J.; Kim, D. *Journal of Materials Chemistry* **2009**, *19*, 1057-1062.

(14) Rohatgi-Mukherjee, K. K. *Fundamentals of Photochemistry*; Wiley Inc.: New York, 1978.

(15) Bajema, L.; Gouterma.M; Rose, C. B. *Journal of Molecular Spectroscopy* **1971**, *39*, 421.

(16) Karolczak, J.; Kowalska, D.; Lukaszewicz, A.; Maciejewski, A.; Steer, R. P. *Journal of Physical Chemistry A* **2004**, *108*, 4570-4575.

(17) Liu, X.; Yeow, E. K. L.; Velate, S.; Steer, R. P. *Physical Chemistry Chemical Physics* **2006**, *8*, 1298-1309.

(18) Dolphin, D. *The Porphyrins: Physical Chemistry, Part C*; Academic Press: New York, 1978; Vol. 5.

(19) Smith, K. M. *Porphyrins and Metalloporphyrins*; Elsevier Scientific Amsterdam, 1975.

(20) Yu, H. Z.; Baskin, J. S.; Zewail, A. H. *Journal of Physical Chemistry A* **2002**, *106*, 9845-9854.

(21) Li, Y.; Steer, R. P. *Chemical Physics Letters* **2003**, *373*, 94-99.

(22) Khairutdinov, R. F.; Serpone, N. *Journal of Physical Chemistry* **1995**, *99*, 11952-11958.

(23) Andersson, M.; Davidsson, J.; Hammarstrom, L.; Korppi-Tommola, J.; Peltola, T. *Journal of Physical Chemistry B* **1999**, *103*, 3258-3262.

(24) Lukaszewicz, A.; Karolczak, J.; Kowalska, D.; Maciejewski, A.; Ziolek, M.; Steer, R. P. *Chemical Physics* **2007**, *331*, 359-372.

(25) O'Brien, J. A.; Rallabandi, S.; Tripathy, U.; Paige, M. F.; Steer, R. P. *Chemical Physics Letters* **2009**, *475*, 220-222.

(26) O'Brien, J.; Lu, Y.; Hooley, E.; Ghiggino, K. P.; Steer, R. P.; Paige, M. F. *Canadian Journal of Chemistry* **2010**, submitted.

(27) Baluschev, S.; Keivanidis, P. E.; Wegner, G.; Jacob, J.; Grimsdale, A. C.; Mullen, K.; Miteva, T.; Yasuda, A.; Nelles, G. *Applied Physics Letters* **2005**, *86*, 3.

(28) Baluschev, S.; Yakutkin, V.; Miteva, T.; Wegner, G.; Roberts, T.; Nelles, G.; Yasuda, A.; Chernov, S.; Aleshchenkov, S.; Cheprakov, A. *New Journal of Physics* **2008**, *10*, 12.

(29) Baluschev, S.; Yakutkin, V.; Wegner, G.; Miteva, T.; Nelles, G.; Yasuda, A.; Chernov, S.; Aleshchenkov, S.; Cheprakov, A. *Applied Physics Letters* **2007**, *90*, 3.

(30) Baluschev, S.; Yakutkin, V.; Miteva, T.; Avlasevich, Y.; Chernov, S.; Aleshchenkov, S.; Nelles, G.; Cheprakov, A.; Yasuda, A.; Mullen, K.; Wegner, G. *Angewandte Chemie-International Edition* **2007**, *46*, 7693-7696.

(31) Baluschev, S.; Yakutkin, V.; Wegner, G.; Minch, B.; Miteva, T.; Nelles, G.; Yasuda, A. *Journal of Applied Physics* **2007**, *101*, 4.

(32) Baluschev, S.; Miteva, T.; Yakutkin, V.; Nelles, G.; Yasuda, A.; Wegner, G. *Physical Review Letters* **2006**, *97*, 3.
(33) Baluschev, S.; Jacob, J.; Avlasevich, Y. S.; Keivanidis, P. E.; Miteva, T.; Yasuda, A.; Nelles, G.; Grimsdale, A. C.; Mullen, K.; Wegner, G. *Chemphyschem* **2005**, *6*, 1250-1253.

(34) Islangulov, R. R.; Lott, J.; Weder, C.; Castellano, F. N. *Journal of the American Chemical Society* **2007**, *129*, 12652.

(35) Singh-Rachford, T. N.; Islangulov, R. R.; Castellano, F. N. *Journal of Physical Chemistry A* **2008**, *112*, 3906-3910.

(36) Islangulov, R. R.; Castellano, F. N. *Angewandte Chemie-International Edition* **2006**, *45*, 5957-5959.

(37) Islangulov, R. R.; Kozlov, D. V.; Castellano, F. N. *Chemical Communications* **2005**, 3776-3778.

(38) Monguzzi, A.; Tubino, R.; Meinardi, F. *Physical Review B* **2008**, *77*, 4.

(39) Stelmakh, G. F.; Tsvirko, M. P. *Acs Symposium Series* **1986**, *321*, 118-127.

(40) Stelmakh, G. F.; Tsvirko, M. P. *Optika I Spektroskopiya* **1980**, *49*, 511-516.

(41) Sevchenko, A. N.; Stelmakh, G. F.; Tsvirko, M. P. *Optika I Spektroskopiya* **1979**, *46*, 893-897.

(42) Sugunan, S. K.; Tripathy, U.; Brunet, S. M. K.; Paige, M. F.; Steer, R. P. *Journal of Physical Chemistry A* **2009**, *113*, 8548-8556.

(43) Furuto, T.; Lee, S. K.; Amao, Y.; Asai, K.; Okura, I. *Journal of Photochemistry and Photobiology a-Chemistry* **2000**, *132*, 81-86.

(44) Nakamura, Y.; Aratani, N.; Osuka, A. *Chemical Society Reviews* **2007**, *36*, 831-845.

(45) Moerner, W. E.; Fromm, D. P. *Review of Scientific Instruments* **2003**, *74*, 3597-3619.

(46) Tinnefeld, P.; Sauer, M. *Angewandte Chemie-International Edition* **2005**, *44*, 2642-2671.

(47) Deschenes, L. A.; Vanden Bout, D. A. *Science* **2001**, *292*, 255-258.

(48) Weston, K. D.; Carson, P. J.; DeAro, J. A.; Buratto, S. K. *Chemical Physics Letters* **1999**, *308*, 58-64.

(49) Basche, T.; Ambrose, W. P.; Moerner, W. E. *Journal of the Optical Society of America B-Optical Physics* **1992**, *9*, 829-836.

(50) Tchenio, P.; Myers, A. B.; Moerner, W. E. *Journal of Physical Chemistry* **1993**, *97*, 2491-2493.

(51) Tchenio, P.; Myers, A. B.; Moerner, W. E. *Chemical Physics Letters* **1993**, *213*, 325-332.

(52) Myers, A. B.; Tchenio, P.; Zgierski, M. Z.; Moerner, W. E. *Journal of Physical Chemistry* **1994**, *98*, 10377-10390.

(53) Trautman, J. K.; Macklin, J. J.; Brus, L. E.; Betzig, E. *Nature* **1994**, *369*, 40-42.

(54) Kowalska, D.; Steer, R. P. *Journal of Photochemistry and Photobiology a-Chemistry* **2008**, *195*, 223-227.

(55) Park, M.; Cho, S.; Yoon, Z. S.; Aratani, N.; Osuka, A.; Kim, D. *Journal of the American Chemical Society* **2005**, *127*, 15201-15206.

(56) Yang, J.; Cho, S.; Yoo, H.; Park, J.; Li, W. S.; Aida, T.; Kim, D. *Journal of Physical Chemistry A* **2008**, *112*, 6869-6876.

(57) Yang, J.; Park, M.; Yoon, Z. S.; Hori, T.; Peng, X. B.; Aratani, N.; Dedecker, P.; Hotta, J. I.; Uji-I, H.; Sliwa, M.; Hofkens, J.; Osuka, A.; Kim, D. *Journal of the American Chemical Society* **2008**, *130*, 1879-1884.

(58) Yang, J. S.; Yoo, H.; Aratani, N.; Osuka, A.; Kim, D. *Angewandte Chemie-International Edition* **2009**, *48*, 4323-4327.

(59) Yoo, H.; Yang, J.; Nakamura, Y.; Aratani, N.; Osuka, A.; Kim, D. *Journal of the American Chemical Society* **2009**, *131*, 1488-1494.

(60) Macho, E.; Alegria, A.; Colmenero, J. *Journal of Applied Physics* **1988**, *64*, 642-646.

(61) Kano, K. *Journal of Porphyrins and Phthalocyanines* **2004**, *8*, 148-155.

(62) Hooley, E. *Honours Thesis, University of Melbourne* **2008**.

(63) Dixon, J. M.; Taniguchi, M.; Lindsey, J. S. *Photochemistry and Photobiology* **2005**, *81*, 212-213.

(64) VandenBout, D. A.; Yip, W. T.; Hu, D. H.; Fu, D. K.; Swager, T. M.; Barbara, P. F. *Science* **1997**, *277*, 1074-1077.

(65) Yip, W. T.; Hu, D. H.; Yu, J.; Vanden Bout, D. A.; Barbara, P. F. *Journal of Physical Chemistry A* **1998**, *102*, 7564-7575.

(66) Bagh, S.; Paige, M. F. *Canadian Journal of Chemistry* **2005**, *83*, 435-442.

(67) Lu, Y.; Paige, M. F. *Journal of Fluorescence* **2007**, *17*, 739-748.

(68) Sharma, S. K.; Wang, Z. F.; vanderLaan, S. *Journal of Raman Spectroscopy* **1996**, *27*, 739-746.

List of Figures in Appendix

Appendix

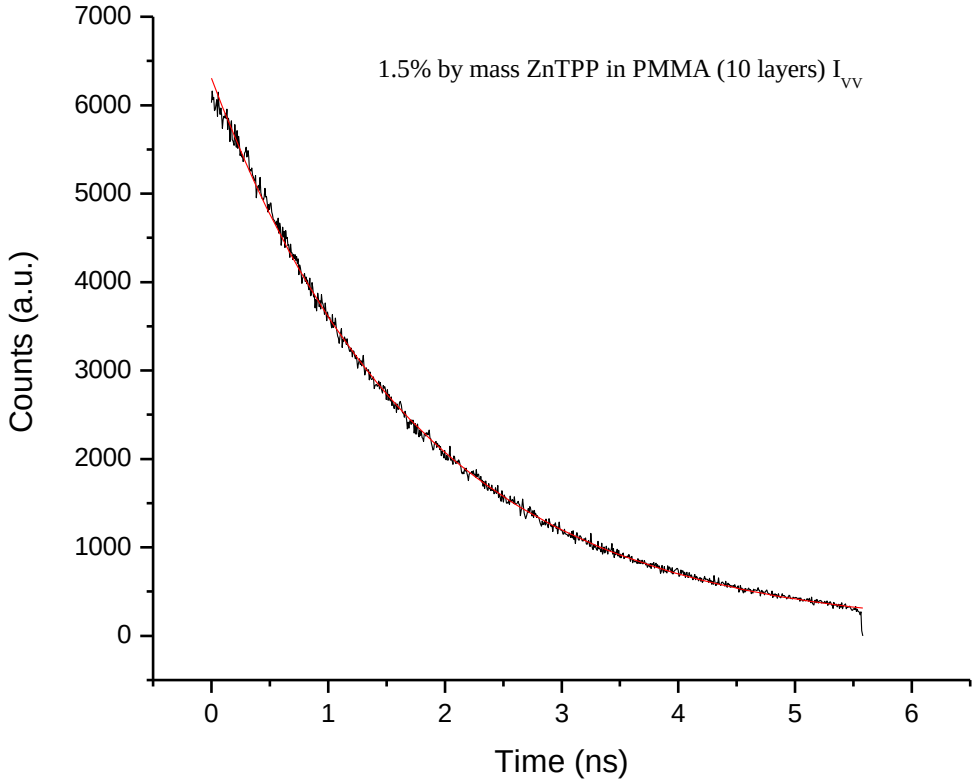

Figure A.1 Vertically polarized fluorescence decay curve a for 1.5% by mass ZnTPP in PMMA film (10 layers), and the best single exponential fit (red). λ_{ex} = 400 nm (pulsed), 120 μW (average power), τ = 1.78 ns.

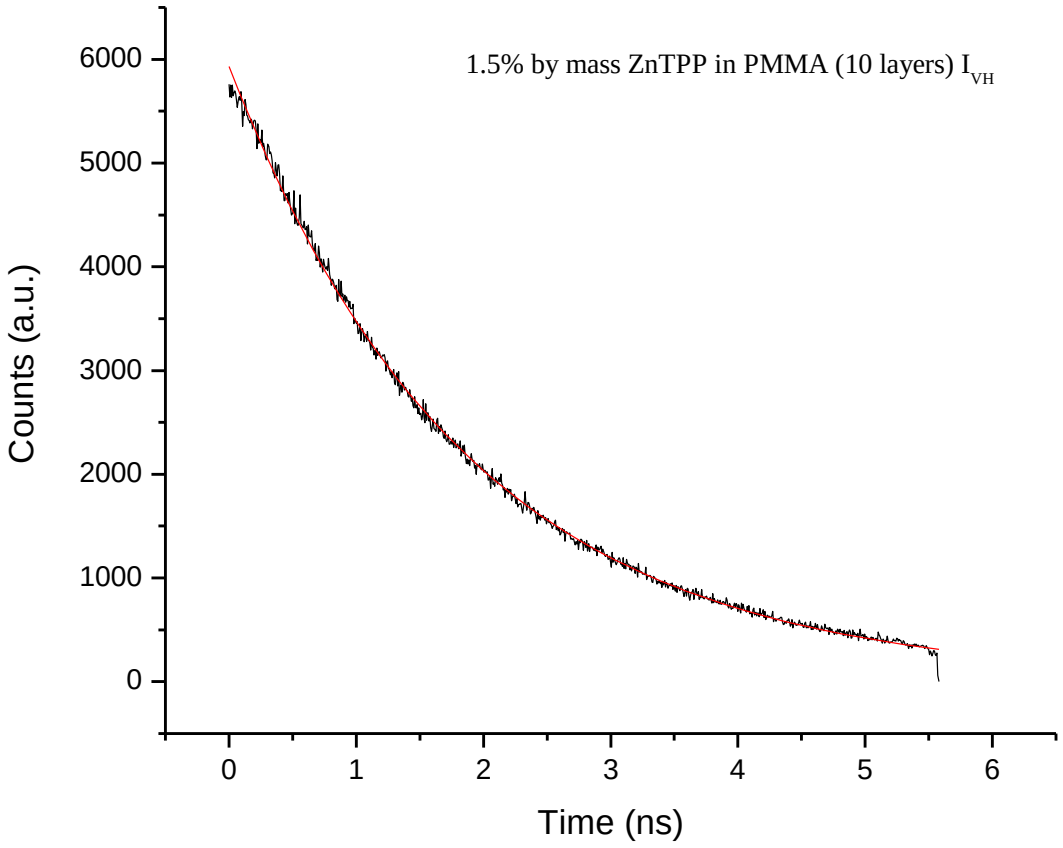

Figure A.2 Horizontally polarized fluorescence decay curve for a 1.5% by mass ZnTPP in PMMA film (10 layers), and the best single exponential fit (red). λ_{ex} = 400 nm (pulsed), 120 μW (average power), τ = 1.86 ns.

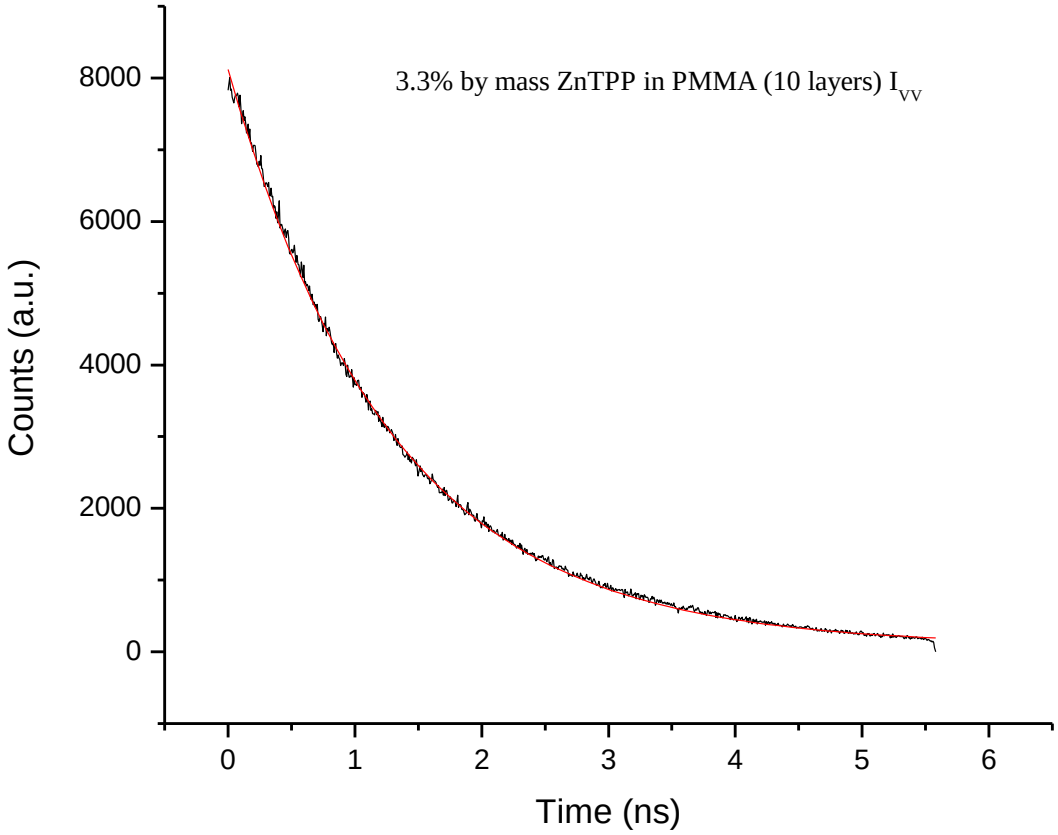

Figure A.3 Vertically polarized fluorescence decay curve for a 3.3% by mass ZnTPP in PMMA film (10 layers), and the best single exponential fit (red). λ_{ex} = 400 nm (pulsed), 120 μW (average power), τ = 1.29 ns.

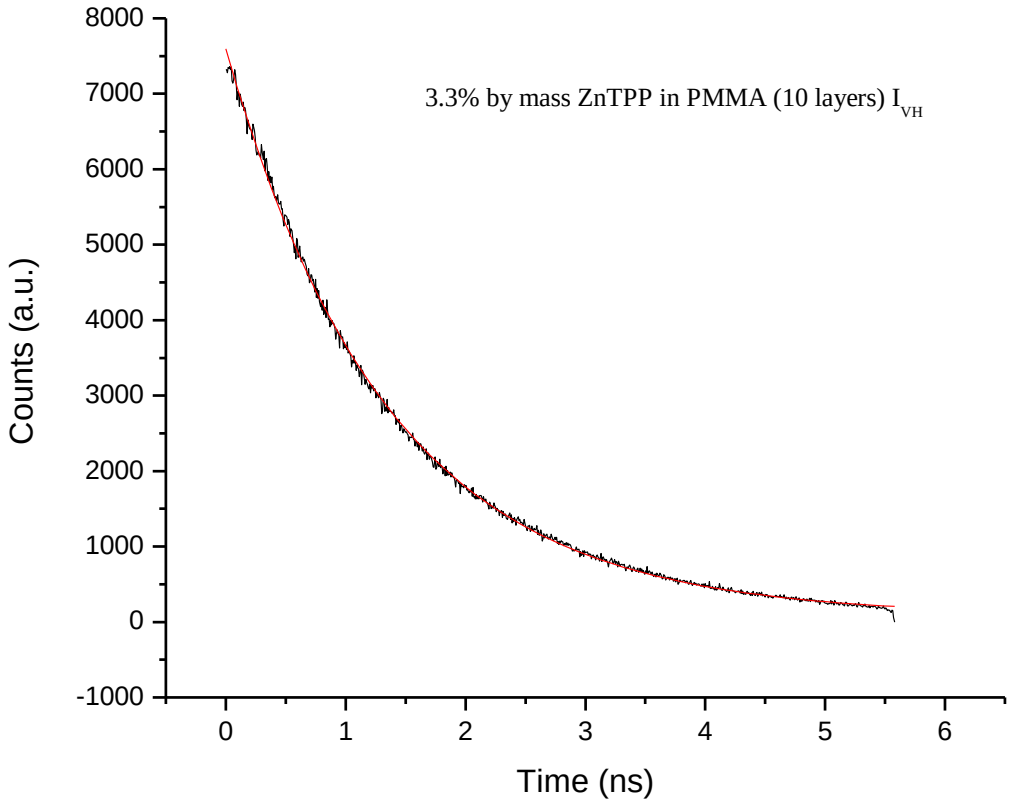

Figure A.4 Horizontally polarized fluorescence decay curve for a 3.3% by mass ZnTPP in PMMA film (10 layers), and the best single exponential fit (red). λ_{ex} = 400 nm (pulsed), 120 μW (average power), τ = 1.35 ns.

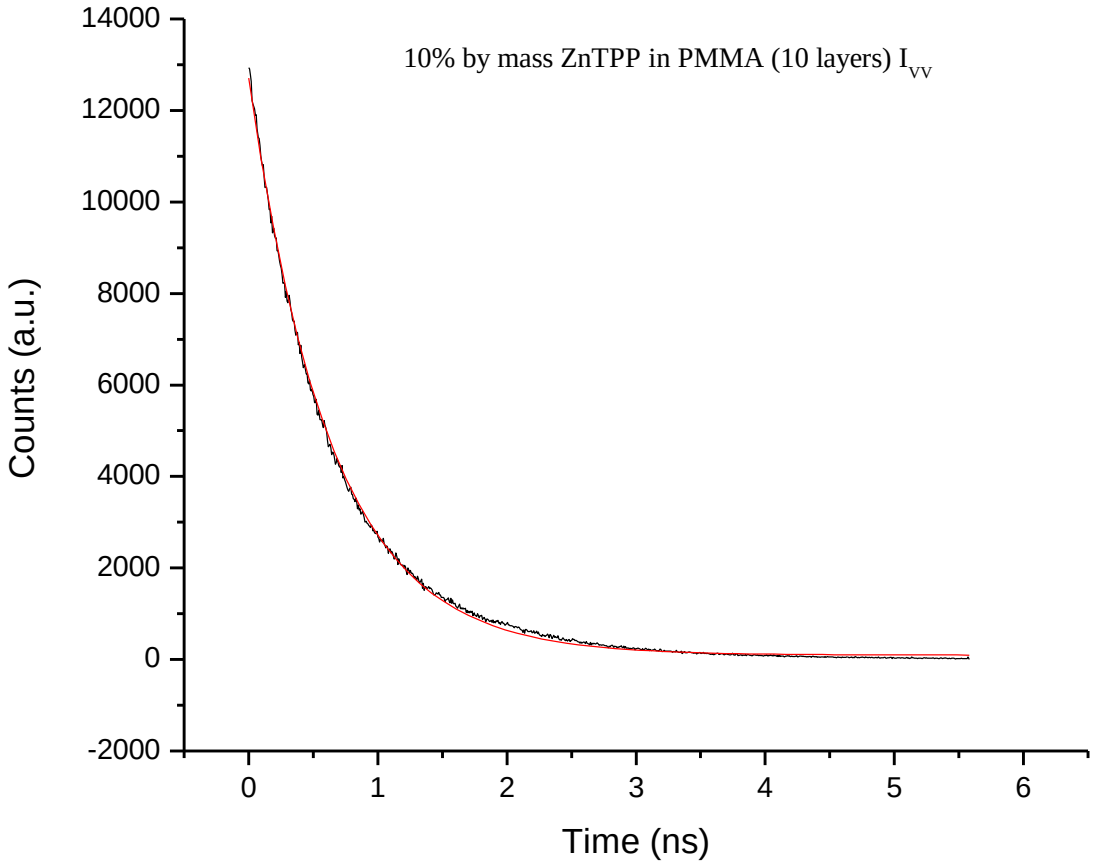

Figure A.5 Vertically polarized fluorescence decay curve for a 10 % by mass ZnTPP in PMMA film (10 layers), and the best single exponential fit (red). λ_{ex} = 400 nm (pulsed), 120 μW (average power), τ = 0.63 ns.

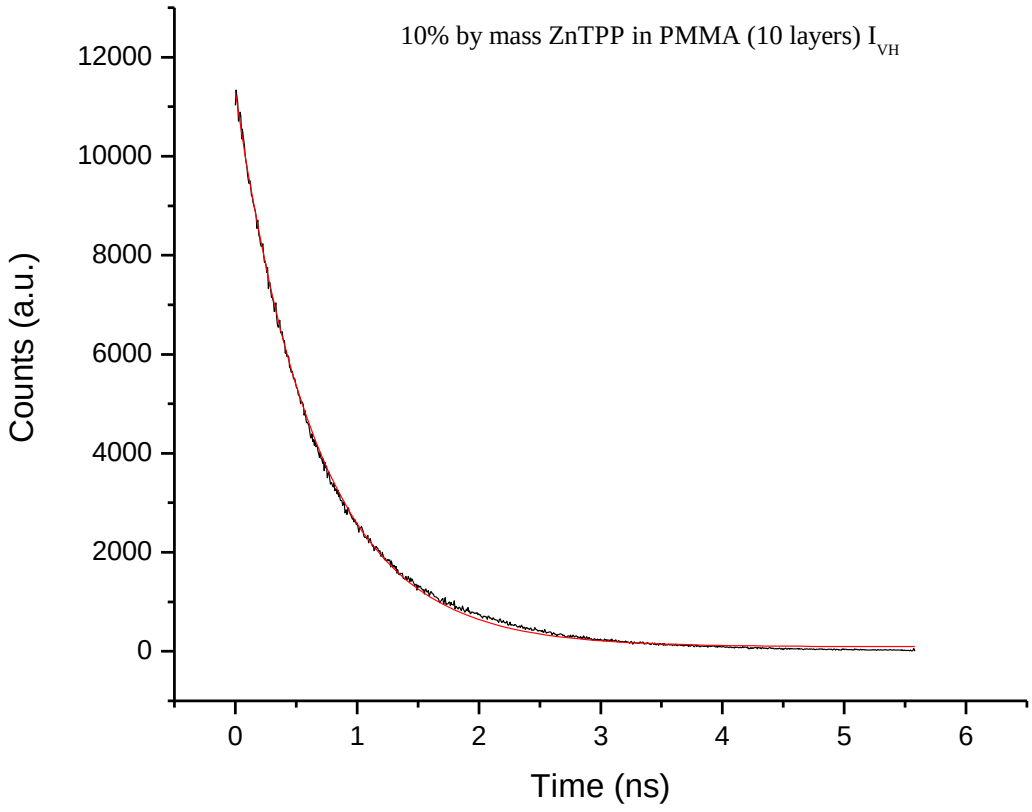

Figure A.6 Horizontally polarized fluorescence decay curve for a 10 % by mass ZnTPP in PMMA film (10 layers), and the best single exponential fit (red). λ_{ex} = 400 nm (pulsed), 120 μW (average power), τ = 0.66 ns.

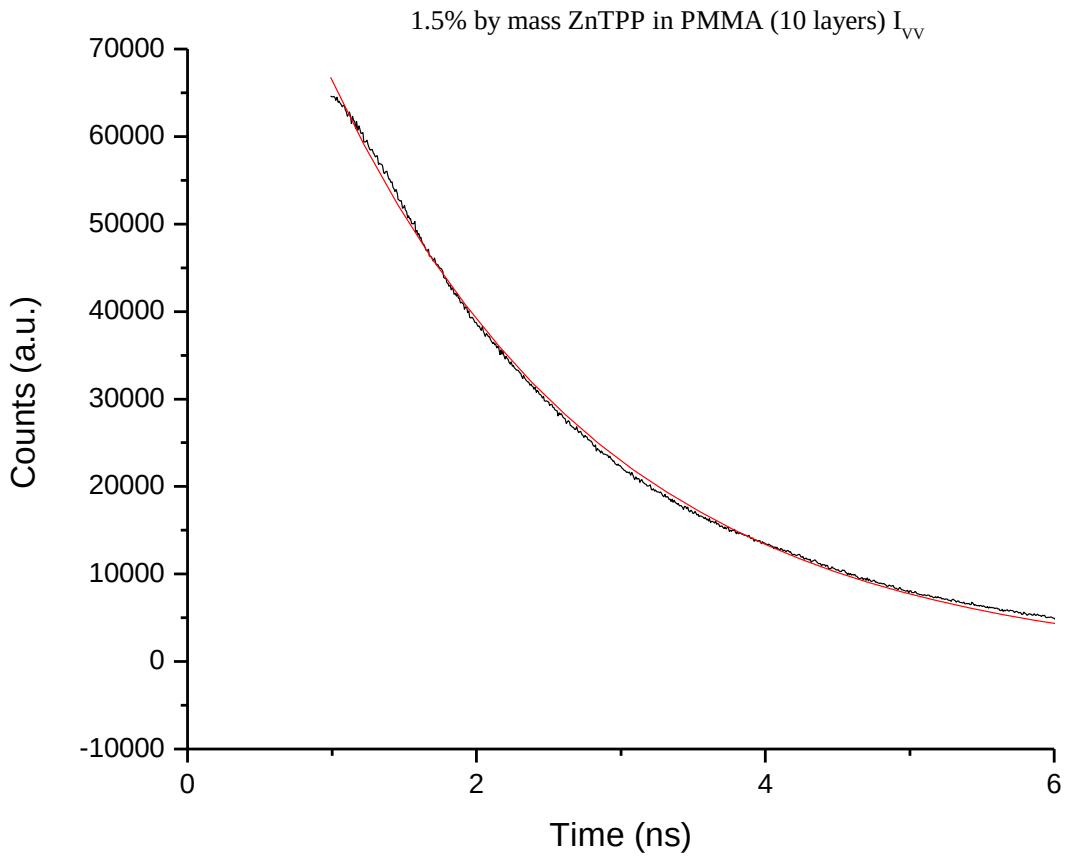

Figure A.7 Vertically polarized fluorescence decay curve for a 1.5 % by mass ZnTPP in PMMA film (10 layers), and the best single exponential fit (red). λ_{ex} = 400 nm (pulsed), 140 μW (average power), τ = 1.91 ns.

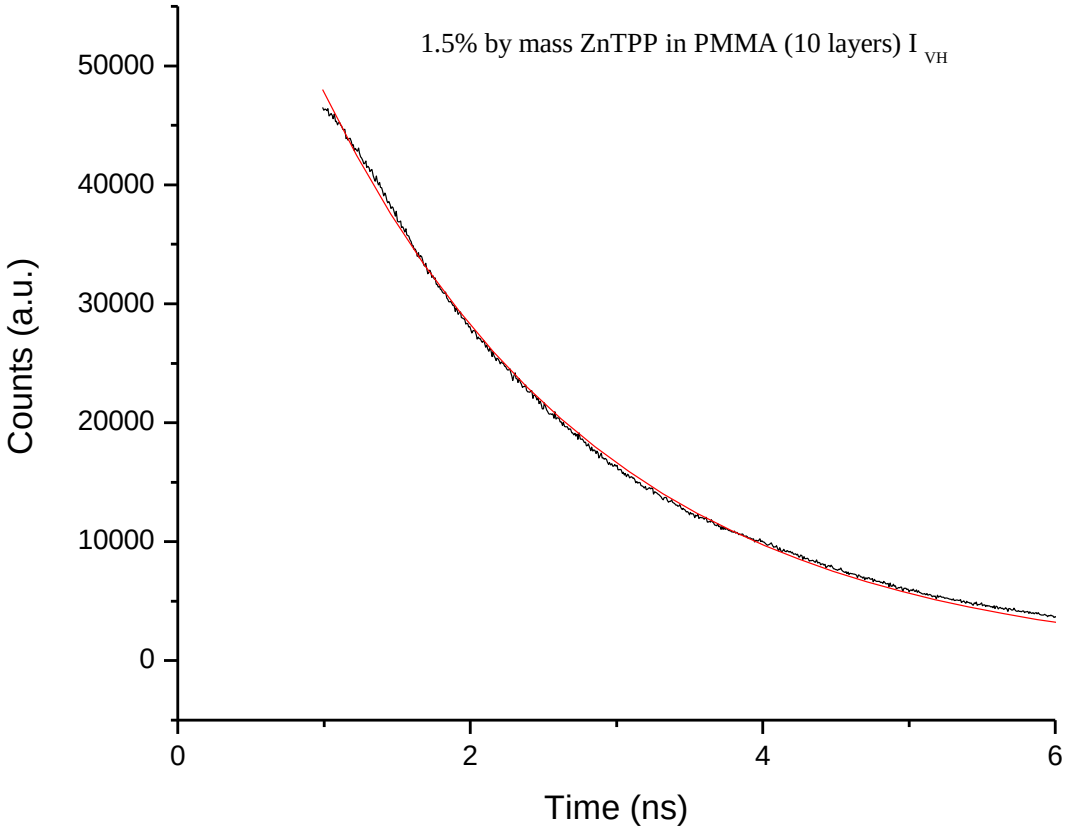

Figure A.8 Horizontally polarized fluorescence decay curve for a 1.5 % by mass ZnTPP in PMMA film (10 layers), and the best single exponential fit (red). λ_{ex} = 400 nm (pulsed), 140 μW (average power), τ = 1.92 ns.

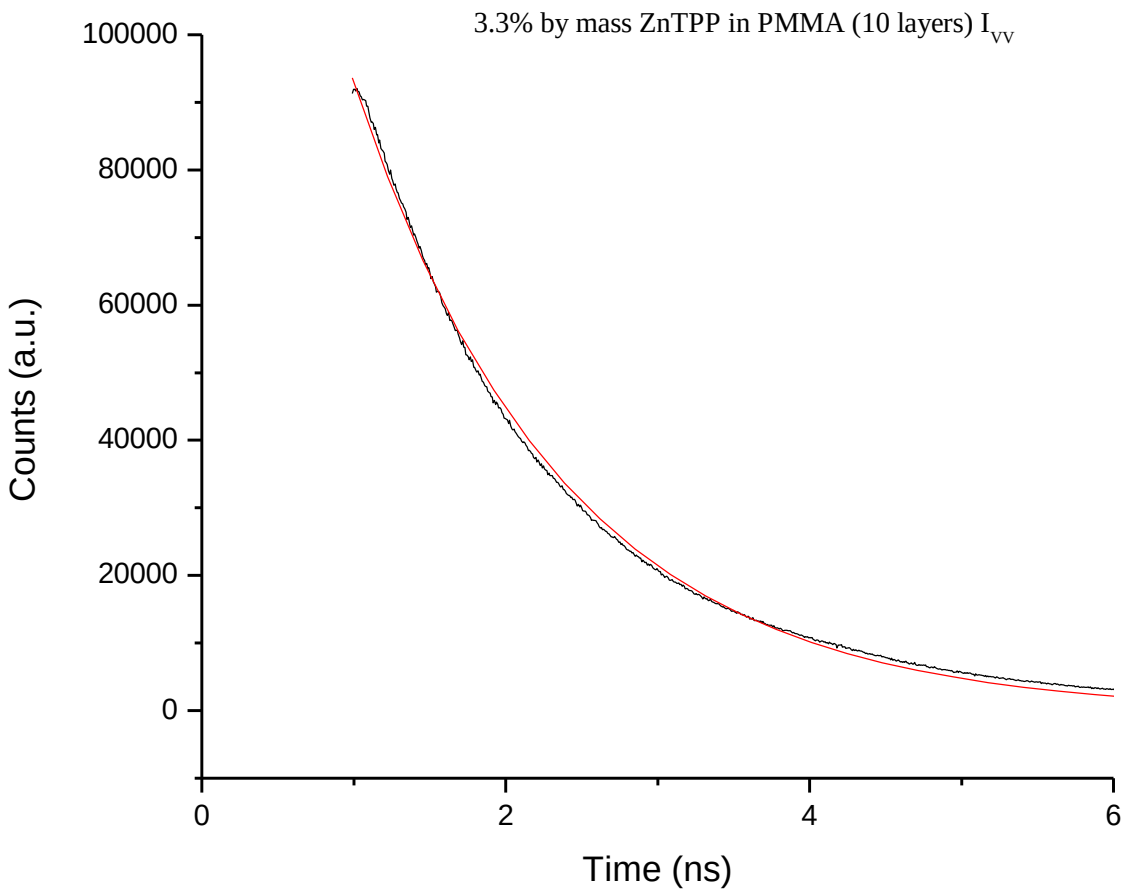

Figure A.9 Vertically polarized fluorescence decay curve for a 3.3 % by mass ZnTPP in PMMA film (10 layers), and the best single exponential fit (red). λ_{ex} = 400 nm (pulsed), 140 μW (average power), τ = 1.37 ns.

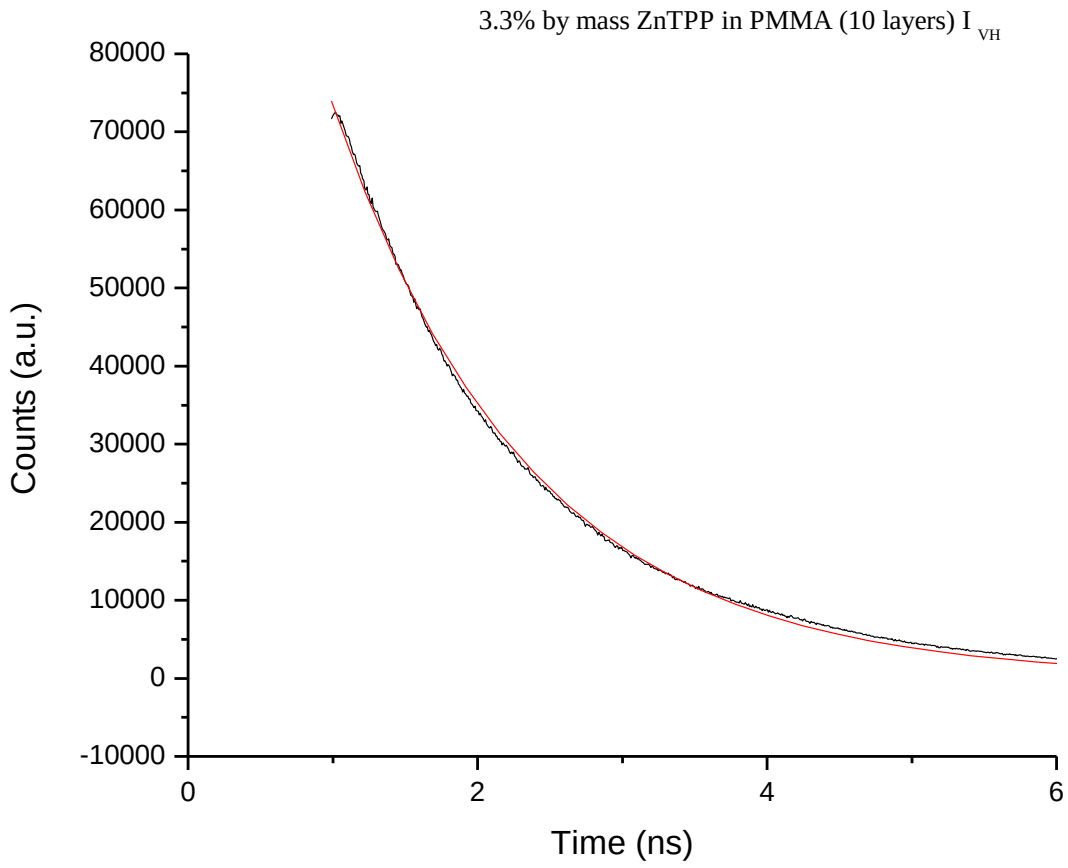

Figure A.10 Horizontally polarized fluorescence decay curve for a 3.3 % by mass ZnTPP in PMMA film (10 layers), and the best single exponential fit (red). λ_{ex} = 400 nm (pulsed), 140 μW (average power), τ = 1.35 ns.

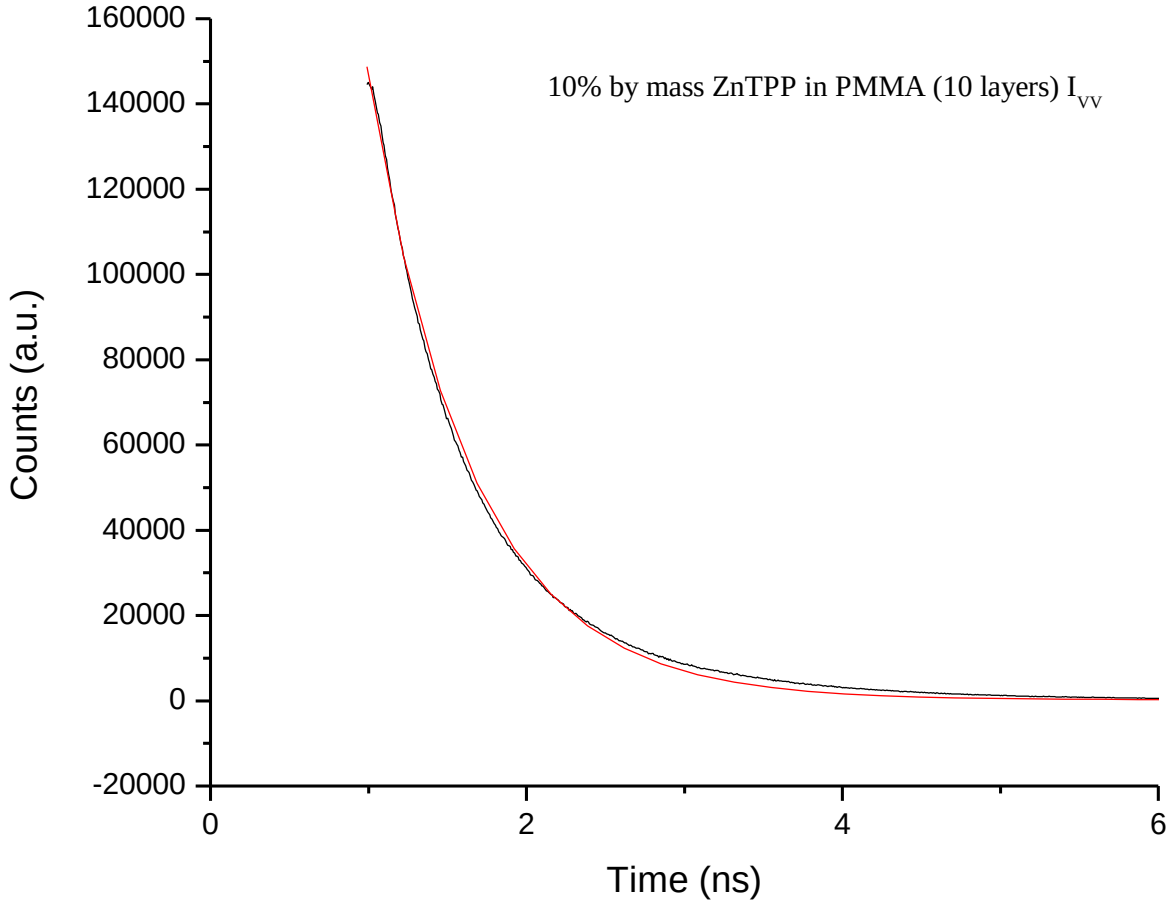

Figure A.11 Vertically polarized fluorescence decay curve for a 10 % by mass ZnTPP in PMMA film (10 layers), and the best single exponential fit (red). λ_{ex} = 400 nm (pulsed), 140 μW (average power), τ = 0.65 ns.

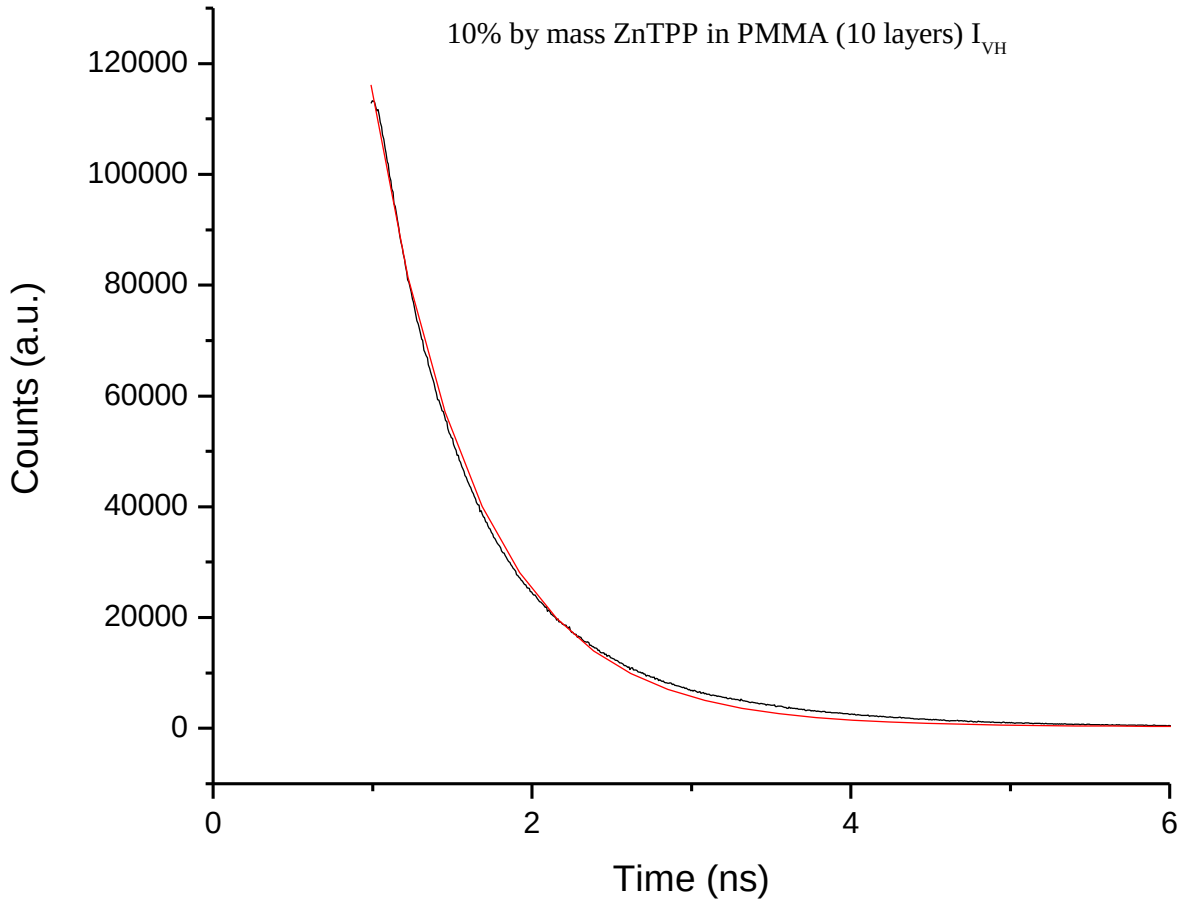

Figure A.12 Horizontally polarized fluorescence decay curve for a 10 % by mass ZnTPP in PMMA film (10 layers), and the best single exponential fit (red). λ_{ex} = 400 nm (pulsed), 140 μW (average power), τ = 0.65 ns.

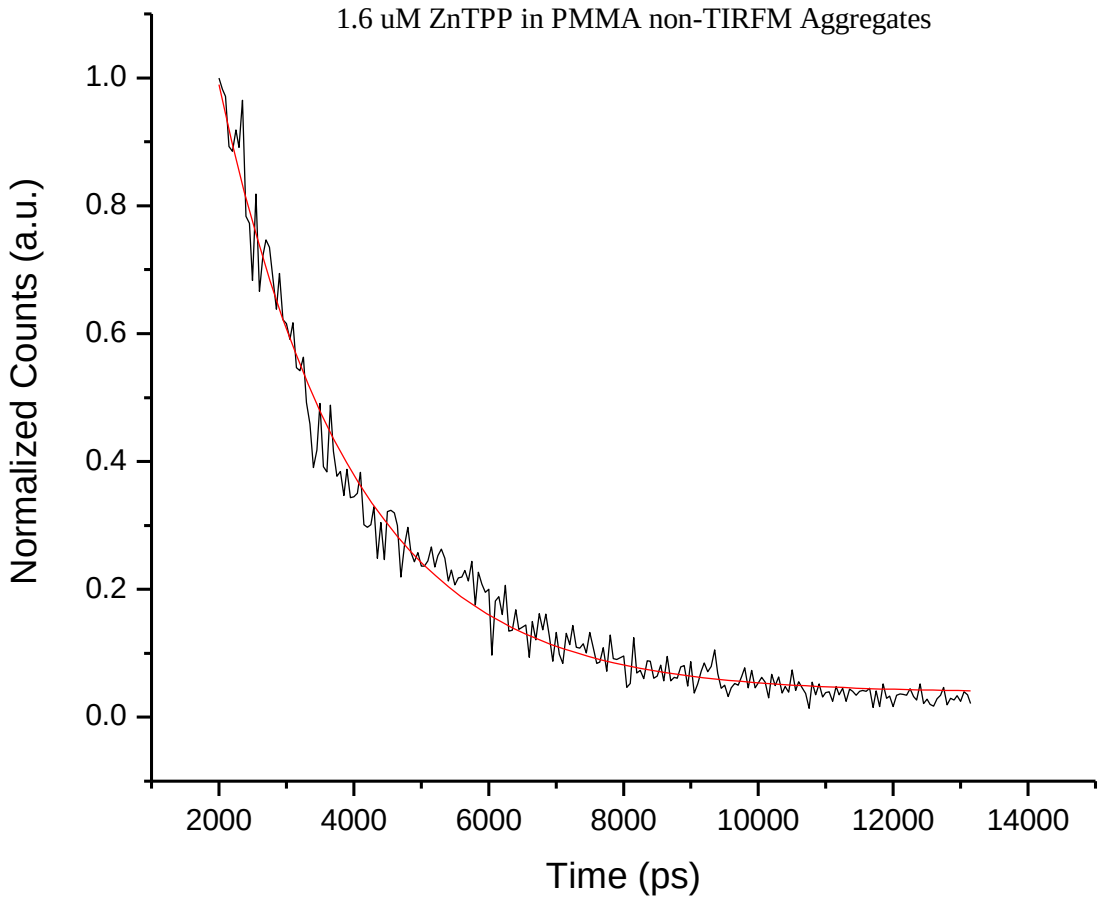

Figure A.13 Normalized fluorescence decay for an area on a 1.6 μM ZnTPP in PMMA film where aggregates are expected to be (collected in non-TIRFM mode), and the best single exponential fit (red). λ_{ex} = 400 nm, pulsed excitation at an average power of 0.4 mW, τ = 1.95 ns.

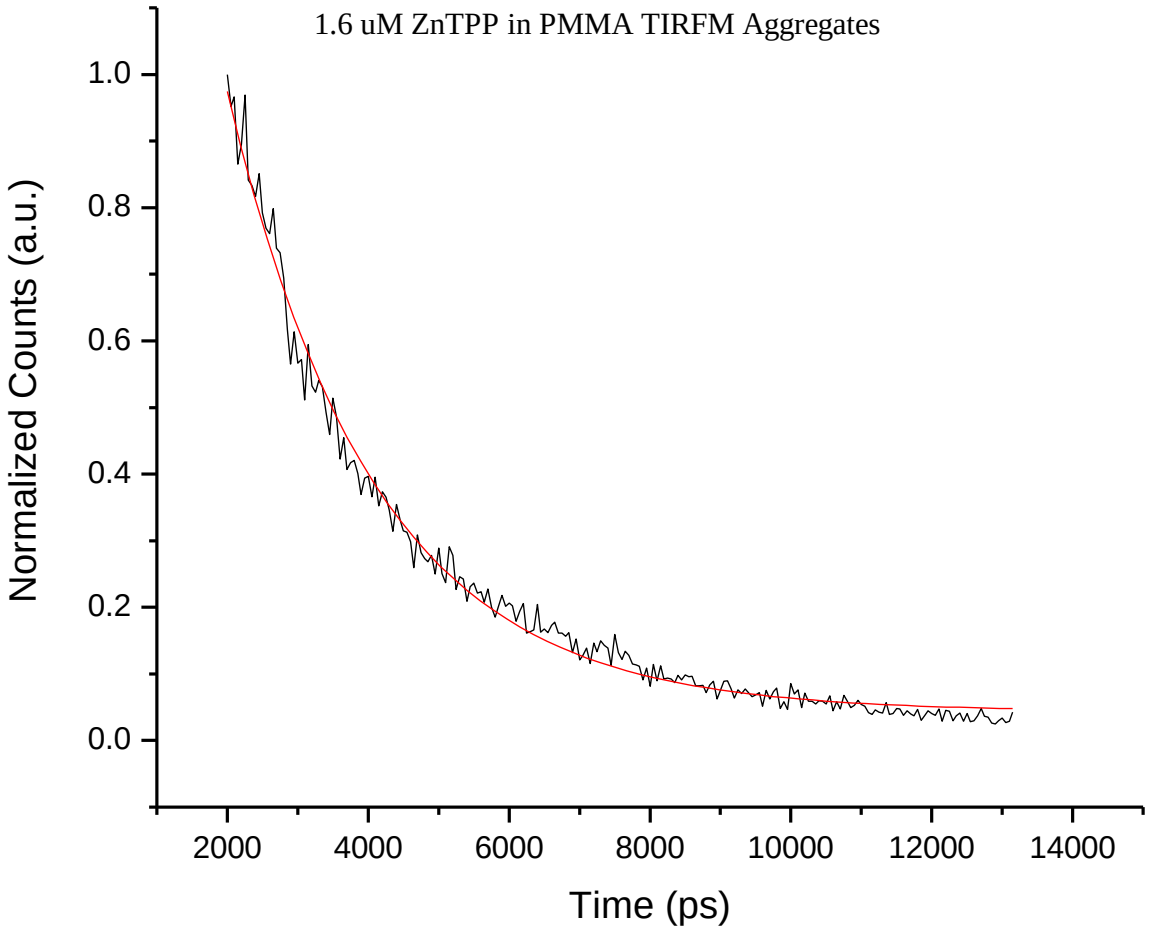

Figure A.14 Normalized fluorescence decay for an area on a 1.6 μM ZnTPP in PMMA film where aggregates are expected to be (collected in TIRFM mode), and the best single exponential fit (red). λ_{ex} = 400 nm, pulsed excitation at an average power of 0.4 mW, τ = 2.09 ns.

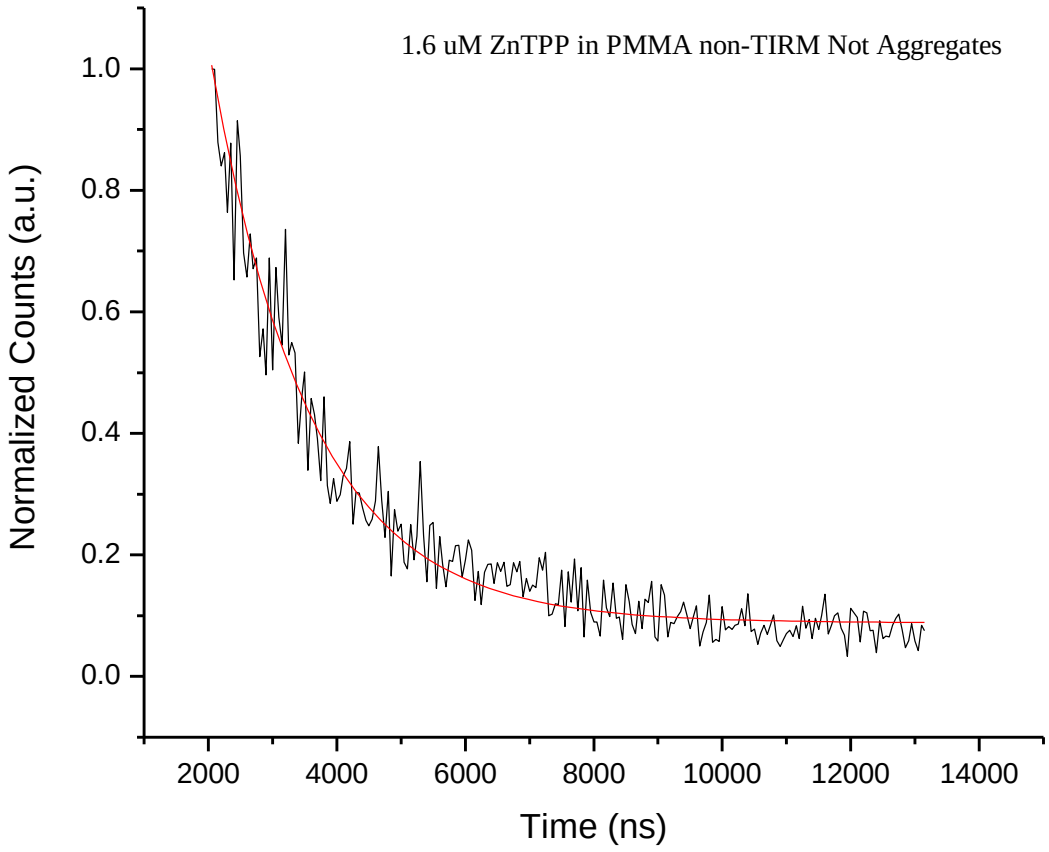

Figure A.15 Normalized fluorescence decay for an area on a 1.6 μM ZnTPP in PMMA film where aggregates are not expected to be (collected in non-TIRFM mode), and the best single exponential fit (red). λ_{ex} = 400 nm, pulsed excitation at an average power of 0.4 mW, τ = 1.56 ns.

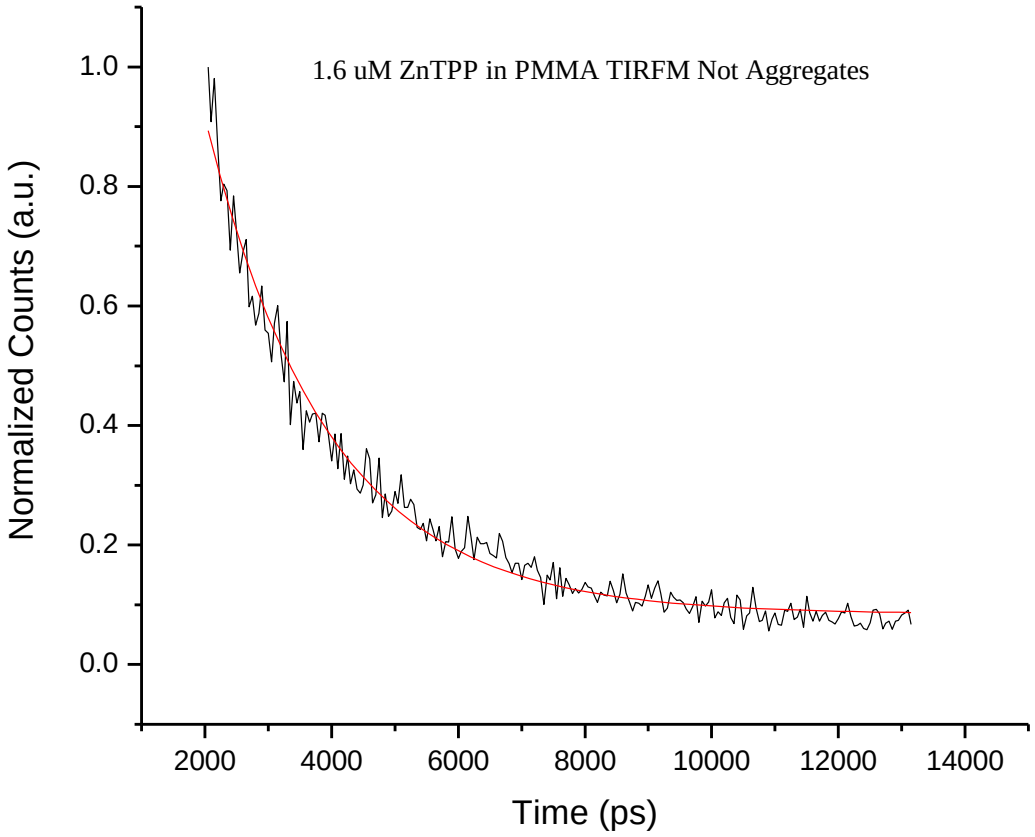

Figure A.16 Normalized fluorescence decay for an area on a 1.6 μM ZnTPP in PMMA film where aggregates are not expected to be (collected in TIRFM mode), and the best single exponential fit (red). λ_{ex} = 400 nm, pulsed excitation at an average power of 0.4 mW, τ = 1.94 ns.

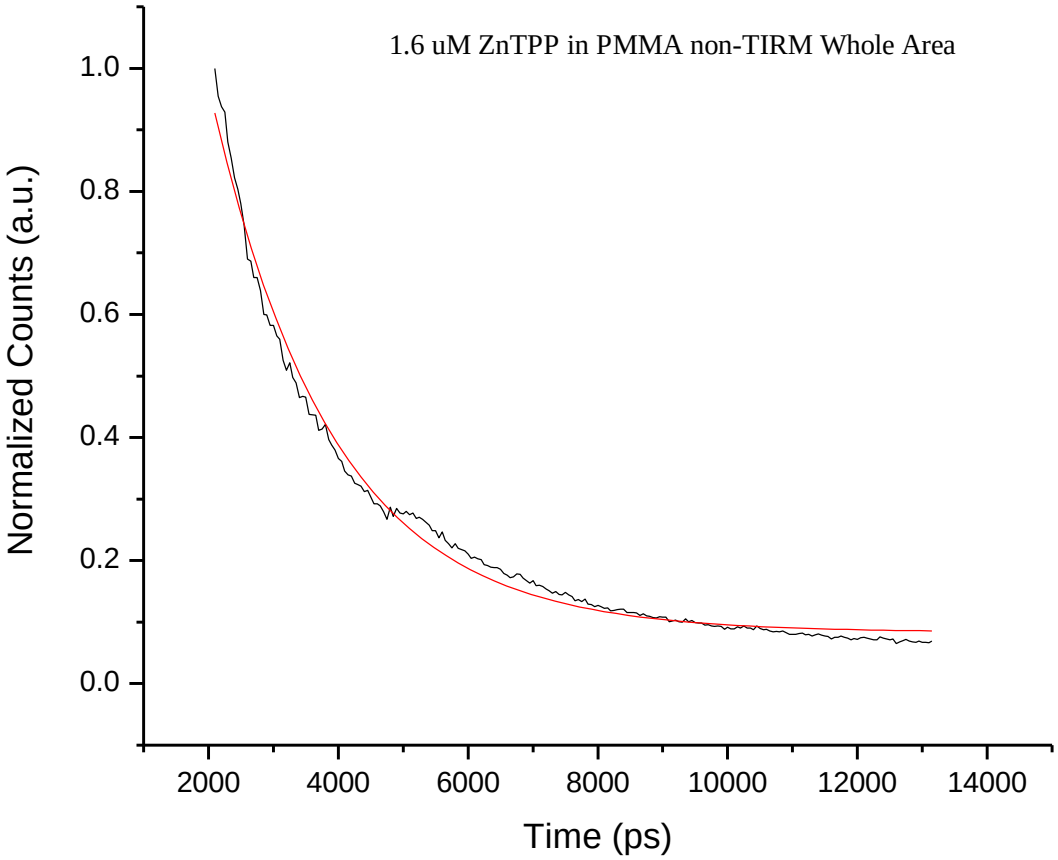

Figure A.17 Normalized fluorescence decay for the whole area of a 1.6 μM ZnTPP in PMMA film (collected in non-TIRFM mode), and the best single exponential fit (red). λ_{ex} = 400 nm, pulsed excitation at an average power of 0.4 mW, τ = 1.86 ns.

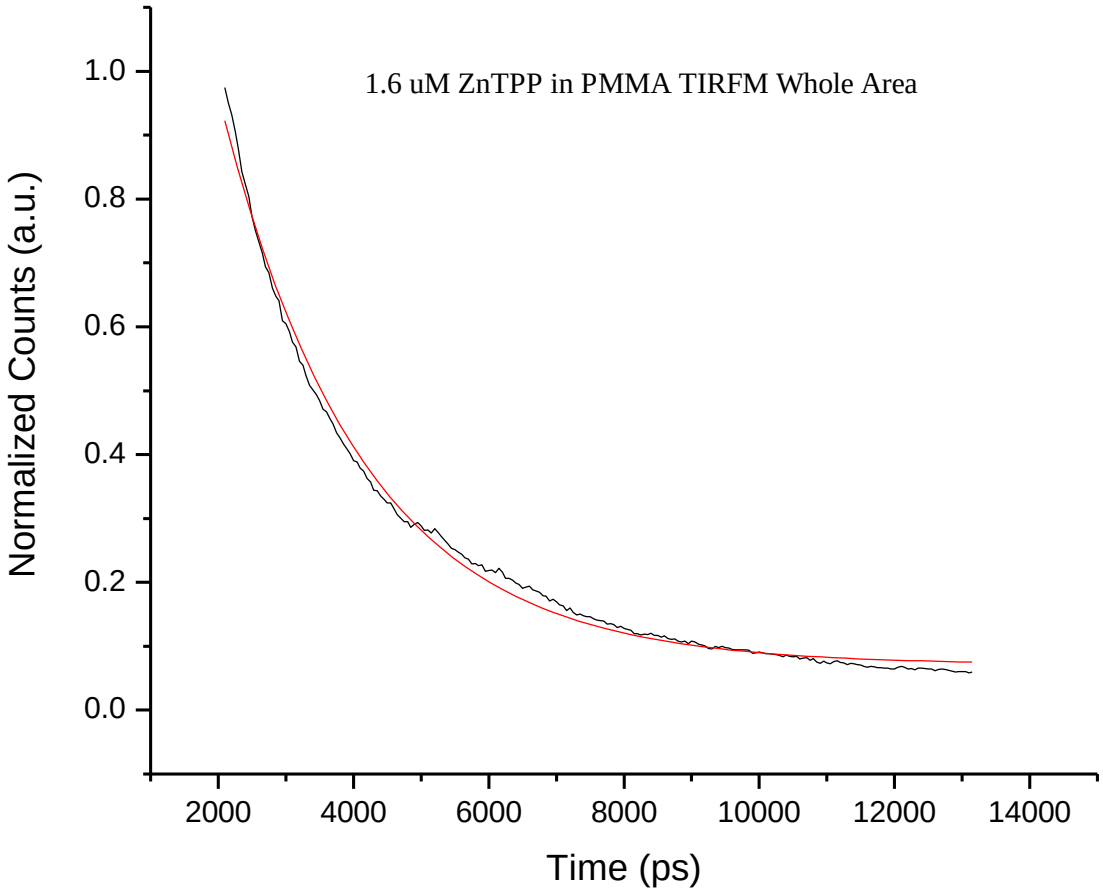

Figure A.18 Normalized fluorescence decay for the whole area of a 1.6 μM ZnTPP in PMMA film (collected in TIRFM mode), and the best single exponential fit (red). λ_{ex} = 400 nm, pulsed excitation at an average power of 0.4 mW, τ = 2.07 ns.

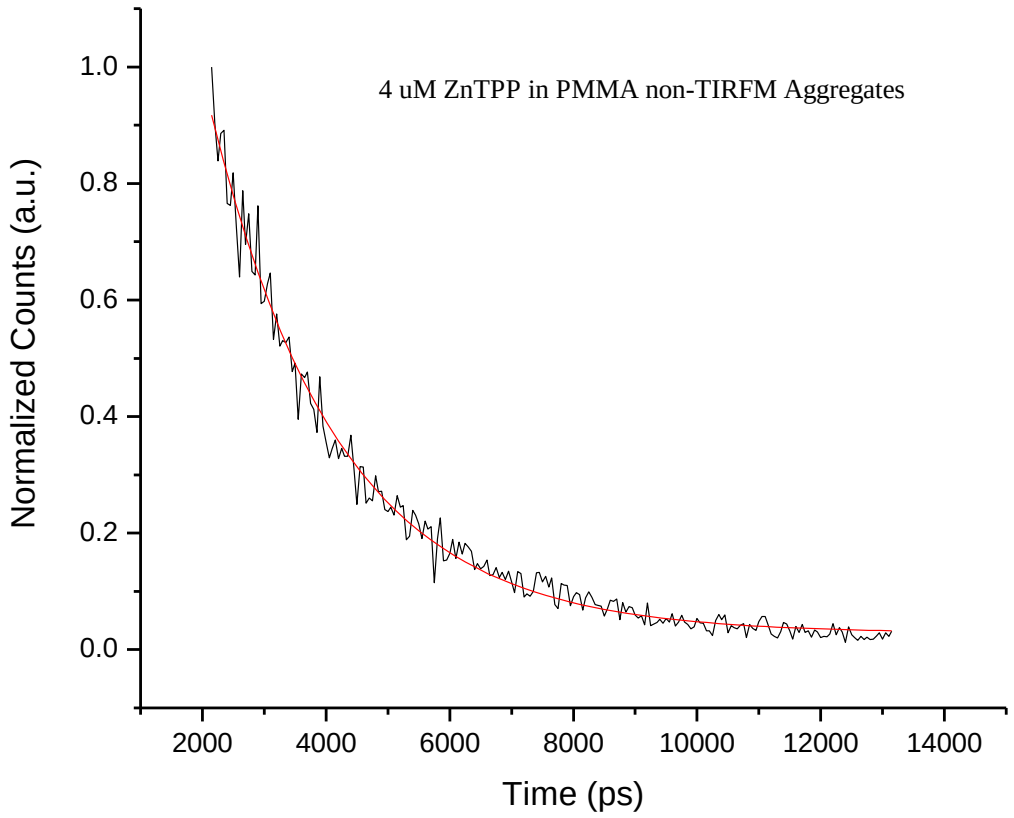

Figure A.19 Normalized fluorescence decay for an area on a 4 μM ZnTPP in PMMA film where aggregates are expected to be (collected in non-TIRFM mode), and the best single exponential fit (red). λ_{ex} = 400 nm, pulsed excitation at an average power of 0.4 mW, τ = 2.07 ns.

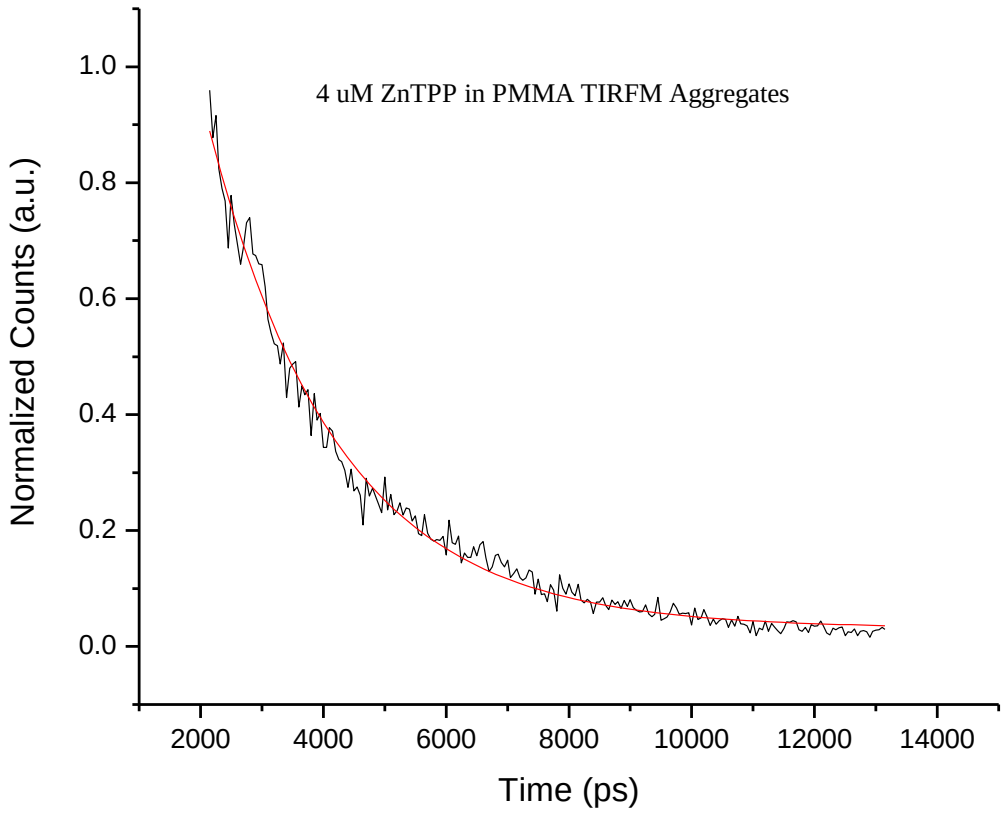

Figure A.20 Normalized fluorescence decay for an area on a 4 μM ZnTPP in PMMA film where aggregates are expected to be (collected in TIRFM mode), and the best single exponential fit (red). λ_{ex} = 400 nm, pulsed excitation at an average power of 0.4 mW, τ = 2.10 ns.

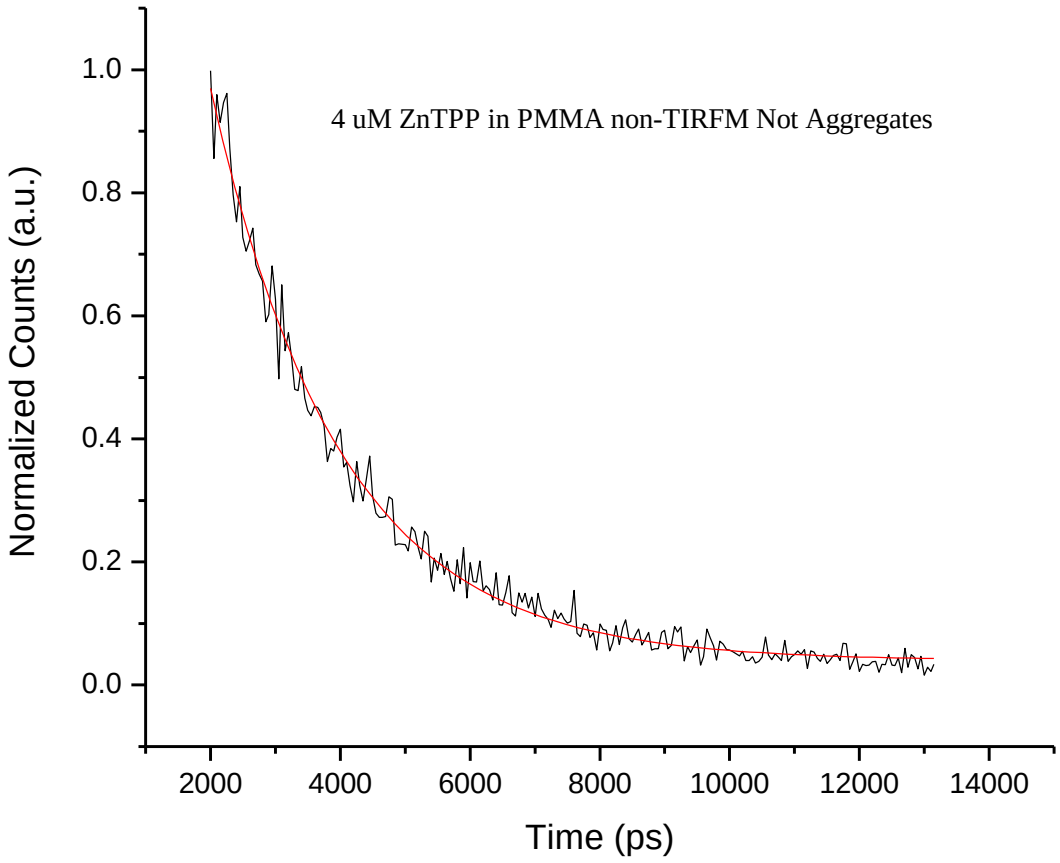

Figure A.21 Normalized fluorescence decay for an area on a 4 μM ZnTPP in PMMA film where aggregates are not expected to be (collected in non-TIRFM mode), and the best single exponential fit (red). λ_{ex} = 400 nm, pulsed excitation at an average power of 0.4 mW, τ = 1.99 ns.

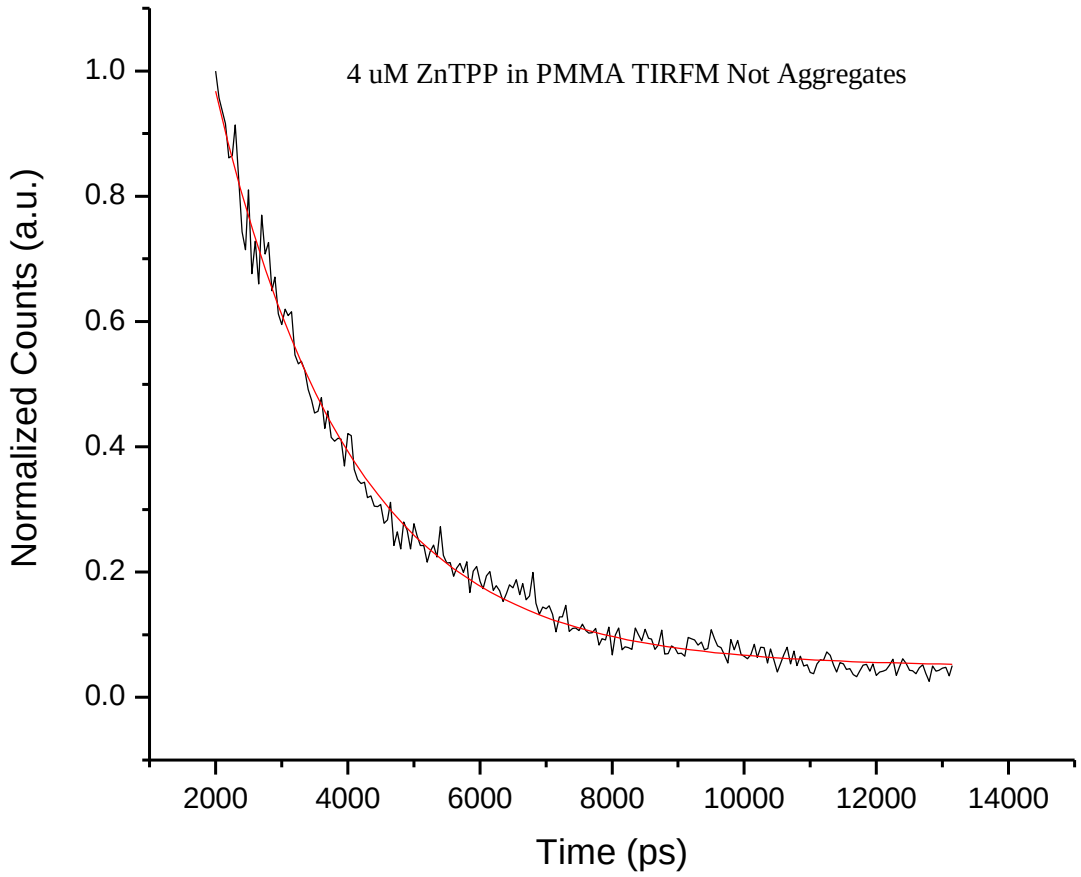

Figure A.22 Normalized fluorescence decay for an area on a 4 μM ZnTPP in PMMA film where aggregates are not expected to be (collected in TIRFM mode), and the best single exponential fit (red). λ_{ex} = 400 nm, pulsed excitation at an average power of 0.4 mW, τ = 2.03 ns.

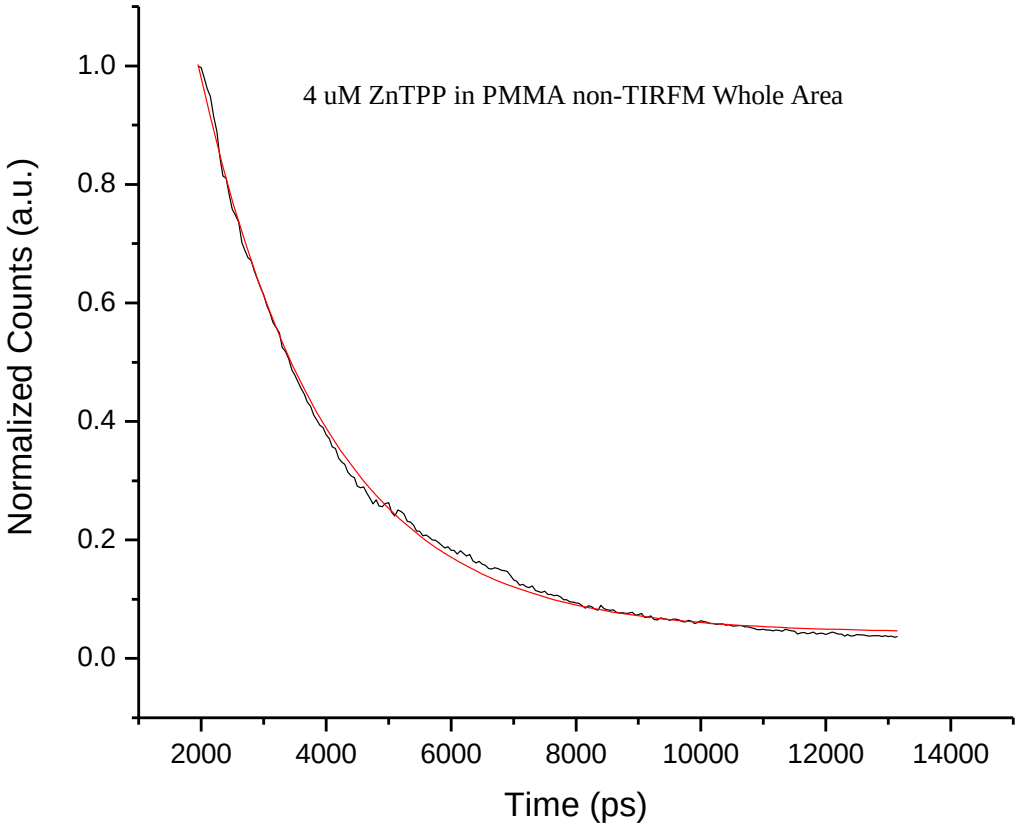

Figure A.23 Normalized fluorescence decay for the whole area of a 4 μM ZnTPP in PMMA film (collected in non-TIRFM mode), and the best single exponential fit (red). λ_{ex} = 400 nm, pulsed excitation at an average power of 0.4 mW, τ = 2.01 ns.

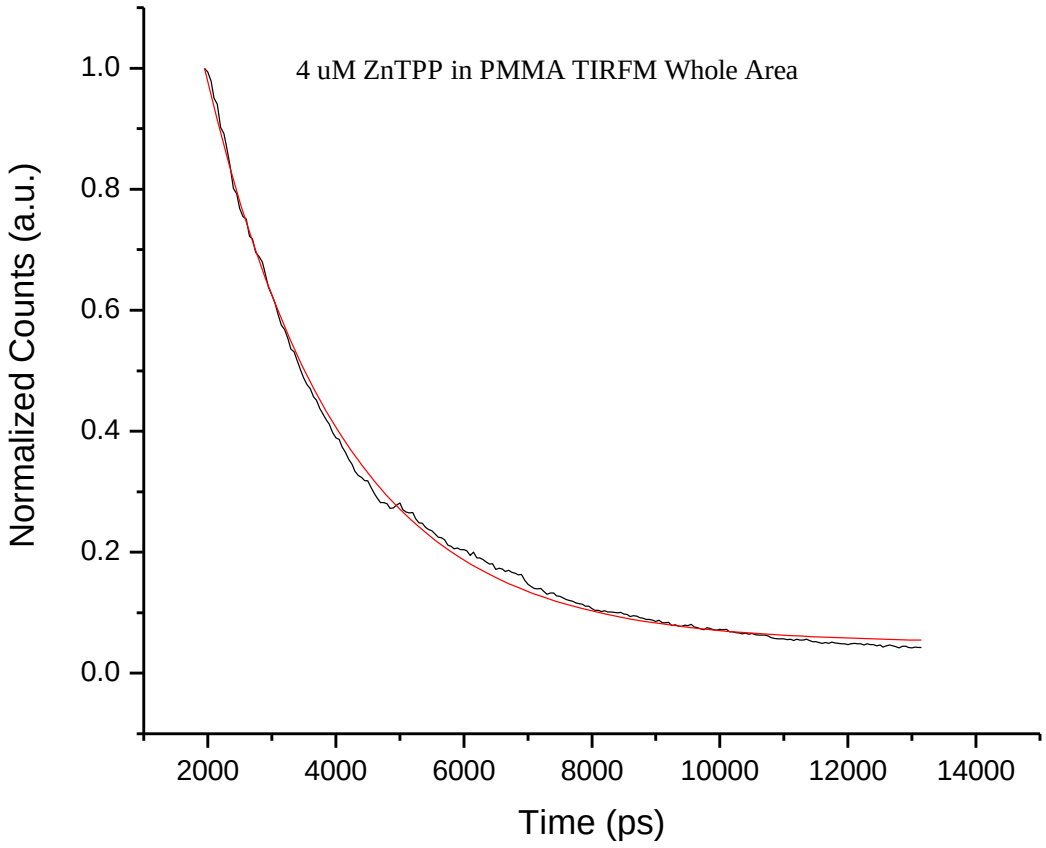

Figure A.24 Normalized fluorescence decay for the whole area of a 4 μM ZnTPP in PMMA film (collected in TIRFM mode), and the best single exponential fit (red). λ_{ex} = 400 nm, pulsed excitation at an average power of 0.4 mW, τ = 2.09 ns.